

REVIEWS OF TOPICAL PROBLEMS

PACS numbers: **12.20.–m**, 42.60.Jf, **52.38.–r**, 52.40.Mj

Dynamics and radiation of charged particles in ultra-intense laser fields

S V Popruzhenko, A M Fedotov

DOI: https://doi.org/10.3367/UFNe.2023.03.039335

Contents

Abstract. The current state of research on high-intensity laser fields and their interaction with charged particles is reviewed. Data on petawatt-class laser facilities are presented, and advanced methods for characterizing ultra-intense laser pulses are discussed. Effects that occur in the interaction of such pulses with matter in the regime dominated by radiation friction are considered. Methods applied to describe nonlinear quantum-electrodynamic processes, including higher-order effects, are described in detail. Some theoretical results and concepts are criticized, including the predicted influence of strong laser fields on decays of nuclei and elementary particles and the concept of Unruh radiation.

Keywords: ultra-intense laser fields, nonlinear quantum electrodynamics, electromagnetic wave radiation, quantum processes, radiation friction, decays of nuclei and elementary particles

S V Popruzhenko (1,*), **A M Fedotov** (2,†)
(1) Prokhorov General Physics Institute, Russian Academy of Sciences, ul. Vavilova 38, 119991 Moscow, Russian Federation
(2) National Research Nuclear University MEPhI (Moscow Engineering Physics Institute), Kashirskoe shosse 31, 115409 Moscow, Russian Federation
E-mail: (*) sergey.popruzhenko@gmail.com, (†) AMFedotov@MEPhI.ru

Received 28 August 2021, revised 13 March 2023
Uspekhi Fizicheskikh Nauk **193** (5) 491 – 527 (2023)
Translated by M Zh Shmatikov

Dedicated to the memory of Nikolai Borisovich Narozhny and Vladimir Stepanovich Popov, with whom the authors were fortunate to work for many years

1. Introduction

This review presents the current state of research on the physics of the interaction of electromagnetic fields of ultrahigh intensities with charged particles. In recent decades, the terms ‘ultra intense laser field’ and ‘extreme light physics’ [1] have become commonly used. The criterion for which fields should be called extremely strong naturally depends on the processes under consideration. Therefore, we begin by explaining what this term means in this review. First, we discuss pulses of electromagnetic radiation with an intensity at the limit of the capabilities of super-powerful laser facilities, both those currently operating and those that are expected to be commissioned in the foreseeable future. This range spans intensities from 10^{21} W cm^{-2} to 10^{24} W cm^{-2}. Second, we discuss electromagnetic fields with an intensity of $\simeq 10^{24} - 10^{25}$ W cm^{-2} and higher, the availability of which will make it possible to study new nonlinear effects of the interaction of radiation with matter and, in the future, with a vacuum. It is not yet clear how soon intensities exceeding 10^{24} W cm^{-2} will become available in laser laboratories, but the success of recent years in the development and creation of super-powerful laser systems allows us to expect that this milestone will be reached in the foreseeable future.

Theoretical studies that laid the foundation for the physics of superstrong laser fields were already published in the first half of the 1960s [2–5], several years after lasers were invented. Experimental schemes aimed at observing the effects of nonlinear quantum electrodynamics (QED) in strong external fields have been proposed and discussed since the late 1960s [6, 7]. A detailed review of the theoretical results with a focus on their possible application to experiments on the nonlinear scattering of laser radiation by fast electrons is given in [8]. However, due to the lack of technologies for producing sufficiently powerful laser sources, until the mid-1990s, the physics of extreme light fields mainly remained an area of theoretical research.

The widespread use of petawatt laser systems [9, 10] in experiments on relativistic nonlinear optics and plasma physics, which began in the mid-1990s, brought abundant experimental results and stimulated new theoretical research. Articles [11, 12] contain a general overview of the state of the art in this field of research and the results obtained at that time. More specialized reviews have discussed in more detail radiation friction [13, 14], acceleration of ions by superstrong laser fields [14–16], collective effects due to photon–photon scattering [17], and nonlinear QED effects [18–22].

Quite a lot of time has passed since the publication of the listed studies, during which, first, several new laser facilities have been completed, which made it possible to raise the peak intensity level by at least an order of magnitude, and second, a large number of theoretical studies devoted to the analysis of new modes of interaction and physical effects in the fields of extreme intensity have been published. Our estimates show that at present at least 100 papers are published annually in renowned physical journals, which are devoted to the production of ultra-intense laser fields, their use in experiments, and the development of the theory of processes occurring in superstrong light fields. Such an abundance of new material requires regular systematization. Therefore, a review of recent achievements in the physics of extreme light fields is, in our opinion, an urgent task.

In selecting the material, we could not but take into account that the physics of extreme light fields is now a field of research that is already too wide to fit an overview of all its current trends in a single publication. Such an attempt would inevitably reduce the review to listing numerous results, while for deep insight into the subject it is sometimes more useful to analyze a few issues in detail than to become superficially acquainted with many topics. Therefore, in our opinion, it would be more relevant to discuss in detail several important problems that are currently attracting the attention of researchers in this field. The range of issues under consideration is primarily limited by QED effects, which could be observed at intensities that are achievable in the foreseeable future. Therefore, the discussion is focused of the effects of the interaction of individual charged particles with laser pulses, while interactions with plasma are only considered briefly, mainly in the context of the problem of radiation friction. It is in no way claimed that the list of problems within the designated topic is complete and, of course, the list is influenced by the scientific preferences of the authors. It includes the following items: options available currently for obtaining ultrahigh-intensity laser beams and prospects for the next decade, and methods for diagnosing extreme light fields (Section 2); effects of radiation friction, which manifest themselves in the interaction of superstrong electromagnetic fields with charged particles (Section 3); elementary QED processes in strong external fields and radiation friction in the quantum regime (Section 4); higher-order processes in an external field, including self-sustaining cascades, radiative corrections, and the hypothesis of their amplification in an intense field (Section 5). In addition, we considered it useful to critically analyze some of the erroneous concepts that have gained popularity in the area of physics under consideration. These issues include a discussion about the possibility of increasing the rate of radioactive decays of nuclei and elementary particles in a strong laser field (Section 6) and the Unruh radiation concept (Section 7).

With such a limited selection of topics, many of the most important questions remain outside the scope of this review. In particular, many recent papers are devoted to the production of electron–positron pairs in various schemes of interaction of laser radiation with targets and laser acceleration of charged particles, the generation of secondary radiation by laser plasma, and the effects of radiation friction in the quantum regime. To get acquainted with these issues, the reader is referred to the aforementioned reviews [14–22] and recently published review papers [23–29].

2. Record high intensities of electromagnetic radiation

2.1 Role of field intensity

In superstrong fields, electrodynamic processes usually proceed in a non-linear mode; in particular, the probabilities of these processes are nonlinear functions of the field strength. While, at a sufficiently high radiation intensity, the manifestation of certain effects is also determined by other characteristics of laser radiation, including the pulse duration, its energy, spatial distribution, and field polarization, at an intensity below a certain threshold, the probabilities of these effects become vanishing, in principle excluding the possibility of their observation. This circumstance distinguishes the intensity from other characteristics of laser radiation.

The intensity, which is usually defined as the absolute value of the Poynting vector, is not a relativistically invariant quantity; therefore, the probabilities of the processes are not directly determined by its value, but are expressed through invariant parameters. In addition to two invariants [30],

$$\mathcal{F} = \mathbf{E}^2 - \mathbf{H}^2\,, \qquad \mathcal{G} = \mathbf{E}\mathbf{H}\,, \tag{1}$$

determined by the strengths of the electric $\mathbf{E}$ and magnetic $\mathbf{H}$ fields, two more dimensionless invariant quantities play an important role in classical and quantum electrodynamics:

$$a_0 = \frac{eE_0}{mc\omega}\,, \tag{2}$$

$$\chi = \frac{e\hbar}{m^3c^4}\sqrt{-(F_{\mu\nu}p^{\nu})^2}\,, \tag{3}$$

which are known as the relativistic and quantum parameters, respectively. The invariants a_0 and χ were introduced in [3], and their meaning was discussed in detail in [31]. Here, e and m are the absolute value of the charge and mass of the particle, p^{μ} is its momentum 4-vector, c is the speed of light, $F_{\mu\nu}$ is the electromagnetic field tensor, ω is the electromagnetic wave frequency, and E_0 is the characteristic value of the field strength. In this review, we define the last quantity as

$E_0 = \langle \mathbf{E}^2 \rangle^{1/2}$, where angle brackets denote time averaging. The amplitude value E_{m} of the electric or magnetic field is also often used as E_0. Parameter (2) is equal to the ratio of the characteristic momentum of a charged particle oscillating under the action of a wave to mc, while (3) is the ratio of the electric field of the wave in the rest frame of the particle to the critical field of QED [32–34],

$$E_{\mathrm{cr}} = \frac{m^2 c^3}{e\hbar} \,. \tag{4}$$

For an electron, $E_{\mathrm{cr}} = 1.32 \times 10^{16}$ W cm^{-1}. Conditions $a_0 \gtrsim 1$ and $\chi \gtrsim 1$ define the regions of the relativistic (also known in the literature as multiphoton or field-nonperturbative) and quantum interaction regimes, respectively. Although the intensity does not uniquely determine the values of (2) and (3), it is clear that the most direct way to increase the parameters a_0 and χ is to use laser pulses with the highest possible intensity. Since the most powerful laser sources operate at wavelengths[1] $\lambda \simeq 1$ μm, the frequency ω in (2) cannot be below the limit $\simeq 10^{15}$ s^{-1}. The energies and momenta of particles can vary over a wide range, and nonlinear QED effects in some cases can be experimentally observed by increasing the electron beam energy, rather than the laser field strength. Examples include the well-known experiment E-144 on observing the Breit–Wheeler effect at the SLAC (Stanford Linear Accelerator Center) facility [8, 37, 38] and recent studies of nonlinear Thomson scattering of intense laser radiation by ultrarelativistic electron beams [39, 40]. However, in many cases, the energies of charged particles in the experiment are not given external parameters, but are determined by the nature of the processes of scattering and radiation in the plasma arising from the interaction of a powerful laser beam with a target.[2] Thus, it is the intensity of laser fields that is the characteristic parameter, the possible increase of which determines the prospects for research in this area of physics to the greatest extent.

Recall that, in a plane-wave field, the intensity $\mathcal{I}$ is connected to the amplitude value E_{m} of the electric field and the ellipticity δ by the relation

$$\mathcal{I} = \frac{c}{8\pi}\, E_{\mathrm{m}}^2 (1 + \delta^2) \,, \tag{5}$$

where $\delta = 0$ for linear polarization and $\delta = \pm 1$ for circular polarization. In tightly focused beams, the field of which can differ greatly from that of a plane wave, the relationship between $\mathcal{I}$ and E_0 or another quantity, including invariants (1)–(3), is not universal and is determined by the distribution of fields $\mathbf{E}$ and $\mathbf{H}$ in the focal area. In some cases, for example, in the problem of the production of electron–positron pairs from a vacuum, an arbitrarily high intensity does not yet indicate the possibility of observing the effect, the probability of which is determined by the values of invariants (1) equal to zero in the plane wave field. Here, dependence $\mathcal{F}(\mathcal{I})$, determined by the nature of focusing, plays a fundamental role. An analysis of such a dependence via the example of exact solutions of Maxwell's equations for tightly focused beams is presented in [42, 43].

[1] Record high intensities of electromagnetic radiation can also be attained using X-ray lasers with a photon energy of $\simeq 1$ keV [35, 36]; however, in such fields, due to the small wavelength, the relativistic regime of interaction, $a_0 \gg 1$, is not achieved.

[2] Such a scheme is referred to in publications as an all-optical setup [41].

2.2 Multipetawatt laser facilities

The history of the increase in the maximum intensity of laser radiation from 1960 to the present is shown in Fig. 1. Also plotted are the intensity values that are expected to be achieved in the nearest future (see also Fig. 1 in review [44] and Fig. 2 in review [28]). A sharp increase in peak intensity began in the mid-1980s due to the introduction of Chirped Pulse Amplification (CPA) technology [45] and its modification using Optical Parametric CPA (OPCPA) [46]. The operating principle of CPA is based on the stretching of a laser pulse in time by several orders of magnitude, its repeated amplification to the maximum power determined by the destruction threshold of the active medium of the laser system, and subsequent compression to the initial duration of the femtosecond time scale. The development of CPA technology, which enabled an increase in the laser radiation intensity by about eight orders of magnitude, was awarded the Nobel Prize in Physics for 2018. The second plateau, at the level of $\approx 10^{21}$ W cm^{-2}, is a manifestation of the saturation of the maximum power of laser radiation P_{L}, which was reached at the end of the 20th century [47] and remained virtually unchanged until the beginning of the 2020s.

To increase the peak power beyond $\simeq 1$ PW, it is necessary to further increase the transverse dimensions of the amplifying and optical elements of laser systems, which requires resolving significant technological problems. As a result, the transition from power $\simeq 1$ PW to $\simeq 10$ PW lasted for decades. By the time of writing this review, several 10-petawatt-class installations had been built, including the Extreme Light Infrastructure (ELI) in Hungary, Romania, and the Czech Republic [50, 51], Apollon in France [52], the Superintense Laser Facility (SULF) [53–56] in China, and the facility operated at the Advanced Photonics Research Institute (APRI) and the Center for Relativistic Laser Science (CoReLS) in South Korea [57]. Installations designed to achieve a 100–200 petawatt power level are still at the design stage [58–60].

Using the known laser radiation power $P_{\mathrm{L}} \simeq W_{\mathrm{L}}/\tau_{\mathrm{L}}$, where W_{L} and τ_{L} are the pulse energy and duration,

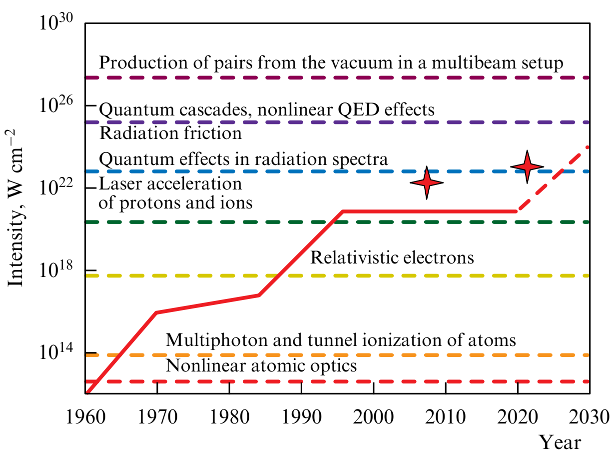

Figure 1. Maximum intensity of laser radiation in various years (solid broken line) and the expected progress in this quantity in the coming years (dashed segment of the broken line). Stars mark record values, the achievement of which was reported in [48, 49]. These reports have not yet been confirmed by the observation of physical effects characteristic of the declared intensity values. Horizontal straight lines show approximate thresholds for observing large groups of nonlinear electrodynamic effects or interaction regimes.

respectively, we can estimate the maximum intensity at the focus as

$$\mathcal{I}_{\max} \simeq \kappa \frac{P_{\mathrm{L}}}{\lambda^2} . \tag{6}$$

The coefficient κ depends on the ratio between the beam convergence angle and the diffraction angle [44]. For short focus mirrors used in obtaining tightly focused beams, the minimum value of $\kappa \approx 0.5$ and estimate (6) for $\lambda = 1$ μm and $P_{\mathrm{L}} = 1$ PW gives $\mathcal{I}_{\max} \approx 5 \times 10^{22}$ W cm^{-2}. Under the same conditions, a laser pulse with a power of 200 PW [58] would make it possible to achieve a peak intensity of about 10^{25} W cm^{-2}.

The maximum intensity values achieved under laboratory conditions may be lower than those predicted by Eqn (6). Petawatt lasers seem to provide stable radiation power on a target of 300–400 TW and an intensity of about 5×10^{21} W cm^{-2}. In some cases, it is possible to achieve an intensity of $\simeq 10^{22}$ W cm^{-2} [48, 61–63] or higher with petawatt and even subpetawatt lasers. Finally, in a recent paper [49], it was announced that an intensity of $\approx 10^{23}$ W cm^{-2} was achieved at a 4-PW CoReLS laser facility. Although it is desirable to confirm this result by direct measurement of the intensity at the focus (for methods of measuring ultrahigh intensities, see Section 2.3), there is no reason to doubt that experiments with laser beams with an intensity of $\simeq 10^{22} - 10^{23}$ W cm^{-2} will become routine.

2.3 Methods for direct measurement of extreme intensities

The distributions of the electromagnetic field in a beam, including intensity and phase, are easily measured by optical methods at a reduced laser power. The results of such measurements can then be extrapolated to the region of high powers, assuming that the passage of the beam through the optical systems of the laser weakly depend on the power. It is in this way that the estimates of record intensities were obtained in [48, 49]. An alternative approach to estimating high intensity values is based on the observation in the focal region of physical effects that feature high sensitivity to the magnitude of the electromagnetic field. In connection with the expected transition to intensities of $10^{22} - 10^{24}$ W cm^{-2}, the selection of the effects that could be used for such measurements has been actively discussed in recent years. Several methods for calibrating ultrahigh intensities have been proposed. The following is required:

(1) use of low-density targets, otherwise the plasma fields emerging in the interaction will significantly affect the processes under study, and the total field of the laser wave and the plasma system rather than the laser beam field would be measured;

(2) use of preferably local effects, the probabilities of which are determined by the instantaneous value of the electromagnetic field at the point of interest in space;

(3) availability of a highly nonlinear mode of interaction, in which the cross sections of the processes depend sharply on the intensity, which would allow, taking into account conditions 1 and 2, a sufficiently accurate measurement to be carried out.

Several processes satisfy these requirements to some extent: nonlinear Thomson scattering [64–66]; electron scattering [66, 67]; scattering of ions, including protons [68]; and tunneling ionization of atoms [69–74]. Below, we briefly comment on each of them.

Nonlinear Thomson scattering. Since at the considered intensities and wavelengths the relativistic parameter (2) $a_0 \gg 1$, the motion of the electron becomes essentially nonlinear, and the emission spectrum contains a significant number of harmonics of the fundamental frequency. In the classical limit $\chi \ll 1$, such a harmonic emission process is known as nonlinear Thomson scattering (NTS) [75]. Where an electron moves in the field of a monochromatic plane wave, the spectral and angular distributions of radiation were studied in detail, for example, in [75], and for the more general case of nonlinear Compton scattering (NCS), when the recoil of emitted photons plays a significant role, in [4, 76]. The theory of NCS is discussed in detail in Section 3.2. In both cases, the shape of the angular distributions and emission spectra depends substantially on a_0, which in principle enables an estimation of the intensity. In addition, in short pulses, the shape of the distributions also depends on the duration and type of time envelope, which potentially makes it possible to extract data on these characteristics of laser radiation as well.

Study [64] proposes to measure the intensity value using the cutoff value of the angular distribution of the radiation of an ultrarelativistic electron undergoing a head-on collision with a laser pulse. The theoretical analysis presented in [64] shows that an intensity of $\simeq 4 \times 10^{22}$ W cm^{-2} can be determined with a 10% accuracy if an electron beam with an energy spread of $\approx 5\%$ is used and the position of the cutoff angle is measured with an accuracy of $\approx 10\%$. In Ref. [66], it is proposed to concurrently study the emission of an electron beam and its scattering by a laser pulse, also in the setup with a head-on collision. In this case, a high accuracy in determining the intensity can be achieved if the conditions $\gamma \gg a_0$ and $b \ll w_0$ are fulfilled, where γ is the relativistic gamma factor of electrons, b is the electron beam width, and w_0 is the laser beam width. It is shown that, in this case, the concurrent measurement of the width of the angular distribution of radiation and the average electron energy before and after the collision makes it possible to determine the value of a_0 with an accuracy of about 10%. Thus, both approaches can provide a high measurement accuracy, but they are difficult to implement in practice, since they require the use of an external relativistic electron beam with a high quality of control over its parameters.

Schemes that are more convenient for experimental implementation are based on the use of electron radiation generated due to the action of the laser beam under study on the target. In experiment [65], the maximum value of the laser beam intensity was measured using the shift of the second harmonic of the fundamental frequency emerging due to the ponderomotive effect, which can also be interpreted as the appearance of an effective mass for an electron oscillating in a light field [75, 77]. The NTS process was observed with electrons that appear during the ionization of molecular nitrogen at a low ($\approx 10^{-3}$ atm) pressure, which excludes the influence of collisions and collective plasma effects. The intensity value of $\approx 10^{18}$ W cm^{-2} found in this way turned out to be in good agreement with the results of measurements of the distribution of the laser radiation energy in the focal spot at a reduced beam power. The main inaccuracy of such a measurement technique is due to the frequency shift of the emitted harmonics being dependent not only on the intensity but also on the initial conditions of the electron motion determined by the moment of ionization. In the experiment under discussion, single tunneling ionization of nitrogen molecules occurred at the leading edge of the laser pulse, which made it possible to consider the electron to be at rest before the onset of interaction. At higher intensities, ionization of the inner shells of atoms will occur, as a result of which electrons will be ejected into the continuum almost constantly during the action of the laser pulse. This will lead to the disappearance of a one-to-one relationship between the value of a_0 and the frequency of the harmonic; under such conditions, the latter will be significantly broadened. Additional factors that broaden the spectrum of harmonics and deteriorate the measurement accuracy are the small size of the focal spot and the laser pulse duration. Thus, the scheme based on observation of the Thomson scattering spectrum becomes less reliable with increasing intensity. However, it should be noted that, at $\mathcal{I} > 10^{25}$ W cm^{-2}, the NTS of light on protons will be observed, which can be used for the same purposes [65].

Scattering of electrons and ions on laser beams. The options for determining the peak intensity of a laser beam based on the scattering of electrons and protons by that beam have been theoretically analyzed in many studies, including recent ones [67, 68, 78, 79]. The momentum distributions of electrons or protons that interact with a laser beam contain detailed information about the distribution of electromagnetic fields in the beam, but its extraction requires solving an inverse problem, which in most cases is extremely difficult, if not impossible. To simplify such calculations, certain assumptions about the field distribution at the focus are usually required [67]. Similar to the case of Thomson scattering, experimental implementation can be simplified if an external beam is not involved, the parameters of which must be precisely controlled, and the momentum distributions of charged particles formed inside the focus due to ionization are measured. Such a diagnostic method based on measuring the momentum distributions of protons that emerge in the process of hydrogen ionization by an intense laser beam was theoretically analyzed in [68]. It was shown that at intensities $\mathcal{I} \leqslant 10^{24}$ W cm^{-2}, for which protons remain nonrelativistic, the energy spectrum cutoff is determined by the peak value of the intensity. The cutoff position of the spectrum of heavy ions formed in the process of multiple tunneling ionization can be used for the same purpose [79].

Tunnel ionization of heavy atoms. Tunneling ionization of atoms and ions is the most 'local' method for determining the intensity, since the detachment of an electron from an atom occurs in a spatial region comparable in scale to the atomic size, in a time much shorter than the oscillation period of the electromagnetic wave of the laser pulse. The ionization probability highly depends on the strength of the electromagnetic wave field and — in the tunneling mode, which is realized for the parameters under consideration by a large margin — is primarily determined by the tunneling exponential [80–82]:

$$w(t) \sim \exp\left(-\frac{2E_{\text{ch}}}{3E(\mathbf{r}, t)}\right), \tag{7}$$

where $E(\mathbf{r}, t)$ is the absolute value of the electric field of the wave at the moment of ionization t at the location of the ion, $E_{\text{ch}} = E_{\text{at}}(I_{\text{p}}/I_{\text{H}})^{3/2}$ is the characteristic field for the bound state with the ionization potential I_{p}, $E_{\text{at}} = 5.14 \times 10^9$ V cm^{-1} is the atomic field, and $I_{\text{H}} = 13.6$ eV is the ionization potential of the ground state of the hydrogen atom. In the region of extreme laser fields of interest to us, due to the strong nonlinearity of probability (7), the degree of ionization of a multielectron atom turns out to be very sensitive to the peak value of the intensity; this enables development of a measurement method based on the observation of multiply charged ions arising upon ionization of low-density gas jets. The method was experimentally tested for intensities $\mathcal{I} \simeq 10^{19}$ W cm^{-2} in [69, 70]. In [71], the observation of multiply charged ions arising from the ionization of neon and krypton atoms at the Sandia Z petawatt laser facility also demonstrated the possibility of determining the intensity by this method.

The strong dependence of the tunneling probability on the applied field amplitude in Eqn (7) results in the population of the level in an atom or ion characterized by certain values of the ionization potential I_{p}, the charge of the atomic residue Z (for neutral atoms $Z = 1$; the charge is included in the probability through the value of the effective principal quantum number $\nu = Z\sqrt{I_{\text{H}}/I_{\text{p}}}$), and orbital l and magnetic m quantum numbers, which behaves almost like a step function of the laser field strength $E(t)$ (see, for example, Fig. 3 in [72]). Due to this, a simple criterion for the complete ionization of a level with potential I_{p} can be formulated [72]:

$$\begin{gathered} E_{\text{m}} > E_{\text{ion}} = 0.05(2I_{\text{p}})^{3/2}, \\ \mathcal{I} > \mathcal{I}_{\text{ion}} = 8.79 \times 10^{-7}\left(\frac{I_{\text{p}}}{I_{\text{H}}}\right)^3 \; [10^{20} \text{ W cm}^{-2}]. \end{gathered} \tag{8}$$

According to the evaluation formula (8), at an intensity $\mathcal{I} = 10^{20}$ W cm^{-2}, electrons will be removed from all levels with $I_{\text{p}} < 1.4$ keV, which corresponds to the complete ionization of neon ($I_{\text{p}}(\text{Ne}^{9+}) = 1362$ eV), and, at an intensity $\mathcal{I} = 2 \times 10^{24}$ W cm^{-2}, full ionization of xenon should be expected. Even at such high intensities, nonrelativistic formulas are adequate for calculating the ionization probabilities [72, 83]. Figure 2 shows the function $I_{\text{p}}(\mathcal{I})$ (i.e., the dependence inverse to Eqn (8)) with the values of the ionization potentials of some ions plotted on the vertical axis. This qualitative dependence makes it possible to choose

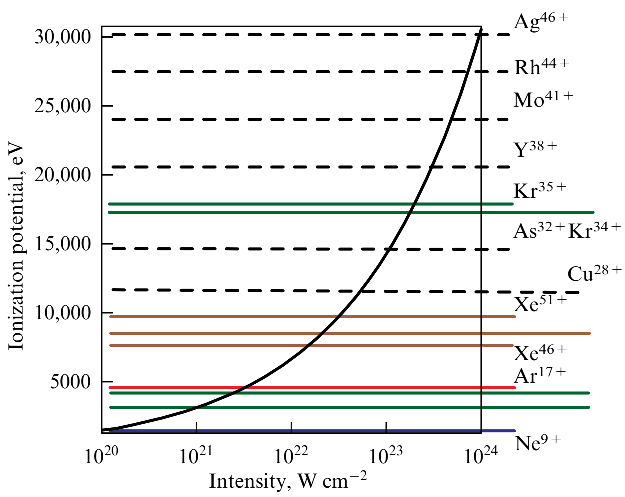

Figure 2. Dependence (8) of the maximum value of the ionization potential, at which a fast detachment of an electron still occurs, as a function of laser radiation intensity. Vertical axis shows the ionization potentials of some multiply charged noble gas and metal ions. Observation of these ions in the laser focus will allow localizing the peak value of the intensity in the chosen interval. (From [72].)

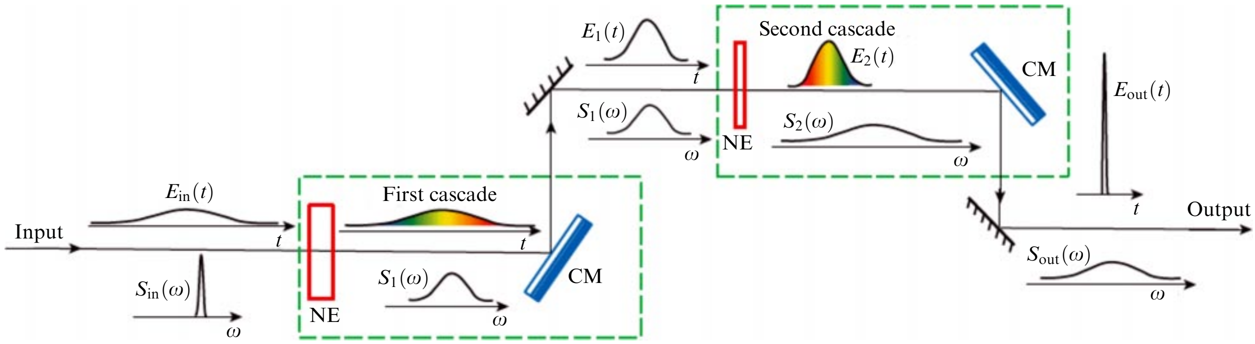

Figure 3. Schematic diagram of the CafCA method implemented in [89]. Laser pulse $E_{in}(t)$ with a total energy of 17 J, a central wavelength of 910 nm, and a duration of 54 to 74 fs, obtained using the PEARL setup, was transmitted through a nonlinear element (NE) (quartz plate), which led to spectrum broadening $S(\omega)$ and phase modulation $\varphi(\omega)$ with respect to their original values $S_{in}(\omega)$ and $\varphi_{in}(\omega)$. Reflection of a pulse from two chirped mirrors (CMs) changes the function $\varphi(\omega)$, so the pulse duration tends to the limit, decreasing to 11 fs. (From [89].)

an atom whose ionization could be used to calibrate the laser radiation intensity in a given range.

The ionization measurement method features, in addition to sensitivity to the local value of the electromagnetic field, another significant advantage: the quantitative theory of tunnel ionization is well developed and is described by simple and fairly accurate analytical formulas for the ionization rate of atomic levels [80, 84, 85]. Studies [72–74] analyze in detail various factors that can affect the possibility of measuring the intensity by this method. It is shown that the deviation from the tunnel ionization regime towards the above-barrier regime and the averaging of the ion signal over the laser focus introduce significant uncertainties into the accuracy of extracting the peak intensity value; nevertheless, a measurement accuracy of 30–50% can be expected.

2.4 Options for further increasing peak intensity values

There is no reason to doubt that intensities of several units of 10^{23} W cm^{-2} will be achieved with new 10-petawatt power-level facilities, and that the *in situ* measurement methods described above will enable their reliable calibration. However, a further increase in the peak intensity of laser radiation is of undoubted interest, since most of the unexplored nonlinear effects of classical and quantum electrodynamics are located in the region of $\mathcal{I} > 10^{24}$ W cm^{-2} (see Fig. 1). The most direct way is to increase the power to a level of 100 PW or more. Existing projects of sub-exawatt laser systems are currently under development [58–60], and the scope of engineering and technical solutions that will be required to reach such a power level is not yet completely clear. Alternative ways to increase the intensity, which make it possible to stay within the already achieved powers of 1–10 PW, consist in the use of multibeam technology, optimization of the intensity distribution at the focus using adaptive optics, and a further decrease in the laser pulse duration.

The technically challenging but nevertheless feasible [86–88] splitting of a laser beam into several beams in the case of reliable control of the relative phase, which provides constructive interference during beam addition, will make it possible to obtain a spatial distribution of the field with intensity values and other important parameters locally higher than in the initial beam. An example of such a parameter is the invariant $\mathcal{F}$, which determines the probability of the production of electron–positron pairs. It was shown in [43] that the use of a multibeam scheme can lead to a decrease in the threshold for the production of electron–positron pairs from a vacuum by almost two orders of magnitude. Successful examples of correcting the laser beam wavefront, which makes it possible to significantly improve the pattern of the intensity distribution at the focus, are presented in a recent paper [49]. Finally, a further decrease in the duration of an already amplified laser pulse can provide a severalfold increase in the peak intensity

In [44, 89–91], a laser pulse recompression method called CafCA (Compression after Compression Approach) was developed and implemented on the basis of the PEARL (PEtawatt pARametric Laser) facility operated by the Institute of Applied Physics of the Russian Academy of Sciences. An approach involving nonlinear compression of laser pulses, shown in Fig. 3 (see also [91, Fig. 1]), was proposed as early as the 1960s [92, 93]. It consists in the broadening of the spectrum of a laser pulse when it passes through a nonlinear optical element. As a result, the laser pulse, the duration of which after the CPA process is close to the limiting one, $\tau_{min} \simeq 1/\Delta\omega$, where $\Delta\omega$ is the spectrum width, can be additionally compressed several more times with virtually no loss of energy. This method of reducing the pulse duration and correspondingly increasing its peak intensity can now be applied regardless of the laser power, which makes it a suitable tool for further enhancing the laser radiation intensity without increasing the pulse energy. The efficiency of the CafCA method was demonstrated in [89, 91] using the example of compression of a laser pulse with an initial duration of 60–70 fs to 11 fs at the PEARL facility. The peak radiation power increased to 1.5 PW. Taking into account the applicability of the method to a wide range of high-power laser systems, it can be expected that, with its use, laser sources with a seed power of $\simeq 10$ PW and a pulse duration of $\simeq 50$ fs will reach intensities $\mathcal{I} > 10^{24}$ W cm^{-2}. A detailed description of the CafCA method, including the history of its development and examples of its application in high-power lasers, is presented in review [44] and publications [89–91].

Although to date the highest intensities have been achieved using infrared lasers, powerful sources of coherent short-wave radiation are being considered as an alternative to these sources. The main advantage of using ultraviolet and X-ray radiation to achieve extreme intensities is related to focusing the beam in a much smaller volume of $\sim \lambda^3$, which significantly reduces the requirements for the total energy per pulse. State-of-the-art free-electron lasers make it possible to achieve intensities of at least 10^{20} W cm^{-2} [94]. Possible schemes for the conversion of high-power laser pulses into short-wavelength ones and their tight focusing are also discussed. In particular, the idea of a relativistic plasma mirror [95, 96] was realized in experiments [97, 98]. Simulation of the reflection of a high-power laser pulse from a concave plasma surface [99] also demonstrated that tight focusing of high harmonics generated upon reflection is possible, and extreme intensity values can be attained in such a scheme.

3. Radiative friction in the classical regime

The force of radiation friction, which arises due to the momentum transfer from a system of charged particles to the radiation emitted by these particles, has been studied in detail in classical physics. The fundamental problem of introducing the classical force of radiation friction as a self-action of a radiating charge is removed, as is known, by a perturbative interpretation of the Abraham–Lorentz–Dirac equation [100, 101], which leads to an expression for this force in the Landau and Lifshitz form [30]. The fundamentals of the theory of radiation friction in classical electrodynamics, with a discussion of problems in which it plays a significant role, are contained in popular books [30, 102, 103] and in original papers, references to which can be found in reviews [11, 12, 24]. In these papers and in review [104], several exactly solvable problems of electrodynamics are discussed, which turned out to be useful in constructing various models that describe the effects of radiation friction and in analyzing basic theoretical issues, such as the effective difference between different forms of recording the radiation friction force. Since a recent review [24] devoted to the problem of radiation friction in classical and quantum physics provides a detailed description of the current state of the art of the theory, numerical simulation, and experiment, in this paper we only discuss the threshold for 'switching on' radiation friction with an increase in intensity and the possibility of observing collective effects generated by radiation friction in a laser plasma.

3.1 Transition to the regime of radiation friction dominance

It is known from classical electrodynamics [30, 102, 103] that, with the exception of some special cases, such as *longitudinal* motion in a uniform electric or crossed field, for ultrarelativistic particles with $\gamma \gg 1$, the classical force of radiation friction $\mathbf{F}_{\rm rad}$ increases quadratically with increasing particle energy $\mathcal{E}$ and field strength E:

$$\mathbf{F}_{\rm rad} \sim -\mathcal{E}^2 E^2 \mathbf{n}_{\rm v} \,. \tag{9}$$

Here, E sets the order of magnitude of not only the electric but also the magnetic field and $\mathbf{n}_{\rm v}$ is a unit vector directed along the particle velocity. This dependence follows from the formula for the force of radiation friction $\mathbf{F}_{\rm rad} = -P\mathbf{n}_{\rm v}/c$, valid under the condition $\gamma \gg 1$, where P is the radiation power,

$$P = -\frac{2}{3}\, e^2 c \,\frac{{\rm d}u^\mu}{{\rm d}s}\,\frac{{\rm d}u_\mu}{{\rm d}s} \sim \alpha\chi^2 \,. \tag{10}$$

Here, u^μ is the 4-vector of velocity and s is the interval.

The Lorentz force $\mathbf{F}_{\rm L}$ is linear in the field. As a result, with an increase in the electromagnetic field strength and the energy of charged particles, a situation known as the *dominance of radiation friction* should be realized, i.e., such a mode of interaction in which the forces $F_{\rm L}$ and $F_{\rm rad}$ are at least comparable in magnitude, and possibly $F_{\rm L} \ll F_{\rm rad}$.

The regime in which radiation friction dominates has been studied in detail in the physics of cosmic rays and charged particle accelerators, i.e., in a situation where the condition $F_{\rm L} \ll F_{\rm rad}$ is satisfied due to the high kinetic energies of the radiating particles. In this case, the electromagnetic fields in the laboratory frame of reference can be quite weak. One of the well-known examples of this kind is the deceleration of electrons with super-high energies, $\mathcal{E} \simeq 10^{18}$ eV, in Earth's magnetic field with a strength of $\simeq 1$ G. Superstrong laser fields provide an alternative option to achieve a similar mode of interaction — by increasing the field strength. Since, in this case, charged particles, unless they are injected into the laser focus from the outside with a given high energy, have an energy of $\mathcal{E} \sim mc^2 a_0$, the force of radiation friction increases very rapidly with increasing laser wave intensity:

$$F_{\rm rad} \sim a_0^4 \,. \tag{11}$$

As discussed in Section 2.1, interaction regimes are determined by the values of invariant parameters, among which (2) and (3) play an important role. We now introduce another parameter responsible for 'switching on' the radiation friction. To determine it, it is convenient to consider radiation in the field of a circularly polarized electromagnetic wave and set the energy emitted by an electron over a period [75] equal to its kinetic energy. Such an estimate determines the following condition on the boundary that separates two modes of interaction — with weak and strong radiation friction:

$$\xi = \frac{P}{\omega\gamma mc^2} \,. \tag{12}$$

Substituting into Eqn (12) the formula for the radiation power and the gamma factor of an electron moving in the field of a wave (it can be done in the easiest way in a reference frame where the electron is at rest on average), we obtain

$$\xi = \frac{4\pi}{3}\,\frac{r_0}{\lambda}\, a_0^3 \,, \tag{13}$$

where $r_0 = 2.8 \times 10^{-13}$ cm is the classical radius of the electron, and the wavelength λ of laser radiation is measured in the special reference frame defined above. With this in mind, the parameter ξ is relativistically invariant. For $\lambda = 0.8$ μm, $\xi = 1$ at $a_0 \approx 400$, which corresponds to an intensity of $\mathcal{I} \approx 7 \times 10^{23}$ W cm^{-2}. Consequently, the characteristics of the multipetawatt laser facilities currently being put into operation are close to reaching the regime of dominance of radiation friction (see Fig. 1), not only for individual electrons or low-density beams but also for dense plasma formed upon the interaction of a laser pulse with solid targets.

With a further increase in the intensity of laser radiation, the quantum effects associated with recoil during the emission of photons by an electron are increasingly significant. The transition from the regime of non-linear Thomson scattering to the nonlinear Compton effect occurs when the quantum parameter χ (3) approaches unity. At $\chi \simeq 1$, the momentum lost by an electron in a single radiation event is large, so the concept of a classical trajectory loses its meaning, and, at the same time, the formulas for the force of radiation friction derived in classical electrodynamics become inapplicable. In this mode, the effects of radiation friction are primarily described by modeling sequential radiation events by the Monte Carlo method (see Sections 5.1 and 5.2). A detailed description of radiation friction in the quantum regime is beyond the scope of this review; a more detailed discussion of modern approaches and recent results in this area can be found in [24, 28, 29]. It should be noted that quantum effects begin to noticeably affect the radiation process and the magnitude of the radiation friction force as early as at $\chi \lesssim 1$. In this region, the quasiclassical description developed in [31, 105, 106] is well applicable. Moreover, the radiation power and the radiation friction force are described by classical formulas, in which the Gaunt suppression correction factor is introduced; the latter turns out to be significant already at $\chi \simeq 0.1$ [107–109].

3.2 Inverse Faraday effect induced by radiation friction

At $\xi \simeq 1$, trajectories of charged particles in the electromagnetic wave field begin to noticeably deviate from those calculated taking into account only the Lorentz force, and, at $\xi \gg 1$, these deviations qualitatively change the dynamics. The changes are especially well seen in examples of exactly solvable problems of the motion of an electron in a plane wave field [110] and of a homogeneous plasma in the field of a circularly polarized plane wave [104]. The corrections introduced by the force of radiation friction into the dynamics manifest themselves in various effects that arise during the interaction of intense laser radiation with plasma, including the acceleration of charged particles and the spectral and angular distributions of secondary radiation. However, their influence, in particular, on the acceleration of ions, has so far been studied rather fragmentarily — individual simulations carried out do not add up to a complete picture. For example, on the one hand, radiation friction has been shown to have little effect on the acceleration of ions in the light sail mode (thin and highly opaque target) [111–113]. This result seems natural, since in this regime the laser field penetrating into the target to the depth of the skin layer only affects a small part of the target electrons. On the other hand, it was noted that taking into account the radiation friction of electrons can significantly reduce the energy of ions accelerated in a thick opaque target [114]. Finally, radiation friction significantly affects the dynamics of laser plasma in thin optically transparent targets, in which the threshold of relativistically induced transparency, generally speaking, depends on the target thickness, laser pulse intensity [115], its duration [116], and other parameters. In particular, in the last case, radiation friction can lead to an increase in charge separation [117, 118] and the energy of accelerated ions [114, 119, 120].

Of particular interest are plasma phenomena that arise exclusively due to radiation friction. In the classical regime of interaction $\chi \ll 1$, effects of this type notably include the generation of short bursts of γ-radiation in the regime of dominance of radiation friction [121] (see also the references cited in reviews [12, 28]). Another effect of radiation friction, which was theoretically studied recently, is the excitation of a longitudinal quasi-static magnetic field upon reflection of an intense laser pulse from a plasma layer with a supercritical density $n > n_{\mathrm{cr}}$ [122]. Here, n_{cr} is the electron concentration above which a laser wave does not propagate in the plasma [11, 123]. For $n > n_{\mathrm{cr}}$, the laser wave penetrates into the plasma to the depth of the skin layer, which is sufficient to excite powerful electron currents and radiation in the near-surface plasma layer. At the high electron energies attained in a superstrong laser field, the effective frequency of binary collisions is low, and the collisional absorption of the laser radiation energy does not play a significant role, even at high plasma density $n \simeq 10^{21} - 10^{22}$ cm^{-3}. The collisionless approximation underlies many important models and exactly solvable problems in the physics of relativistic laser plasma [11]. Under such conditions, high-frequency radiation, whose properties are close to those of synchrotron radiation, becomes the main mechanism for the dissipation of laser pulse energy in addition to its conversion into the kinetic energy of the translational motion of accelerated electrons and ions. The dissipation coefficient η, which is conveniently defined as the ratio of the energy emitted at high frequencies to the initial energy of the laser pulse, increases with increasing intensity, at least until leaving the classical interaction regime, i.e., at $\chi \ll 1$ [124]. In terms of macroscopic electrodynamics, this implies that the imaginary part of the plasma permittivity, which decreases in magnitude with increasing intensity in the range of $10^{18} - 10^{21}$ W cm^{-2} due to suppression of collisions, again begins to grow with a further increase in $\mathcal{I}$, this time due to radiation friction [125]. As a result, the plasma formed if films or surfaces are irradiated with laser radiation with an intensity of more than 10^{22} W cm^{-2} becomes a dissipative medium in which a circularly polarized wave excites a longitudinal quasi-static magnetic field, a phenomenon known in the literature as the inverse Faraday effect [126–128]. Numerical calculations carried out using the Particle-In-Cell (PIC) method with the inclusion of the classical force of radiation friction in the equations of motion of quasiparticles [122, 124] predict the excitation of a longitudinal magnetic field with a strength of several GG during the interaction of a circularly polarized femtosecond laser pulse with an intensity of $10^{23} - 10^{24}$ W cm^{-2} with a plasma layer of supercritical density in a regime called hole boring, i.e., the formation of a channel in a dense supercritical plasma under the action of laser radiation [129–131].

The analytical model developed in [122, 132] is based on the law of conservation of angular momentum, and macroscopic equations relating the transfer of angular momentum $\Delta L_x \approx \pm \Delta N \hbar$ from the laser field to the plasma (here, ΔN is the number of absorbed laser-wave photons, and the sign depends on its polarization) make it possible to predict the dependence of the maximum value $B_{x\mathrm{m}}$ of the longitudinal magnetic field on the laser wave amplitude E_{m} and the dissipation coefficient η:

$$B_{x\mathrm{m}} \simeq C\eta E_{\mathrm{m}} \,, \quad E_{\mathrm{m}} \equiv a_0 B_0 \,, \quad B_0 = \frac{mc\omega}{e} = 0.134\ \mathrm{GG} \,. \tag{14}$$

Here, $C \approx 0.1 - 0.2$ is a numerical coefficient that primarily depends on the shape of the laser pulse. Estimates of the magnetic field amplitude $B_{x\mathrm{m}}$ and its intensity dependence, which can be made based on Eqn (14), qualitatively agree with the results of the numerical simulation performed by the PIC method, which are displayed in Fig. 4. Simulation shows that, at a laser pulse intensity of $\simeq 10^{24}$ W cm^{-2}, quasi-static magnetic fields with strengths of several GG can be obtained. At $\mathcal{I} \approx 10^{23}$ W cm^{-2}, the effect of the magnetic field is already noticeable in the results of numerical calculations, and its value of ≈ 0.2 GG is sufficient for measurement using standard methods of proton diagnostics.

With a further increase in intensity, the influence of the effects of radiation friction on the trajectories of electrons in

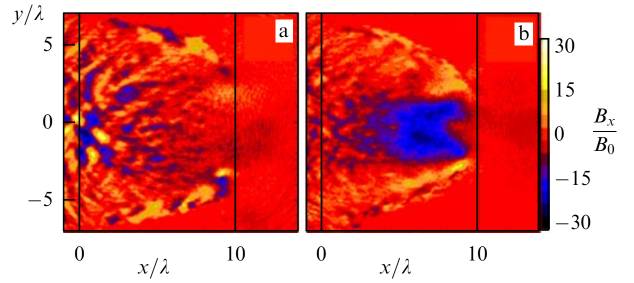

Figure 4. Distribution of component B_x of a magnetic field ≈ 30 fs after the reflection of a circularly polarized laser pulse from a helium plasma target with a concentration of 1.55×10^{23} cm^{-3}. Laser pulse propagates in the direction of the x-axis. Distribution of the magnetic field is symmetric in the yz plane. Color bar shows the ratio B_x/B_0 (14). Distributions correspond to two cases: the force of radiative friction (a) is excluded from the equations of motion, (b) it is present in the equations in the form derived by Landau and Lifshitz. Vertical lines indicate the initial position of the plasma boundary, whose thickness was chosen to be $10\lambda = 8$ μm. Laser pulse intensity $\mathcal{I} = 1.5 \times 10^{24}$ W cm^{-2}, duration $\tau = 10$ fs, transverse radius $r_0 = 3.1$ μm. (From [122].)

plasma and on quantum corrections to the emission spectra leads to a slowdown in the increase in the coefficient η and a kind of 'freezing' of the inverse Faraday effect at intensities of $10^{24}-10^{25}$ W cm^{-2} [124, 132].

4. Simplest quantum processes

Charged particles in an external field exchange energy and momentum with the field. The stronger the field the stronger this exchange. In the classical language, charged particles are simply accelerated and deflected by the field; in the quantum language, they are dressed by interaction with the field, which leads to a modification of the probabilities of all QED processes that involve charged particles [3, 4]. In particular, processes strictly forbidden by the law of conservation of energy–momentum in the absence of a field, generally speaking, become allowed and occur in the presence of a field. Virtual charged particles in the presence of a field may [133] or may not emerge on the mass shell, and the corresponding contributions to the total amplitude of the process interfere with each other. This, along with the modification of kinematics when particles are dressed by a field, leads to a complex nonmonotonic dependence of the probabilities of processes on the field strength and other parameters, so that, depending on them, some processes are enhanced in the presence of a field, while others are suppressed. Despite the availability of a general approach, only the simplest processes can be calculated analytically.

In Sections 4.1–4.4, we consider in more detail the simplest single-vertex processes of photon emission by an electron [3, 134–136] and single-photon production of an electron–positron pair in the field of an electromagnetic wave [2, 3, 136] and in a constant crossed field [3, 4], which allow a relatively simple analytical description.

4.1 Summation of interactions with an external field (Furry picture)

Recall that QED, which describes the interaction of the quantized electron–positron field[3] $\psi(x)$ and the electromagnetic field $A^\mu(x)$, is derived from the Lagrangian [76, 137]

$$\mathcal{L} = \mathcal{L}_{e^-e^+} + \mathcal{L}_\gamma + \mathcal{L}_{\rm int}\,, \tag{15}$$

where[4] $\mathcal{L}_{e^-e^+} = \bar\psi(i\gamma^\mu\partial_\mu - m)\psi$ is the Lagrangian of the free electron–positron field, $\mathcal{L}_\gamma = -(16\pi)^{-1}F_{\mu\nu}F^{\mu\nu}$ is the Lagrangian of the free electromagnetic field, $\mathcal{L}_{\rm int} = -J^\mu A_\mu$ is the interaction Lagrangian, and $J^\mu = J^\mu_{e^+e^-} = -e\bar\psi\gamma^\mu A_\mu\psi$ is the electron–positron current. In the interaction picture, the operators evolve with time as free ones, while the evolution of the Fock states is governed by the interaction. Namely, the initial Fock state $|\Psi_{\rm i}\rangle$ evolves to the final state $|\Psi_{\rm f}\rangle = S|\Psi_{\rm i}\rangle$, where S is the evolution operator (S-matrix) over the interaction time,

$$S = \sum_{n=0}^{\infty}\frac{(-i)^n}{n!}\int d^4x_1\ldots\int d^4x_n\,{\rm T}\big[\mathcal{L}_{\rm int}(x_1)\ldots\mathcal{L}_{\rm int}(x_n)\big]\,. \tag{16}$$

The probability amplitude of the process $|\Psi_{\rm i}\rangle \to |\Psi_{\rm f}\rangle$ is determined by the matrix element $S_{\rm i\to f} \equiv \langle\Psi_{\rm f}|S|\Psi_{\rm i}\rangle$; the square of its modulus determines the probability of the considered process $W_{\rm i\to f} = |S_{\rm i\to f}|^2$. In practice, due to the smallness of the coupling constant, the fine structure constant $\alpha = e^2 = 1/137.035999084(21)$ [138], calculations are carried out according to perturbation theory, truncating the series in Eqn (16) and disregarding higher-order corrections. Usually, QED considers processes that involve a small number of charged particles and photons. However, if in addition to them there are remote classical currents $J^{\rm (ext)}_\mu$ that create a classical field $A^{\rm (ext)}_\mu$, the total field has the form $A_\mu = A^{\rm (ext)}_\mu + A^{\rm (q)}_\mu$, where $A^{\rm (q)}_\mu$ is its quantized part. Then, abstracting from the emission of photons by distant sources, QED processes can be effectively described by the same Lagrangian (15), in which the interaction Lagrangian includes the contribution of both fields: $\mathcal{L}_{\rm int} = -J^\mu_{e^+e^-}(A^{\rm (ext)}_\mu + A^{\rm (q)}_\mu)$. Further, for brevity, we omit the superscript 'ext,' so A_μ denotes the classical part of the field (the external field). The introduced concept of an external field is exactly equivalent [139, 140] to the full quantum description of processes in which the electromagnetic field is initially in an arbitrary coherent state [141], or approximately equivalent to such a full description if an initial state contains a large number of photons in the states occupying a small phase volume, and only a small part of them is involved in the process under consideration [140, 142]. Precisely this situation is apparently realized in a real laser field.

The main method of calculation in problems with a strong external field is the diagram technique in the Furry picture [76, 143], which is equivalent to the exact summation of all interactions of charged particles with an external field A_μ.

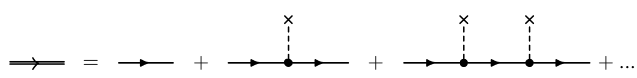

Figure 5. External line of an electron dressed with an external field.

[3] And other charged fields that are included in the theory in a similar way.

[4] Sections 4 and 5 use the same system of units as in [76], in particular, $\alpha = e^2/\hbar c$ and $\hbar = c = 1$. When compared with the results of early original and modern studies (in particular, [137]), one should have in mind that they usually use the Heaviside system of units, in which $\mathcal{L}_\gamma = -(1/4)F_{\mu\nu}F^{\mu\nu}$, the external lines of photons do not contain factors $\sqrt{4\pi}$, the photon propagator does not have the factor 4π, and $\alpha = e^2/(4\pi\hbar c)$. As a consequence, all results, expressed in terms of α, are the same.

Diagrams depicting the incoming external line of a dressed electron are shown in Fig. 5. Analytically, their sum is expressed as a series,

$$\Psi_p^{(A)} = \left\{ 1 + \frac{\mathrm{i}}{\not{\tilde{p}} - m} (-\mathrm{i}e\not{A}) + \frac{\mathrm{i}}{\not{\tilde{p}} - m} (-\mathrm{i}e\not{A}) \frac{\mathrm{i}}{\not{\tilde{p}} - m} (-\mathrm{i}e\not{A}) + \ldots \right\} \Psi_p^{(0)} , \quad (17)$$

where the factor $\Psi_p^{(0)} = C_p \exp(-\mathrm{i}px) u_p$ that satisfies the equation $(\not{\tilde{p}} - m)\Psi_p^{(0)} = 0$ corresponds to the external line of a free electron, $\mathrm{i}/(\not{\tilde{p}} - m)$ is its propagator, u_p is the bispinor that satisfies the equation $(\not{p} - m)u_p = 0$, C_p is the normalization constant, and $-\mathrm{i}e\not{A}$ is the vertex of interaction with the external field A_μ, according to the standard Feynman notation $\not{A} = \gamma^\mu A_\mu$ [137].

Assuming $\not{\tilde{p}} - m \sim m$, we reveal that the expansion parameter in Eqn (17) is the previously introduced dimensionless parameter (2). This fact can also be interpreted differently if we note that, in the presence of a background of photons from an external field, the interaction vertex (coupling constant) is effectively multiplied by the Bose factor [144]

$$\sqrt{\alpha} \mapsto \sqrt{\alpha}\sqrt{\bar{N}_\gamma^{\mathrm{ext}}} \simeq \frac{e}{\sqrt{\hbar c}} \sqrt{\left(\frac{\hbar}{mc}\right)^2 \frac{2\pi c}{\omega} \frac{E^2}{4\pi\hbar\omega}} \simeq \frac{eE}{m\omega c} \simeq a_0 ,$$

where the number $\bar{N}_\gamma^{\mathrm{ext}}$ of external-field photons that participate in the process is estimated as the product of their characteristic density $E^2/(4\pi\hbar\omega)$ and the volume of a tube of Compton thickness $\hbar/(mc)$ that surrounds the section of the electron trajectory with a length equal to the external field wavelength $\lambda = 2\pi c/\omega$. Thus, if $a_0 \gtrsim 1$, the interaction of an electron with an external field is nonperturbative, and interaction with it should be taken into account in all orders [31]. We note that, in the classical description, this regime corresponds to the relativistic transverse motion of an electron in an external field [30].

To implement such a summation, we represent (17) in the form of an equation,

$$\Psi_p^{(A)} = \Psi_p^{(0)} + \frac{\mathrm{i}}{\not{\tilde{p}} - m} (-\mathrm{i}e\not{A})\Psi_p^{(A)} , \quad (18)$$

which we multiply by the Dirac operator $\not{\tilde{p}} - m$. As a result, we arrive at the equation

$$(\not{\tilde{p}} - e\not{A} - m)\Psi_p^{(A)} = 0 , \quad (19)$$

called the Dirac equation in an external field [76] (or otherwise, in the Furry picture [143]). Equation (19) only allows an analytical solution in certain simplified cases, in particular, in a Coulomb field, in constant homogeneous fields, and in a plane-wave field [145].

The case of a plane wave describes a laser beam or a pulse in a vacuum without focusing and is therefore of particular interest. This field has the form

$$A_\mu = A_\mu(\varphi) , \quad \varphi = kx , \quad k^2 = kA = 0 , \quad (20)$$

i.e., it is transverse and only depends on the phase $\varphi = kx$, and the wave 4-vector k^μ is lightlike. The Dirac equation in a plane-wave field can be solved exactly in an analytical way due to the availability of a sufficient number of the quantities that are conserved in this field. Namely, conserved in the plane wave are $p_- = p_0 - p_\parallel$ and $\mathbf{p}_\perp$, where the components of electron momentum parallel and perpendicular to the wave propagation direction are separated [76, 145].

A solution of Eqn (19) in field (20), which is referred to as the Volkov solution, has the form [76, 146, 147]

$$\Psi_p^{(A)}(x) = C_p E_p(x) u_p , \quad E_p(x) = \exp\big(\mathrm{i}S_p(x)\big)\Sigma_p(\varphi) , \qquad \Sigma_p = 1 + \frac{e}{2kp} \not{k}\not{A} , \quad (21)$$

where

$$S_p = -px + \mathcal{S}_p(\varphi) , \qquad \mathcal{S}_p(\varphi) = -\frac{e}{kp}\int_{\varphi_0}^{\varphi} \left(pA(\varphi) - \frac{e}{2} A^2(\varphi) \right) \mathrm{d}\varphi , \quad (22)$$

the matrix $E_p(x)$ is called the Ritus E_p-function [148], $\Sigma_p(\varphi)$ is the spin factor (it can be easily seen that the spinor $\Sigma_p(\varphi)u_p$ precesses in the wave according to the Bargmann–Michel–Telegdi equation [149] with $g = 2$), S_p is the classical action, and $\mathcal{S}_p$ is its part that depends only on the phase $\varphi = kx$. Solutions (21) are labelled by quantum numbers p_- and $\mathbf{p}_\perp$. The explicitly semiclassical form of exact Volkov solution (21) corresponds to the motion in the wave field being semiclassical for any values of these quantum numbers.

The separation from the action of the part that depends only on the phase is not unique. For example, if the field is turned on and off (i.e., a pulse of finite duration is considered), setting $\varphi_0 = -\infty$, we see that the 4-vector p^μ (satisfying the mass-shell equation $p^2 = m^2$) in Eqn (22) has the meaning of the momentum of the electron before it enters the wave. If the bispinor u_p is normalized using the standard condition $\bar{u}_p u_p = 2m$, the normalization of solution (21) to one particle per unit volume before entering the field corresponds to the choice $C_p = 1/\sqrt{2p_0}$.

If the wave is periodic (for definiteness, 2π-periodic in phase φ), in particular, monochromatic, and bipolar (average $\langle A_\mu \rangle = 0$), it is more convenient to separate from the action the part that only depends on the phase in an alternative way:

$$S_p = -qx + \tilde{\mathcal{S}}_q(\varphi) , \quad (23)$$

where

$$q^\mu = p^\mu - \frac{e^2\langle A^2 \rangle}{2kp} k^\mu , \qquad \tilde{\mathcal{S}}_q(\varphi) = -\frac{e}{kq}\int_{\varphi_0}^{\varphi} \left[qA(\varphi) - \frac{e}{2}\big(A^2(\varphi) - \langle A^2 \rangle\big) \right] \mathrm{d}\varphi . \quad (24)$$

Since $\tilde{\mathcal{S}}_q(\varphi)$ is a periodic function, the 4-vector q^μ defined in such a way has the meaning of quasi-momentum:

$$\Psi_p^{(A)}(x + \Delta x) = \exp(-\mathrm{i}q\Delta x)\Psi_p^{(A)}(x) \quad \text{at } k\Delta x = \Delta\varphi = 2\pi \times \text{integer} , \quad (25)$$

and its square

$$q^2 = m^2 \left(1 - \frac{e^2}{m^2} \langle A^2 \rangle \right) = m^2(1 + a_0^2) = m_*^2 \quad (26)$$

determines the effective mass m_* of an electron in a wave [4, 134]. In the classical theory, the effective mass includes the average energy of transverse oscillations in the wave [77, 150],

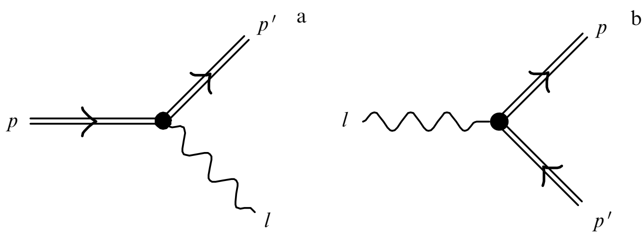

Figure 6. Feynman diagrams of (a) photon emission in an external field (nonlinear Compton effect); (b) production of an electron–positron pair by a photon (nonlinear Breit–Wheeler process). Double lines denote an electron dressed by an external field (see Fig. 5).

and its dependence on the envelope leads to the ponderomotive effect [151]. Note that $q_- = p_-$ and $\mathbf{q}_\perp = \mathbf{p}_\perp$. The density of particles in a monochromatic wave periodically depends on the phase, so in this case it is natural to normalize solution (21) to the unit average density of particles in the wave, which corresponds to the choice $C_p = 1/\sqrt{2q_0}$ [3].

4.2 Photon emission by an electron in a plane-wave field and in a constant field

We consider in more detail the process $\mathrm{eL} \to \mathrm{e}\gamma\mathrm{L}$, the radiation of a photon by an electron in a plane monochromatic wave [13, 134, 135], where L denotes that the process occurs in a laser field. This process, which has a classical analog — nonlinear Thomson scattering [75, 152] — is often also called nonlinear Compton scattering [153]. Its amplitude is determined by the formula [5] (Fig. 6a)

$$S_{\mathrm{e}\to\mathrm{e}\gamma} = -\mathrm{i}e \int \mathrm{d}^4 x\, \bar{\Psi}_{p'}^{(A)}(x)\, \not{\varepsilon}_l^{\,*}\, \frac{\exp(\mathrm{i}lx)\sqrt{4\pi}}{\sqrt{2\Omega}}\, \Psi_p^{(A)}(x)\,, \quad (27)$$

where $\Psi_p^{(A)}$ and $\Psi_{p'}^{(A)}$ are the initial and final Volkov states of an electron with 4-quasi-momenta $q^\mu = \{\mathcal{E}, \mathbf{q}\}$ and $q'^\mu = \{\mathcal{E}', \mathbf{q}'\}$, respectively,[6] and $l^\mu = \{\Omega, \mathbf{l}\}$ and ε_l^μ are the 4-momentum and 4-vector of polarization of the emitted photon ($l^2 = l\varepsilon_l = 0$). As discussed above, the Volkov functions accurately take into account the interaction of an electron with a wave before and after the emission of a photon, which can be interpreted as the emission and absorption of wave photons by the electron. Substituting into Eqn (27) Volkov solutions (21) and expanding in them the factors that periodically depend on the phase in a Fourier series, we obtain

$$S_{\mathrm{e}\to\mathrm{e}\gamma} = (2\pi)^4 \sum_{s=1}^{\infty} \delta^{(4)}(q' + l - q - sk)\, \frac{M_{\mathrm{e}\to\mathrm{e}\gamma}}{\sqrt{(2\mathcal{E})(2\mathcal{E}')(2\Omega)}}\,, \quad (28)$$

where $M_{\mathrm{e}\to\mathrm{e}\gamma}^{(s)}$ is the invariant amplitude of photon emission with the final absorption of s photons from the wave over the period of the field,

$$M_{\mathrm{e}\to\mathrm{e}\gamma}^{(s)} = -\mathrm{i}e \int_0^{2\pi} \frac{\mathrm{d}\varphi}{2\pi} \exp\left[\mathrm{i}\left(s\varphi + \tilde{\mathcal{S}}_q(\varphi) - \tilde{\mathcal{S}}_{q'}(\varphi)\right)\right] \times \bar{u}_{p'} \bar{\Sigma}_{p'}(\varphi)\, \not{\varepsilon}_l^{\,*}\, \Sigma_p(\varphi) u_p\,. \quad (29)$$

The delta function included in (28) corresponds to the conservation of the 4-quasi-momentum taking into account the photons absorbed from the field. Equation (28) takes into account that, since the emission of a photon by a free electron is forbidden by conservation laws, only processes with $s \geqslant 1$ can actually contribute (see below).

Thus, the kinematics of the process coincide with those for the usual linear Compton effect. In particular, in the reference frame where the electron is initially at rest on average ($\mathbf{q} = 0$), the frequency of the emitted photon Ω when s photons are absorbed from the field is related to the angle θ between the direction $\mathbf{l}$ of its radiation and the direction of wave propagation $\mathbf{k}$ by the formula [31]

$$\Omega_s(\theta) = \frac{s\omega}{1 + (s\omega/m_*)(1 - \cos\theta)}\,, \quad s \geqslant 1\,. \quad (30)$$

The main difference from the linear Compton effect is that Eqn (30) contains instead of the electron mass m an effective mass m_*, which depends on the field intensity. As noted, this is a purely classical effect associated with transverse oscillations of an electron in the field of a wave, but its manifestation (difference of the denominator from unity) is already associated with the quantum recoil effect during radiation. In the classical approximation, the recoil disappears in this reference frame; the radiation becomes isotropic and occurs strictly on the harmonics $s\omega$ of the wave frequency. However, in the reference frame where the electron is at rest before entering the wave (in this system, $\mathbf{p} = 0$), the frequency of the emitted photons is given by the formula [8, 134, 135]

$$\Omega_s(\theta) = \frac{s\omega}{1 + (s\omega/m + a_0^2/2)(1 - \cos\theta)}\,, \quad s \geqslant 1\,, \quad (31)$$

where now θ is the radiation angle in this system. Thus, in such a system, even in the classical limit, the radiation remains anisotropic, and the harmonic frequencies, with the exception of radiation strictly in the direction of wave propagation ($\theta = 0$), decrease with increasing wave intensity, which is due to the Doppler effect when an electron is dragged by the wave due to the ponderomotive effect.

The differential probability per unit time of a process with unpolarized electrons is determined by the standard formula [76]

$$\mathrm{d}R_{\mathrm{e}\to\mathrm{e}\gamma} = \frac{1}{(2\pi)^2} \sum_s \left\langle |M_{\mathrm{e}\to\mathrm{e}\gamma}^{(s)}|^2 \right\rangle_{\mathrm{pol}} \times \delta^{(4)}(q' + l - q - sk)\, \frac{\mathrm{d}^3 q'\, \mathrm{d}^3 l}{(2\mathcal{E})(2\mathcal{E}')(2\Omega)}\,, \quad (32)$$

where $\left\langle |M_{\mathrm{e}\to\mathrm{e}\gamma}^{(s)}|^2 \right\rangle_{\mathrm{pol}}$ is the square of the modulus of the invariant amplitude (29) averaged over the initial electron polarization and summed over its final polarization and the polarization of the emitted photon. The rather cumbersome calculation of this quantity includes the calculation of Dirac traces and the integral over phases included in Fourier coefficient (29). Due to the nonlinearity in the field, the result depends on the wave polarization. However, the result is

[5] Strictly speaking, in recording the amplitude, one should distinguish between the in and out states corresponding in Eqns (21) and (24) to the choice $\varphi_0 = \mp\infty$ and the electron before and after the action of the wave, and describe the initial electrons by the 'in' state, and the final electrons by the 'out' state. However, in this case, this only leads to the appearance of an additional phase factor that drops out at the stage of transition from the amplitude to the probability of the process.

[6] The introduction from the very beginning of the quasi-momentum to describe the initial and final states of an electron is convenient but not mandatory. The Volkov functions $\Psi_p^{(A)}$ are labelled by quantum numbers $p_- = q_-$ and $\mathbf{p}_\perp = \mathbf{q}_\perp$. The mass shift, which is conveniently interpreted in terms of a quasi-momentum, arises dynamically in the law of 4-momentum conservation in a monochromatic plane wave due to the dependence of the invariant amplitude (29) on s [154].

substantially simplified for the case of a circularly polarized wave, in which $A^\mu(\varphi) = (ma_0/e)(\epsilon_1^\mu \cos\varphi + \epsilon_2^\mu \sin\varphi)$, where $\epsilon_i^2 = -1$ and $k\epsilon_i = \epsilon_1\epsilon_2 = 0$, so that $A^2 = -(ma_0/e)^2 = \text{const}$, and the Fourier coefficient reduces to Bessel functions [75, 135, 136].

The total probability, which is given by the integral of Eqn (32) over the quasi-momentum of the final electron and the momentum of the emitted photon, depends on the invariant parameters a_0 and $\chi = a_0(ql)/m^2$. It is convenient to represent the differential probability as a distribution over the quantum parameter of the emitted photon $\varkappa = a_0(kl)/m^2$ or final electron $\chi' = a_0(q'l)/m^2$ connected by the conservation law $\chi = \chi' + \varkappa$. For a given s, the final quasi-momentum of an electron $\mathbf{q}'$ is uniquely determined by the momentum of the emitted photon $\mathbf{l}$ by the conservation law (and *vice versa*), while the spatial components of the delta function remove the integration over d^3q' (or, conversely, over d^3l). The remaining time component of the delta function determines the discrete frequencies at which radiation occurs with absorption from the field of a various number of photons, depending on the direction of radiation (in the frame where the electron is initially at rest on average, determined by Eqn (30)). Integration over the remaining photon momentum (consequently, the final quasi-momentum of the electron) is simplified if it is performed before summing over s in the center-of-mass system (depending on the number of absorbed photons s), where $\mathbf{q} + s\mathbf{k} = 0$. In the considered case of a circularly polarized wave, the integral over the azimuthal angle is idle; the energy integral removes the remaining delta function; and the polar angle integral is transformed into an integral over the invariant variable $\varkappa$:

$$\int \frac{d^3q'\,d^3l}{(2\mathcal{E}')(2\Omega)}\,\delta^{(4)}(q' + l - q - sk)\ldots = \frac{\pi}{2}\int \frac{d\varkappa}{\chi}\ldots. \quad (33)$$

Taking this into consideration, we finally obtain [76, 135, 136]

$$R_{e\to e\gamma} = \frac{\alpha m^2}{\mathcal{E}}\int_0^\chi \frac{d\varkappa}{\chi}\sum_{s=s_0(\varkappa)}^{\infty}\left[-J_s^2(z) + \frac{a_0^2}{2}\left(\frac{\varkappa^2}{2\chi\chi'} + 1\right)\right.$$
$$\left.\times\left(J_{s+1}^2(z) + J_{s-1}^2(z) - 2J_s^2(z)\right)\right], \quad (34)$$

where $\chi' = \chi - \varkappa$,

$$z = \frac{2a_0}{\sqrt{1 + a_0^2}}\sqrt{s_0(\varkappa)\big(s - s_0(\varkappa)\big)}, \quad s_0(\varkappa) = \frac{\varkappa a_0(1 + a_0^2)}{2\chi\chi'}. \quad (35)$$

Here, the overall factor α corresponds to the first order of the process with respect to the quantized field; the factor $m/\mathcal{E}$ takes into account relativistic time dilation in the reference frame, in which the electron is initially at rest on average, while the remaining part of the formula determines the dependence on invariant dimensionless parameters a_0 and χ and the distribution (now continuous) over the variable $\varkappa$, which is convenient for theoretical analysis. Of greater importance for experiment are, naturally, the angular and energy distributions, which are related to derived Eqn (34) taking into account the definition $\varkappa = a_0(\omega\Omega/m^2)(1 - \cos\theta)$. However, it is only reasonable to derive such distributions for the parameters of particular experiments [8]. The quantity $s_0(\varkappa)$, which is the minimal number of photons absorbed from the wave kinematically allowed for the given $\varkappa$, can also be found using the Kibble kinematic inequality $(\varepsilon_{\mu\nu\lambda\rho}q^\nu k^\lambda l^\rho)^2 \leqslant 0$ [76]. On the contrary, for a fixed s, the inequality $s \geqslant s_0(\varkappa)$ limits $\varkappa$ from above by a value $\varkappa_s$, which is the Compton edge for the absorption of s photons from a wave.

It can be shown [76, 135, 136] that, in the weak-field limit, $a_0 \ll 1$, Eqn (34) is dominated by the component with $s = 1$, and it transforms into a product of the Klein–Nishina cross section [76, 137] and the photon flux density $E^2/(4\pi\omega) = m\omega a_0^2/(4\pi e^2)$ in a wave, and, in the classical limit, $\chi \ll 1$ (34) (with corresponding changes in notations, in particular, after transition from probability to intensity of radiation), into the classical Schott formula [30] for radiation of an electron in a constant perpendicular magnetic field. This result is natural, since the classical motion of an electron, which is on average at rest in the field of a circularly polarized wave, as well as in a constant magnetic field, is a uniform circular motion.

In the most interesting limiting case $a_0 \to \infty$ (at $\omega \to 0$ and constant field strengths $E_0 = m\omega a_0/e$ and χ), the effective values of s in (34) determined by the condition $s \lesssim z$ turn out to be $s \simeq 2s_0$. This shows that, for large a_0, the values of $s \propto a_0^3$ included in the sum are very large [31, 136]. Taking this circumstance into account, we can proceed from summation over s to integration over a new variable τ defined according to $s = 2s_0(1 + \tau/a_0)$, for which the ratio $z/s \approx 1 - (1 + \tau^2)/(2a_0^2)$ is close to unity, and use the asymptotic form [30, 155]

$$J_s(z) \approx s_0^{-1/3}\,\mathrm{Ai}\left[\left(\frac{s_0}{a_0^3}\right)^{2/3}(1 + \tau^2)\right]. \quad (36)$$

With the same accuracy, the lower integration limit $-a_0$ can be replaced with $-\infty$. The dependence on a_0 then disappears, and after transformation and calculation of the integral over τ using the properties of the Airy function, we arrive at [76, 156]

$$R_{e\to e\gamma} \approx R_{e\to e\gamma}^{\mathrm{CCF}}(\chi) = -\frac{\alpha m^2}{\mathcal{E}}\int_0^\chi \frac{d\varkappa}{\chi}\left\{\mathrm{Ai}_1(x)\right.$$
$$\left. + \left(\frac{2}{x} + \varkappa\sqrt{x}\right)\mathrm{Ai}'(x)\right\}, \quad x = \left(\frac{\varkappa}{\chi\chi'}\right)^{2/3} \quad (37)$$

(since in this limit the quasi-momentum no longer has meaning, it is reasonable to also change the normalization so that $\mathcal{E}$ is now p_0 rather than q_0. Equation (37) coincides with the result for a constant crossed field [31] and, as can be seen from its derivation, the approximation under discussion, applicable at $a_0 \gg \max\{1, (\chi\chi'/\varkappa)^{1/3}\}$, in particular, is always violated at sufficiently small $\varkappa$; however, it is quite applicable in the main radiation region $\varkappa \sim \chi$ provided $a_0 \gg \chi^{1/3} \gtrsim 1$ [31, 157–159].

Figure 7 shows the distributions of $dR_{e\to e\gamma}(\varkappa)/d\varkappa$ over the invariant variable $\varkappa$ at a fixed $\mathcal{E}$ according to Eqn (34), for several values of a_0, and also in comparison with Eqn (37). It can be seen from the figure that the dependence on $\varkappa$ is essentially nonmonotonic, which is due to the closing of absorption channels for a small number of photons as $\varkappa$ increases. It is also seen that, at $\varkappa < \varkappa_1$ and at $a_0 \lesssim 1$, in the entire region, with the exception of only $\varkappa \approx \chi$, the linear Compton effect dominates with the absorption of one photon from the wave. On the contrary, in the region of large $\varkappa$ (the larger a_0, the farther to the left it extends), the contribution of processes with large s is significant, and Eqn (34) transforms there into (37). In accordance with the discussion above, at $a_0 \gg \max\{1, \chi^{1/3}\}$, this region almost completely determines the total probability of radiation. An analysis of the angular and energy distributions in a laboratory system can be found, for example, in [8, 38, 160].

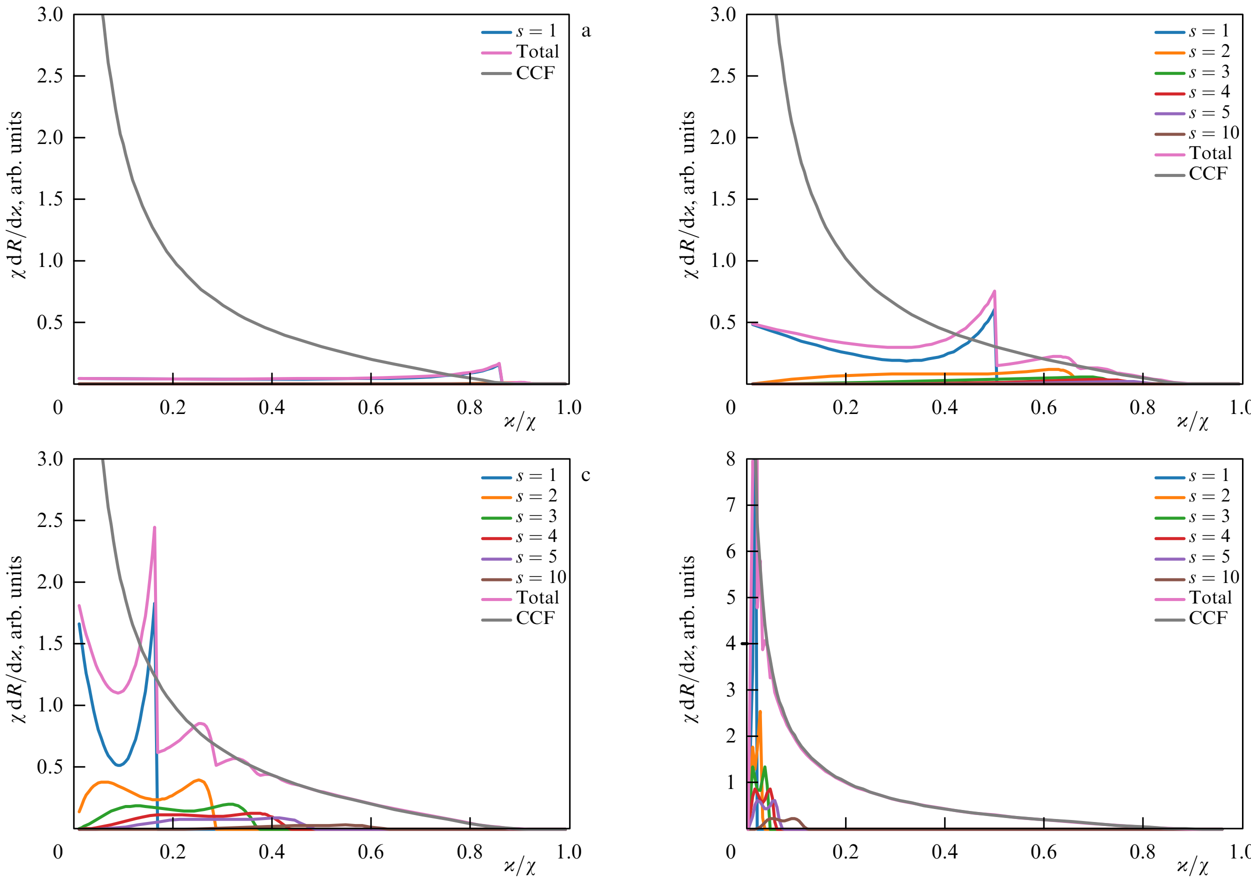

Figure 7. Distribution $\mathrm{d}R_{\mathrm{e}\to\mathrm{e}\gamma}(\varkappa)/\mathrm{d}\varkappa$ over the invariant variable $\varkappa$ according to Eqn (34) (the Total curve) and its comparison with Eqn (37) (curve CCF) at $\chi = 1$ and (a) $a_0 = 0.3$, (b) $a_0 = 1$, (c) $a_0 = 2$, and (d) $a_0 = 5$. Additionally, the contribution of partial processes with absorption of $s = 1-5$ and $s = 10$ photons from the wave is shown.

The dependence of the total probability of emission of a photon by an electron per unit time $R_{\mathrm{e}\to\mathrm{e}\gamma}$ on a_0 is plotted in Fig. 8. It can be seen from the figure that, at $a_0 \lesssim 1$, the main contribution comes from the channel with $s = 1$, while at $a_0 \gg 1$, the contribution of all partial channels decreases, so the probability is determined by processes with the absorption of a large number of photons from the wave. It monotonically increases with increasing a_0, and at $a_0 \gg 1$ (in practice with a significant margin even for $\chi = 1$) asymptotically tends to the probability in a constant crossed field. In the classical theory, this transition corresponds to the transition from the Schott formula to the synchrotron radiation formula [30, 102].

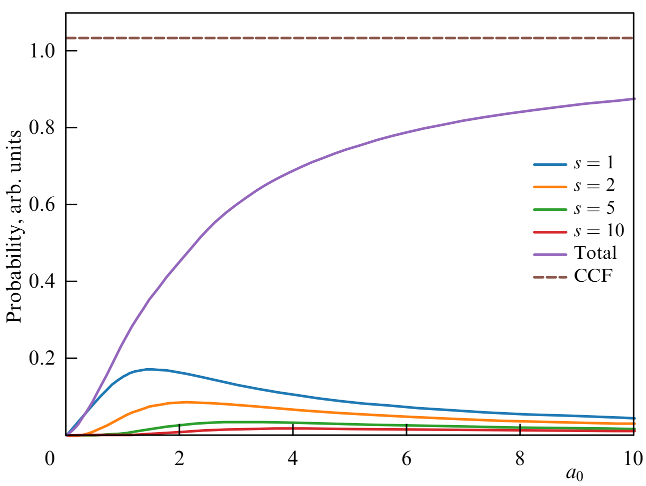

Figure 8. Total probability of emission of a photon by an electron per unit time $R_{\mathrm{e}\to\mathrm{e}\gamma}$ in a plane circularly polarized wave and the contribution of channels with absorption of $s = 1, 2, 5, 10$ photons from the wave as a function of a_0 at $\chi = 1$.

The dependence $\mathrm{d}R^{\mathrm{CCF}}_{\mathrm{e}\to\mathrm{e}\gamma}/\mathrm{d}\varkappa$ on $\varkappa$ shown in Fig. 7, for not too large χ is a monotonic decrease for increasing $\varkappa$. At $\varkappa \to 0$, the spectrum has an integrable singularity $\propto \varkappa^{-2/3}$ [31] due to the assumed infinite extent of the field, and at $\varkappa$ close to χ it decreases exponentially: $\mathrm{d}R^{\mathrm{CCF}}_{\mathrm{e}\to\mathrm{e}\gamma}(u)/\mathrm{d}u \propto \exp\left[-2\varkappa/3\chi(\chi - \varkappa)\right]$. However, at $\chi \gtrsim 16$, a maximum appears at $\varkappa$ close to χ, which is increasingly strongly pronounced with a further increase in χ (Fig. 9a). This maximum, which is even more noticeable in the transition from the probability of radiation to its intensity, is proposed to be used in the creation of a photon collider [161].

The dependence of the total probability of radiation per unit time $R^{\mathrm{CCF}}_{\mathrm{e}\to\mathrm{e}\gamma}(\chi)$ in a constant crossed field on χ at a fixed $\mathcal{E}$ is shown in Fig. 9b. It can be seen that it increases monotonically with increasing χ and has the asymptotic form [4, 31]

$$R^{\mathrm{CCF}}_{\mathrm{e}\to\mathrm{e}\gamma}(\chi) \approx \frac{\alpha m^2}{\mathcal{E}} \begin{cases} 1.44\chi\,, & \chi \ll 1\,, \\ 1.46\chi^{2/3}\,, & \chi \gg 1\,. \end{cases} \tag{38}$$

The first asymptotic formula corresponds to the classical theory, since in the transition from probability to intensity in

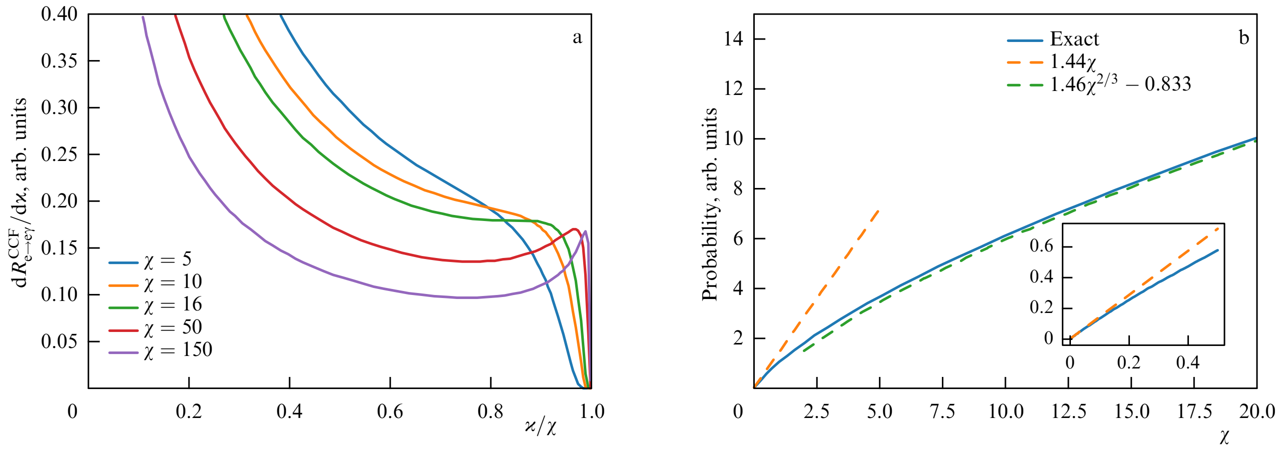

Figure 9. (a) Distributions $dR^{CCF}_{e\to e\gamma}(\varkappa)/d\varkappa$ of photon emission in a constant crossed field over quantum parameter $\varkappa$ of an emitted photon for several values of χ. (b) Total probability of photon emission per unit time $R^{CCF}_{e\to e\gamma}$ in a constant crossed field as a function of χ.

the $\chi \to 0$ limit Planck's constant drops out. In practice, this asymptotic form begins to be significantly violated as early as at $\chi \gtrsim 0.02$ [107, 108]. The second asymptotic formula, on the contrary, corresponds to the quantum regime; its accuracy is 10%, 5%, and 1% at $\chi > 15$, $\chi > 40$, and $\chi > 430$, respectively.

In the case of elliptical (in particular, linear) polarization, the general approach and results are basically similar to those in the case of circular polarization. However, if a_0 is understood not as the root-mean-square but as the amplitude value, some formulas, in particular, the one for the effective mass in (26), which is implicitly included in Eqns (35), need to be corrected accordingly. In addition, the Fourier integral in Eqn (29) reduces to the following functions:

$$A_n(s,\alpha,\beta) = \int_0^{2\pi} \frac{d\varphi}{2\pi} \cos^n \varphi \exp\left[i\big(s\varphi - \alpha \sin\varphi + \beta \sin(2\varphi)\big)\right], \quad n = 0, 1, 2 \qquad (39)$$

(which, in the case of circular polarization $\beta = 0$, in turn reduce to Bessel functions). Finally, in the frame of the center of mass of the initial electron and s wave photons, the distribution is no longer azimuthally symmetric. The corresponding results are discussed in [3, 31].

For a plane wave of finite duration (a laser pulse), the field is not periodic; consequently, the invariant amplitude is not expanded in a series, but is expressed by the Fourier integral (in this case, the variable s becomes continuous and, in essence, acquires the meaning of not a number but the energy of photons absorbed from a wave measured in units of a conventional carrier frequency), and instead of the probability per unit time $R_{e\to e\gamma}$, the total probability of the process $W_{e\to e\gamma}$ is calculated for the entire duration of the pulse. In this case, the initial and final states are determined in asymptotic regions where the field is still or already absent [162], and therefore there is no need to explicitly introduce quasimomenta and the effective mass of the initial and final states of the electron (at the same time, its dressing inside the pulse, in particular, the formation of the effective mass, is still correctly taken into account in the Volkov solutions and formulas for the process amplitude; notably, it manifests itself in the spectrum of emitted photons) [154]. An analog of Eqn (29) then reduces to integrals of the form

$$A_n(s,\alpha,\beta) = \int_{-\infty}^{+\infty} g^n(\varphi) \exp\left[i\big(s\varphi - f(\varphi)\big)\right] \frac{d\varphi}{2\pi}, \qquad (40)$$
$$f(\varphi) = \alpha \int_{-\infty}^{\varphi} g(\varphi)\, d\varphi - \beta \int_{-\infty}^{\varphi} g^2(\varphi)\, d\varphi,$$

where $n = 0$, 1, 2, and $g(\varphi)$ is the pulse profile (that includes both the carrier and the envelope). Except for artificially simple cases, integrals (40) cannot be determined analytically and should be calculated numerically. However, the integral A_0 formally diverges, and it must first be regularized by integration by parts with the nonintegral term discarded [163]:

$$A_0 \mapsto A_0 - \delta(s) = \frac{1}{s} \int_{-\infty}^{+\infty} f'(\varphi) \exp\left[i\big(s\varphi - f(\varphi)\big)\right] \frac{d\varphi}{2\pi}. \quad (41)$$

The meaning of this procedure is that it eliminates the contribution of the kinematically forbidden process of radiation without absorption of photons from the field, which continues for a formally infinite time and thereby leads to divergence. For short pulses, the resulting spectra and angular distributions strongly depend on their profile [18, 21, 164–168]; however, in the limit of long pulses, the probability of the process is proportional to their duration, and the results for a monochromatic field are reproduced. The process was also calculated for polarized particles in the case of a monochromatic wave [169], for short pulses [170], and in a constant crossed field [171].

Since real high-intensity laser pulses are tightly focused, it is also of interest to take into account focusing effects, which apparently requires going beyond the plane-wave approximation. In the case of fast particles, the operator method [76, 172] dating back to Schwinger [108] can be used to show that the motion of such particles in an arbitrary inhomogeneous field is semiclassical,[7] and their radiation is essentially described by the classical formula, in which the quantum nature of the process in an arbitrary inhomogeneous field only manifests itself in the need to additionally take into account the Doppler effect in the recoil due to the radiation of

[7] Under additional assumption $E, H \ll E_{cr}$. In a plane wave and a constant crossed field, this description becomes accurate, which is reflected in the quasiclassical form (21) of exact solutions of the Dirac equation.

a hard photon and the spin contribution to radiation (spin light [173]). As was recently shown for a plane wave, in which the equation of motion, taking into account that radiation friction is solved exactly in the Landau and Lifshitz approximation [110], the quantum recoil can then be formally taken into account in the classical formula similarly to the exact account for radiation friction in the NTS [174, 175]. An alternative method is based on a generalization of the above approach using approximate solutions of the Dirac equation for fast particles in arbitrary fields, generalizing the Volkov solutions [176–178]. Both approaches make it possible to substantiate the applicability of the locally constant field approximation for fast particles in strong fields, but the corrections have been systematically calculated and analyzed only for the case of a plane wave [158, 159].

The process of nonlinear Compton scattering was observed in the second half of the 1990s at SLAC in the E144 experiment [37, 38], where an electron beam emerging from a linear accelerator with an energy of 46.6 GeV collided at an angle of 17° with laser pulses with a power of $\simeq 1$ TW, duration of 1.5 ps, and wavelength of 1054 nm (527 nm after frequency doubling with an efficiency of $\sim 50\%$). Under these conditions, the values $a_0 \sim 0.5$ and $\chi \sim 0.3$ were reached, and photons emitted with the absorption of $s = 2$, 3, and 4 quanta from the laser pulse were observed — the data agreed with Eqn (34) with an accuracy of $\sim 10\%$. The main problem in carrying out such experiments is the need to combine and synchronize a powerful laser and an electron accelerator. In 2019, the results of experiments at RAL (Rutherford Appleton Laboratory) [39, 40] were published, where the laser pulse was divided into two, and electrons, after being accelerated by a wake plasma wave generated in a gas jet by one of them, collided with another. Such a setup simplifies synchronization, but acceleration instability becomes problematic, due to which most shots turn out to be idle. The contribution of radiation friction to the spectrum of scattered electrons was measured. Finally, experiments on nonlinear Compton scattering are currently being carried out in CoReLS, and, in the near future, the LUXE (Laser Und XLEL Experiment) experiments will begin at DESY (Deutsches Elektronen Synchrotron) [179] and E-320 at SLAC [180], in which it is planned to study in detail the process under consideration for $a_0 \sim 1-5$ and $\chi \sim 1$.

4.3 Photoproduction of a pair

The second elementary process is the production of an electron–positron pair by a photon in an external field $\gamma\mathrm{L} \to \mathrm{e}^+\mathrm{e}^-\mathrm{L}$ (multiphoton Breit–Wheeler process) [2]; its diagram is depicted in Fig. 6b. It can be seen that it is obtained from the diagram of Fig. 6a by interchanging the initial electron with the final photon,

$$S_{\gamma\to\mathrm{e}^+\mathrm{e}^-} = -\mathrm{i}e \int \mathrm{d}^4 x\, \bar{\Psi}^{(A)}_{p'}(x)\, \not{\varepsilon}_l\, \frac{\exp(-\mathrm{i}lx)\sqrt{4\pi}}{\sqrt{2\Omega}}\, \Psi^{(A)}_{-p}(x)\,, \tag{42}$$

and, according to the crossing-symmetry rules, taking into account the same number of initial and final polarization states in both cases, the modulus squared of the invariant amplitude of this process $\langle |M^{(s)}_{\gamma\to\mathrm{e}^+\mathrm{e}^-}|^2\rangle_{\mathrm{pol}}$ averaged and summed over polarizations is obtained from Eqn (29) for the emission of a photon by an electron by making substitutions $l^\mu \to -l^\mu$ and $p^\mu \to -p^\mu$ (in our notation, equivalent to the substitutions $\varkappa \to -\varkappa$ and $\chi \to -\chi$) and a change in the overall sign due to the replacement of the electron density matrix with the positron density matrix [3, 136]. In addition, in the expression for the probability of the process per unit time, integration should now be carried out over the 4-quasi-momenta q^μ of the final positron and q'^μ of the final electron; the corresponding phase volume is

$$\int \frac{\mathrm{d}^3 q\, \mathrm{d}^3 q'}{(2\mathcal{E})(2\mathcal{E}')}\, \delta^{(4)}(q' + q - l - sk) \ldots = \frac{\pi}{2} \int \frac{\mathrm{d}\chi}{\varkappa} \ldots \tag{43}$$

(the distribution over χ' in this case is identical to the distribution over χ).

After corresponding changes are made in Eqn (34), the probability per unit time of the process under consideration with unpolarized photons in a circularly polarized monochromatic wave is expressed as [136]

$$\begin{aligned} R_{\gamma\to\mathrm{e}^+\mathrm{e}^-} &= \frac{\alpha m^2}{\Omega} \int_0^\varkappa \frac{\mathrm{d}\chi}{\varkappa} \sum_{s=s_0(\chi)}^{\infty} \left[J_s^2(z) + \frac{a_0^2}{2} \left(\frac{\varkappa^2}{2\chi\chi'} - 1 \right) \right. \\ &\quad \left. \times \left(J_{s+1}^2(z) + J_{s-1}^2(z) - 2J_s^2(z) \right) \right], \end{aligned} \tag{44}$$

where z and $s_0(\chi)$ are as before determined by Eqns (35), in which, however, now $\chi' = \varkappa - \chi$. An important difference between this process and the nonlinear Compton effect is that the minimum number of photons absorbed from the field is limited by the kinematics:[8]

$$s_{\min} = \min_\chi s_0(\chi) = \frac{2a_0(1 + a_0^2)}{\varkappa}\,; \tag{45}$$

thus, $R_{\gamma\to\mathrm{e}^+\mathrm{e}^-} \propto a_0^{2s_{\min}}$ for $a_0 \ll 1$, and in the classical limit $\varkappa \ll 1$, in which $s_{\min} \to \infty$, the photoproduction of a pair is suppressed exponentially. The distribution of the produced pairs over χ for $a_0 = 0.5$ is shown in Fig. 10a. It is interesting that in this case the contribution of partial processes at small a_0 decreases monotonically with increasing s, while at $a_0 \gtrsim 1$ it first increases, attaining a maximum, and then decreases.

Similar to the case of the photon emission process, for $a_0 \gg \max\{1, (\chi\chi'/\varkappa)^{1/3}\}$, Eqn (44) asymptotically transforms into the result for a constant crossed field [76, 156]:

$$\begin{aligned} R_{\gamma\to\mathrm{e}^+\mathrm{e}^-} &\approx R^{\mathrm{CCF}}_{\gamma\to\mathrm{e}^+\mathrm{e}^-}(\varkappa) \\ &= \frac{\alpha m^2}{\Omega} \int_0^\varkappa \frac{\mathrm{d}\chi}{\varkappa} \left[\mathrm{Ai}_1(x) + \left(\frac{2}{x} - \varkappa\sqrt{x} \right) \mathrm{Ai}'(x) \right], \\ x &= \left(\frac{\varkappa}{\chi\chi'} \right)^{2/3}. \end{aligned} \tag{46}$$

As can be seen from Fig. 10b, with increasing a_0, the total probability (44), which at first varies nonmonotonically, significantly exceeds the probability in a constant crossed field, but at $\varkappa = 1$ already at $a_0 \gtrsim 2$ approaches (46) with good accuracy.

The dependences of the distribution of produced pairs with respect to the variable χ and the total probability of photoproduction of a pair per unit time in a constant crossed field approximation are displayed in Fig. 11. It can be seen that the distribution over χ of the produced pair for small $\varkappa$ is

[8] The number $s_{\min}$ can also be easily found from the inequality $(l + sk)^2 \geqslant 4m_*^2$, which follows from the law of conservation of 4-quasi-momentum taking into account the photons absorbed from the field.

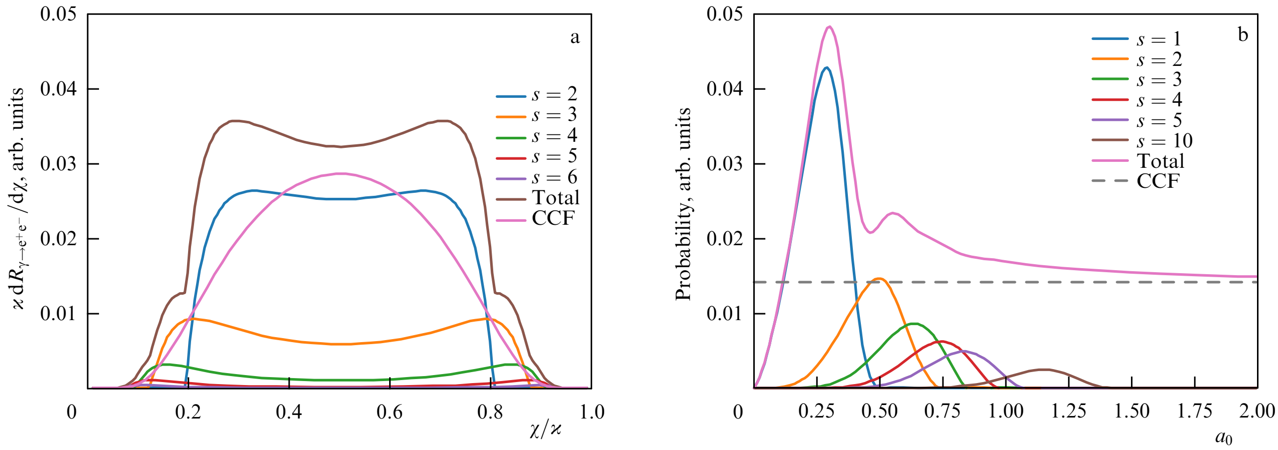

Figure 10. (a) Distribution of produced pairs over invariant variable χ and contributions of channels with various s according to Eqn (44) (Total curve) and comparison with Eqn (46) (curve CCF) at $\varkappa = 1$ and $a_0 = 0.5$. (b) Total probability of pair photoproduction per unit time $R_{\gamma\to e^+e^-}$ in a plane circularly polarized wave and the contribution of channels with various s as a function of a_0 at $\varkappa = 1$.

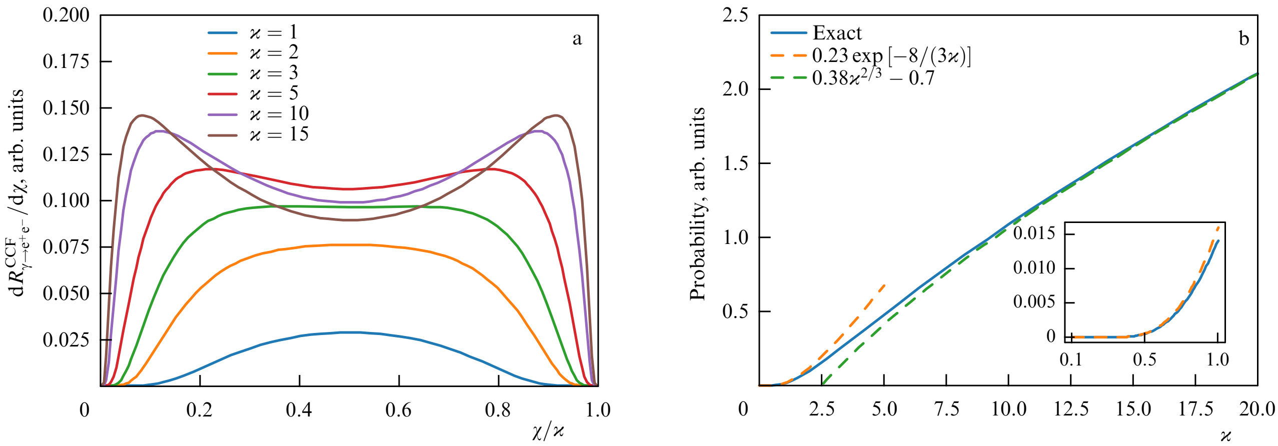

Figure 11. (a) Distributions $\mathrm{d}R^{\mathrm{CCF}}_{\gamma\to e^+e^-}(\chi)/\mathrm{d}\chi$ of photoproduction of a pair in a constant crossed field over quantum parameter χ of an emitted photon as a function of $\varkappa$. (b) Total probability of photoproduction of a pair per unit time $R^{\mathrm{CCF}}_{\gamma\to e^+e^-}$ in a constant crossed field as a function of $\varkappa$.

single-bumped, but for $\varkappa \gtrsim 5$ it exhibits two bumps with a hollow in the middle. The total probability of pair production per unit time in a constant crossed field has the following asymptotic form [4, 31]:

$$R^{\mathrm{CCF}}_{\gamma\to e^+e^-}(\chi) \approx \frac{\alpha m^2}{\Omega} \begin{cases} 0.23\varkappa \exp\left(-\dfrac{8}{3\varkappa}\right), & \varkappa \ll 1\,, \\ 0.38\varkappa^{2/3}\,, & \varkappa \gg 1\,. \end{cases} \tag{47}$$

We note the rapid decrease in the probability of this process in the classical limit $\varkappa \to 0$ and the nonanalytical dependence, similar to that arising in the Schwinger effect [34], on the parameter $\varkappa$, due to the infinite number of photons (of zero frequency) absorbed from the field in the constant field limit.

Similar to the nonlinear Compton effect, pair photoproduction has been studied in detail in pulsed fields (see, for example, [18, 181–185]) and was also observed in the SLAC-E144 experiment [38, 186], where pairs were produced by backscattered electrons at $a_0 \sim 0.2$ and $\varkappa \sim 0.2$ (at the boundary of the perturbative regime) and $\lesssim 0.02$ positrons per shot were detected; nevertheless, the onset of the upper (at $\varkappa \ll 1$) nonperturbative asymptotic form (47) was successfully detected. A more accurate and detailed study of this effect at somewhat more extreme parameters is planned to be carried out in the coming years in the LUXE experiments at DESY [179] and E320 experiment at SLAC [180].

4.4 Characteristic scales, backreaction, and approximation of a locally constant field

We now discuss a number of subtle questions key to understanding the nature of the strong field regime, which are related to the concept of effective mass, the characteristic scales of processes in the strong field regime and their hierarchy, and the meaning and applicability of the external and locally constant field approximations, which sometimes cause confusion in publications. For greater clarity, the discussion is carried out at the level of qualitative assessments.

The concepts of quasi-momentum q^μ and effective mass $m_* = m(1 + a_0^2)^{1/2} \simeq m a_0$ (for simplicity, we assume $a_0 \gtrsim 1$, which corresponds to relativistic transverse motion in the classical theory and nonperturbative dressing in the quantum one) characterize the dressing of particles in an electromagnetic wave and arise already in the classical description of the motion of particles in it, where the effective mass takes into account the part of the energy and momentum $\sim eE/\omega$ associated with the transverse oscillations of a charged particle in the wave, and the quasi-momentum characterizes the motion of the leading center of these oscillations. Hence, it is clear that the characteristic time of their formation is of the order of the wave period, $\tau_d \sim \omega^{-1}$, and m_* is determined by the characteristic work of the field and the transfer of momentum to the particle by the field in time τ_d, $m_* \simeq eE\tau_d$. In quantum theory, dressing by a field is characterized by the processes of exchange of photons with the field, depicted by the diagram in Fig. 5. Let the electron absorb s_{in} photons from the wave and emit s_{out} photons back into the wave.[9] Then, the processes with $s_{in} \lessgtr s_{out}$ in the classical language correspond to the deceleration or acceleration of the leading center upon recoil from radiation (i.e., radiation friction), while those with $s_{in} = s_{out}$ just lead to the formation of an effective mass [31, 187]. Moreover, the characteristic number of external-field photons, $s_d \sim m_*/\omega$, involved in dressing even one electron, can be very large, and the question arises as to whether this process can deplete the field.

Equating the energy density nm_* of the transverse motion of electrons in a wave, where n is their density, to the field energy density $\langle E^2\rangle/(4\pi)$, taking into account the definition of a_0 (2), we find that they become equal when

$$\omega \gtrsim \omega_{pl} = \sqrt{\frac{4\pi e^2 n}{m_*}}, \qquad n \gtrsim n_{cr} = \frac{m_*\omega^2}{4\pi e^2}. \tag{48}$$

The quantity ω_{pl} is called the relativistic plasma frequency, and condition (48) determines the threshold for wave absorption in a relativistic laser plasma [123]. Thus, the external field approximation is applicable in an optically transparent plasma and is only violated under condition (48). In the case of a single particle, the average density can be estimated as $n \sim \omega^3$; hence, it is clear that condition (48) is violated with a large margin for optical-range lasers, so the backreaction (at least for the considered times of $\sim \omega^{-1}$) can be completely neglected. We note that the critical concentration is proportional to a_0, and in regime (48) one should take into account the change in the dispersion relation of the wave and, consequently, the modification of the Volkov solution [188].

However, as we shall now see, the time τ_f characteristic for the formation of photon radiation (and photoproduction of a pair) in a strong field is much shorter. To estimate τ_f, we assume that an ultrarelativistic electron moving in a perpendicular constant electric field of strength E with momentum p and energy $\mathcal{E} = \sqrt{p^2+m^2} \gg m$ radiates forward a photon with frequency Ω and momentum $l = \Omega$. In such a field, the momentum component perpendicular to the field is conserved, but energy is not conserved, since the field does work by deflecting the electron, due to which the process is possible. During the time t, the electron acquires momentum $p_\perp(t) = eEt$ in the direction of the field, and its energy changes as $\mathcal{E}(t) = (p^2 + p_\perp^2(t) + m^2)^{1/2}$. Assuming non-relativistic motion along the field (to which we will return after the estimate is completed), we can make an expansion

$$\mathcal{E}(t) \approx p + \frac{p_\perp^2(t) + m^2}{2p}, \tag{49}$$

and a similar formula for the electron energy $\mathcal{E}'$ after it emits a photon. Then, taking into account the conservation of the momentum component perpendicular to the field $p = p' + l$, the energy mismatch in the process takes the form

$$Q(t) = \mathcal{E}'(t) + \Omega - \mathcal{E}(t) \simeq \frac{\left(p_\perp^2(t) + m^2\right)\Omega}{2\mathcal{E}(\mathcal{E}-\Omega)}. \tag{50}$$

The characteristic time τ_f of the formation of the process is determined in [189–191] from the uncertainty relation $Q(\tau_f)\tau_f \sim 1$. Disregarding the mass (see below), we find in terms of dimensionless quantum parameters $\chi = eE\mathcal{E}/m^3$, $\varkappa = eE\Omega/m^3$, and $\chi' = eE\mathcal{E}'/m^3 = \chi - \varkappa$:

$$\tau_f = \frac{m}{eE}\left(\frac{\chi\chi'}{\varkappa}\right)^{1/3} = \frac{1}{\omega a_0}\left(\frac{\chi\chi'}{\varkappa}\right)^{1/3}. \tag{51}$$

Estimate (51) agrees with the results obtained in [157–159, 192] and in Section 4.2.[10]

For sufficiently small $\varkappa \ll \chi$, time τ_f is large, and the assumptions made are not fulfilled [157–159]; hence, $\tau_f \sim \omega^{-1}$. However, for $\varkappa \simeq \chi$, we have $\tau_f \sim \chi^{1/3}/a_0\omega$, and for $a_0 \gg \chi^{1/3}$ the inequality $\tau_f \ll \tau_d$ is satisfied, which confirms the assumptions made in the derivation of Eqn (51) that the field is constant and it is not necessary to take the effective mass into account. Furthermore, we have $p_\perp(\tau_f) \simeq m\chi^{1/3}$, so neglecting the mass in Eqn (50) is justified at $\chi \gtrsim 1$. Finally, expansion (49) is justified for $p \sim m\gamma \gtrsim m\chi^{1/3}$. Since in a strong field $\gamma \gtrsim a_0$ (where $\gamma \sim a_0$ corresponds to particles captured by the field, and $\gamma \gg a_0$ corresponds to fast particles entering the field), for $a_0 \gg \chi^{1/3}$, this condition is also automatically satisfied, finally confirming that the logic used in the evaluation is correct.

So, under the condition $a_0 \gg \chi^{1/3} \gtrsim 1$ and not too small $\varkappa$, the characteristic time of formation of process (51) is much less than the wave period, and, consequently, the field can be considered locally constant. It is this factor that explains why the effective mass drops out in the transition from Eqn (32) to Eqn (37) and may be not taken into account in the above reasoning. Expressing the radiation formation time in terms of χ and $\mathcal{E}$, $\tau_f = \mathcal{E}/m^2\chi^{2/3}$, it can be easily seen that it determines, in order of magnitude, the process probability scale per unit time in the regime $a_0 \gg \chi^{1/3} \gtrsim 1$ (the lower asymptotics of the total probability in (38)) according to $R^{CCF}_{e\to e\gamma}(\chi) \simeq \alpha/\tau_f$. The factor α apparently means, as is natural for first-order processes, the probability of decay in time τ_f. The same results and conclusions with only the replacement $\chi \to \varkappa$ are apparently valid as well for the photoproduction of a pair, with the exception that, in accordance with its inherent kinematics, the energy mismatch is minimized at $\chi = \chi' = \varkappa/2$ and a special case similar to emission of soft photons does not occur. This explains the universality of the asymptotic forms $\propto \chi^{2/3}$, $\varkappa^{2/3}$ of first-order processes in a constant field for large values of the quantum parameter.

The number Δs of photons absorbed from the wave during emission can be estimated as the ratio of the energy mismatch $Q(\tau_f) \simeq \tau_f^{-1}$ to the frequency of the wave ω, yielding $\Delta s \sim a_0/\chi^{1/3}$. Under the conditions of applicability of the constant field approximation, the number Δs is large, but the question arises as to how this result complies with the

[9] To introduce these numbers in an explicit way, Volkov solutions (21) should be expanded into a Fourier series prior to being substituted into matrix element (27).

[10] The above reasoning was presented in [191] specifically to clarify the derivation of characteristic scales without using the explicit form of the Volkov functions and matrix elements. Of course, the same result can also be obtained directly from the formulas in Section 4.2, since, as follows from the derivation of asymptotic form (36), the integration variable ψ in the integral representation of the Airy function is formally related to the phase of the wave φ by the relation $\psi = a_0(\varkappa/2\chi\chi')^{1/3}\varphi$.

much larger number $s_0 \sim (\Delta s)^3 \gg \Delta s$ appearing in formula (35). The number s_0 only appears if we consider the process of radiation at times $\tau_{\rm d} \gg \tau_{\rm f}$, at which the electron after radiation changes is redressed, and the effective mass is formed [185]. Indeed, in this case, setting $\mathcal{E} = (p^2 + m_*^2)^{1/2}$, $\mathcal{E}' = (p'^2 + m_*^2)^{1/2}$, and proceeding by analogy with the previous reasoning, we arrive instead of (50) at

$$Q_* \simeq \frac{m_*^2 \Omega}{2\mathcal{E}(\mathcal{E} - \Omega)} = \omega s_0 \,, \tag{52}$$

with the same s_0 as in (35). In other words, the number s_0 appearing in (35) is actually the number of photons absorbed from the wave not only in the process of emission itself but also in the subsequent redressing of the electron. However, the time of the latter process is $\tau_{\rm d} \sim \omega^{-1} \gg \tau_{\rm f}$, and it is no longer directly related to radiation. At this stage, the process is already purely classical, which can be seen from the relationship $Q_* \tau_{\rm d} \sim s_0 \gg 1$. Finally, as can be easily seen, at $\gamma \gtrsim a_0$ we always have $s_0 \lesssim s_{\rm d}$; therefore, according to the previous reasoning, despite the seemingly catastrophic increase $\propto a_0^3$ in the number of photons absorbed from the field with an increase in a_0 in redressing the electron in radiating a hard photon [31, 193], the external field approximation is quite applicable up to reaching the opacity limit determined by condition (48).

Apparently, the key and most interesting feature of processes in a strong field, which significantly distinguishes them from ordinary QED processes that involve individual photons, is precisely their multiphoton character. However, the complex form of the spectra in Figs 7a–c and 10a corresponds to the parameters at which the number of photons from the wave involved in the process is small. In particular, the sharp dips in Fig. 7a–c correspond to a change in their number by one. In the multiphoton regime, such oscillations are smoothed out (Fig. 7d) (see also [157]). From this point of view, it is precisely the regime $a_0 \gg \max\{1, (\chi\chi'/\varkappa)^{1/3}\}$ in which the formation time of the process $\tau_{\rm f}$ is short compared to the characteristic time of the change in the field ω^{-1} that should be considered a real strong field regime. In this sense, the locally constant crossed field (LCCF) approximation, in which the interference between radiation occurring in non-overlapping formation intervals is neglected, is a manifestation of the strong field regime. In the LCCF approximation, the probability of a radiation process in an arbitrary field is represented as the sum of incoherent contributions from all formation intervals:

$$W_{{\rm e}\to{\rm e}\gamma} = \int R^{\rm CCF}_{{\rm e}\to{\rm e}\gamma}\big(\chi(t)\big)\,{\rm d}t \,, \tag{53}$$

where $R^{\rm CCF}_{{\rm e}\to{\rm e}\gamma}(\chi)$ is the probability of radiation in a constant crossed field determined by Eqn (37) and $\chi(t)$ is a quantum parameter calculated using the local strengths of the electric and magnetic fields at the current location $\mathbf{r}(t)$ for the current energy $\mathcal{E}(t)$ and momentum $\mathbf{p}(t)$ of an electron along its trajectory in the field under consideration:

$$\chi(t) = \frac{e}{m^3}\left[\Big(\mathcal{E}(t)\mathbf{E}\big(\mathbf{r}(t), t\big) + \mathbf{p}(t) \times \mathbf{H}\big(\mathbf{r}(t), t\big)\Big)^2 - \Big(\mathbf{E}\big(\mathbf{r}(t), t\big)\,\mathbf{p}(t)\Big)^2\right]^{1/2} . \tag{54}$$

The semiclassical nature of the motion of an electron with $\chi \gtrsim 1$ in arbitrary fields $E, H \ll E_{\rm cr}$ is additionally used (which is exactly realized without additional restrictions in the plane-wave field), which makes it possible to introduce the concept of a classical trajectory before and after radiation events, as well as between them [76, 172]. An approximation of the same meaning is used to calculate the spectrum of emitted photons and for other processes, in particular, pair photoproduction. Formally, to justify Eqn (53), derivation can be based on localized wave packets constructed from known solutions (generalizing the Volkov solution) of the Dirac equation in the high-energy approximation (the meaning of which is equivalent to quasi-classical), representing the square of the amplitude modulus (27) in the form of a double integral over ${\rm d}^4x\,{\rm d}^4x'$, passing in it to integration over $X^\mu = (x^\mu + x'^\mu)/2$ and $\xi^\mu = x^\mu - x'^\mu$, expanding the expressions in the exponent and pre-exponential factor in powers of ξ^μ and interpreting $X^\mu = (T, \mathbf{X})$ as the current time and location of the formation interval from which the radiation is considered [177].

As noted, the LCCF approximation is completely synonymous with the strong field regime and, therefore, enables a correct description of any phenomena specific to this regime. However, the experiments currently being carried out and planned for the foreseeable future will be conducted in the regime $\chi \sim a_0 \gtrsim 1$ in which the accuracy of the LCCF approximation is lower than the measurement accuracy. In addition, even in the case of fields with $a_0 \gg 1$, while entering and leaving a strong field region, particles still inevitably pass through a weak field region, in which the LCCF approximation is inapplicable. Although the probability of the considered processes in the region of a relatively weak field is suppressed, nevertheless, for the correct interpretation of experiments in such situations, it is necessary to calculate corrections to the LCCF approximation or develop more general approaches, to which much attention is devoted in today's literature [157–159, 177, 194–198].

5. Higher-order processes

In addition to the simplest first-order processes considered above, apparently, more complex higher-order processes can also occur. They can be classified in different ways. In particular, as in conventional QED, a general diagram contains a skeleton and loops. In sufficiently strong weakly-inhomogeneous fields, $a_0 \gtrsim \alpha m/\omega$, of a general type, tree diagrams of large multiplicity can dominate; such processes are called self-sustaining cascades. The loops determine the radiative corrections to the internal and external lines (moreover, in the presence of a field, the corrections to the external lines do not reduce to renormalization and lead to nontrivial effects) and vertices. For very strong weakly-inhomogeneous fields, $a_0 \gg \chi^{1/3} \gtrsim \alpha^{-1/2}$, the role of radiative corrections can become dominant. In the modern literature, this assertion is known as the Ritus–Narozhny conjecture [199].

5.1 Single-stage and cascade processes

In fields that are not too strong (see Section 5.3), it is sufficient to consider any process in the lowest order in α in the tree approximation. The main differences between higher-order processes in the tree approximation and the main ones are the increased number of initial and final interacting particles and the emergence of internal lines in the diagrams. Internal electron lines in amplitude are associated with a propagator in an external field, which in a plane wave field in the coordinate representation has the form [148, 200]

$$S^{(A)}(x',x) = \int \frac{\mathrm{d}^4 p}{(2\pi)^4}\, E_p(x')\, \frac{\mathrm{i}(\not{p}+m)}{p^2-m^2+\mathrm{i}0}\, \bar{E}_p(x) \qquad (55)$$

(in the monochromatic case in (55) it is convenient to use quasi-momentum instead of momentum, in which case the mass is also replaced by the effective mass).

Since a QED vertex always attaches two electron lines (each of which can be internal or external), it is customary in modern approaches to higher-order processes to redefine the diagram technique by moving the dressing from the electronic external lines and propagators to vertices [148, 201]. Then, the external and internal electronic lines become free, while the vertices are dressed by an external field, $-\mathrm{i}e\gamma_\mu \mapsto -\mathrm{i}e\Gamma^{(s)}_\mu(p',p)$. After such a redefinition, at each dressed vertex, the conservation law $p^\mu + sk^\mu = p'^\mu + l^\mu$ is satisfied, taking into account the absorption of s photons from the wave at such a vertex, and the invariant amplitude includes summation over the numbers of photons absorbed at each of the vertices. For example, in the generally accepted notation, invariant amplitude (29) of the nonlinear Compton effect is represented as $M^{(s)}_{\mathrm{e}\to\mathrm{e}\gamma} = -\mathrm{i}e\bar{u}_{p'}\varepsilon^{\mu *}\Gamma^{(s)}_\mu(p',p)u_p$ (Fig. 12a) (cf. Fig. 6a).

The most studied processes are the second-order ones: trident process $\mathrm{eL}\to\mathrm{ee^+e^-L}$ (Fig. 12b) [202–212] and two-photon radiation $\mathrm{eL}\to\mathrm{e}\gamma\gamma\mathrm{L}$ (nonlinear double Compton effect) (Fig. 12c) [213–219]. The invariant amplitude, for example, of the former process in a plane monochromatic wave in the conventional notation is represented as

$$\begin{aligned} &M^{(s)}_{\mathrm{e^-\to e^-e^+e^-}} \\ &= 4\pi\mathrm{i}e^2 \sum_{s_1} \frac{\left(\bar{u}_{p'}\Gamma^{(s_1)\mu}(p',p)u_p\right)\left(\bar{u}_{p_-}\Gamma^{(s-s_1)}_\mu(p_-,-p_+)u_{-p_+}\right)}{(p+s_1k-p')^2+\mathrm{i}0} \\ &- \{p'\leftrightarrow p_-\}\,, \end{aligned} \qquad (56)$$

the general conservation law having the form $p^\mu + sk^\mu = p'^\mu + p^\mu_+ + p^\mu_-$, and $\{p'\leftrightarrow p_-\}$ symbolizes the contribution of the exchange diagram, in which the final electrons are interchanged.

Since the first-order processes are kinematically allowed in the presence of an external field, a common feature of the processes of the second and higher orders is that virtual particles (a photon in Fig. 12b and an electron in Fig. 12c) can appear on the mass shell. In the case of a monochromatic wave or a constant field, this leads to divergences known as Oleinik resonances [133]. To isolate the divergent contributions, the propagator of each internal line should be split into positive-frequency and advanced parts [220]. The former part contains an additional delta function supported on the mass shell of the virtual particle, which, after squaring, leads to an additional factor $\delta(p^2-m^2)|_{p^2=m^2}$ proportional to the duration of the process τ [203, 206, 221]. This part of the

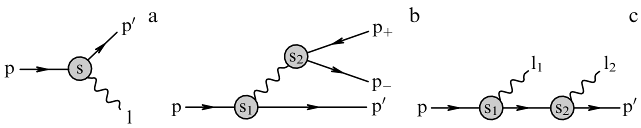

Figure 12. Feynman diagrams in the representation of bare lines and a dressed vertex: (a) photon emission in an external field (nonlinear Compton effect) and second-order processes — (b) trident process and (c) double photon emission.

process is called two-stage or cascade; strictly speaking, it was specifically this part that was observed in the SLAC E-144 experiment [38, 186]. It is easy to see that, in the strong field mode, $a_0 \gg \chi^{1/3}$ (i.e., in the LCCF approximation), its probability $\propto (\alpha\tau/\tau_{\mathrm{f}})^2$ and it factorizes into a convolution of probability distributions of sequential first-order processes.

In practice, to calculate multistage (cascade) processes, numerical simulation is widely used, in which the motion of electrons and positrons in a field is described as classical, that of hard photons is described as ballistic, and the elementary processes of emission of a hard photon by electrons and positrons and photoproduction of a pair are modeled by the Monte Carlo method in the LCCF approximation (see Section 4.4 and Eqns (37) and (46)). This approach, which is now considered standard, is used, for example, in the CAIN [222] and GUINEA-PIG [223] codes for modeling beam collisions in colliders. However, due to the specifics of laser plasma, special codes have been independently developed for modeling processes in strong fields. Several alternative schemes have been proposed for the actual implementation of the main processes considered in Section 4 by the Monte Carlo method [224–229]. In the simplest of the methods [224], the time step Δt of integration of the classical equations of motion of the available particles is chosen so that condition $\Delta t \ll (a_0\omega)^{-1}$ [230] is satisfied, and, in addition, the probability of the process under consideration (for definiteness, photon emission; photoproduction of a pair is included similarly) at this step is small ($R^{\mathrm{CCF}}_{\mathrm{e}\to\mathrm{e}\gamma}\Delta t \ll 1$, which for electrons and positrons with $\chi \gtrsim 1$ is fulfilled automatically due to

$$R^{\mathrm{CCF}}_{\mathrm{e}\to\mathrm{e}\gamma}(\chi)\Delta t \simeq \frac{\alpha m^2\chi^{2/3}}{\mathcal{E}}\,\frac{1}{\omega a_0} \simeq \frac{\alpha}{\chi^{1/3}} \ll 1\,, \qquad (57)$$

taking into account that $\chi \simeq a_0\omega\mathcal{E}/m^2$), and then at each step for each available particle, two pseudo-random numbers $r_{1,2}\in[0,1]$ are generated. If $r_1 < R^{\mathrm{CCF}}_{\mathrm{e}\to\mathrm{e}\gamma}(\chi)\Delta t$, it is assumed that this particle at the considered step emits a photon strictly forward, with the quantum parameter $\varkappa = a_0(kl)/m^2$, determined by the solution of the equation

$$\frac{1}{R^{\mathrm{CCF}}_{\mathrm{e}\to\mathrm{e}\gamma}} \int_0^{\varkappa} \frac{\mathrm{d}R^{\mathrm{CCF}}_{\mathrm{e}\to\mathrm{e}\gamma}}{\mathrm{d}\varkappa}\,\mathrm{d}\varkappa = r_2\,, \qquad (58)$$

where the distribution over $\varkappa$ is defined in Eqn (37) (in practice, to speed up calculations, this distribution is interpolated or tabulated in advance). Such an approach greatly overestimates the probability of emitting soft photons with $\varkappa \ll 1$, for which the LCCF approximation is inapplicable. However, such processes can be ignored, since soft photons certainly do not produce pairs, and their emission has little effect on the electron dynamics. Strictly speaking, based on the meaning of the Monte Carlo method, the simulation results should also be averaged over a large ($> 10^3$) ensemble of simulation implementations; however, for example, when simulating a multiple cascade at long times, it is sufficient to only average over the cascade itself.

We return to the separation of the multi-stage (cascade) part from the amplitude of the process. Other contributions, including interference ones, $\propto \alpha^2\tau/\tau_{\mathrm{f}}$. Therefore, at radiation times $\tau_{\mathrm{r}} \simeq \alpha^{-1}\tau_{\mathrm{f}}$ with an accuracy of $\mathcal{O}(\alpha)$, it is sufficient to take into account only cascade processes, since the remaining contributions (including interference), which correspond to a single-stage process, can significantly manifest themselves only at large times, $\alpha^{-2}\tau_{\mathrm{f}} \sim \alpha^{-1}\tau_{\mathrm{r}}$, and should be modeled in

Monte Carlo codes by separate event generators. Due to the difference between the methods of accounting for cascade and single-stage processes in Monte Carlo codes, the corresponding division of processes into multi- and single-stage processes is of a conceptual nature. In the case of a pulsed field, similar to first-order processes, the sums over s are replaced by integrals, and, instead of the probability per unit time, the total probability of the process over the entire time should be calculated. However, in the case of long pulses ($\tau \gg \tau_{\rm f}$), the total probability of the process again contains contributions proportional to τ^2 and τ, which are identified with two- and one-stage processes, respectively. In addition, proposed in study [208] was an alternative division of the total probability of a process in a finite-duration pulse or the probability over a period in a monochromatic field based on the observation that the probability of a second-order cascade process at $a_0 \gg 1$ is asymptotically $\propto a_0^2$, while the probability of a single-stage process is $\propto a_0$. This approach is reasonable, since a_0 is inversely proportional to the characteristic frequency, i.e., ultimately proportional to the period of the field or its duration. Note that for $a_0 \lesssim 1$ the LCCF approximation is inapplicable, and the division of processes into cascade and single-stage processes breaks down.

Quantitative calculation of spectra and total probabilities even for the simplest second-order processes in the field of a plane wave is only possible numerically. The main problems are the cumbersome contributions due to the mutual interference of the direct process with the exchange and two- and one-stage contributions, and the calculation of the five-fold integral, which remains after removing the delta functions and other simplifications [206, 209]. Although the conceptual possibility of such calculations has been demonstrated in the cited papers, the dependence of the probabilities of processes, spectra, and angular distributions on parameters in all interesting areas of their variation has not yet been fully investigated. It is also worth noting that, according to [209], after complete and accurate consideration of all interference contributions, the probability of a single-stage trident process in a constant crossed field is negative [11] at $\chi \lesssim 20$. The meaning of this result is not yet clear either.

5.2 Self-sustaining quantum electrodynamic cascades

We now consider an ultrarelativistic electron that somehow enters a region of such a strong field that the LCCF approximation is applicable (it has flown into it or has been produced directly in this region (see below)), $a_0 \gg \chi^{1/3}$. Then, according to the discussion above, at times $\tau_{\rm r} \ll \tau \ll \alpha^{-1}\tau_{\rm r}$, cascade (multi-stage) processes dominate in its interaction with the field. In the LCCF approximation, their intensity is determined by the local value (54) of the quantum parameter (3), which in this case is proportional to the component of the Lorentz force acting on it perpendicular to the electron velocity. In the fields close to that of a traveling plane wave, the Poynting vector is nonzero; the value of χ is maximum when the electron moves against the wave and minimum when moving in the direction of the wave. In fields of the standing wave type, the Poynting vector can vanish at the nodes, and then the value of χ is maximum when moving across the field and minimum when moving along it. With the exception of the indicated special geometries, in which the parameter χ is anomalously small, in order of magnitude $\chi \sim (E/E_{\rm cr})\gamma$, where γ is the Lorentz factor of the electron. Therefore, for sufficiently large values of the Lorentz factor, χ can reach the optimal values for the considered processes of ~ 1 even in fields $E \ll E_{\rm cr}$ [31, 186].

In the LCCF approximation, in the course of individual processes of photon emission or the production of a pair by a photon, the value χ of the initial particle is divided between the final ones. In the classical regime $\chi \ll 1$, photons with parameters $\varkappa \sim \chi^2 \ll \chi \ll 1$ are emitted [31], for which the probability of pair production at the next stage of the cascade process is exponentially suppressed. In this regime, the cascade process generated by the electron is reduced to the sequential emission of a large number of soft photons, and the recoil of the electron during the emission of individual photons is negligible and has a cumulative character. This regime corresponds to the classical radiation friction [31, 231] discussed in Section 3. However, at large values of the parameter $\chi \gtrsim 0.1$, the radiation becomes quantum, and its character changes qualitatively. First, most of the energy in the quantum regime is transferred on average to hard photons with quantum parameters $\varkappa \sim \chi$ comparable to the quantum parameter of an electron, so the contribution to the recoil of radiation from individual photons becomes significant. The resulting Doppler shift of radiation to the red region leads to a significant suppression of the average radiation intensity, which can be described by the Gaunt correction factor. Concurrently, radiation due to the precession of the magnetic moment of the electron (spin light) becomes significant. Finally, the so-called straggling effect becomes important. Its essence is that the emission of hard photons, which dominates in the energy balance of radiation, acquires an essentially stochastic character, and the electron moves at times of the order of $\tau_{\rm r}$ between events of their radiation virtually without radiation friction [232, 233].

At $\chi \gtrsim 1$, the emitted hard photons begin to produce pairs, which leads to the development of a QED cascade [234–237]. The same cascades are generated by seed photons entering the region of a strong field with large values of $\varkappa \gtrsim 1$. The cascades generated in a strong field by high-energy particles with $\chi \gg 1$ are quite similar to extensive air showers (EASs) generated in the atmosphere by cosmic rays [238]. The main difference is that the probabilities of emission and production of pairs by photons in a collision with a nucleus are determined by the energy of the incident particle, while in a strong field, by the value of its quantum parameter. At large values of the latter, the multiplicity of the process increases rapidly; however, in the course of its growth, the initial value of the quantum parameter is approximately evenly distributed among the particles of cascade generations, and for the particles, of which the generation consists, it rapidly decreases from generation to generation. When the value of the quantum parameter diminishes to ~ 1, photons cease to produce pairs; the multiplicity stabilizes, and the cascade decays. Therefore, the final multiplicity of such a cascade turns out to be numerically of the order of the value χ of the quantum parameter of the seed particle and cannot be too large. Cascades in the field per se are not exotic either; for example, they are generated by high-energy cosmic rays in Earth's magnetosphere.

However, in a sufficiently strong electric field [12] ($\mathcal{F} > 0$, i.e., $E > H$), a new factor becomes significant, which

[11] The total probability taking into consideration the two-stage contribution is, of course, always positive; this result only refers to the total remaining contribution.

[12] That is, the field that can do work.

fundamentally distinguishes cascades in this field from those generated by fast particles in weak fields or in a medium. Namely, in such a field, electrons can be rapidly accelerated in the interval between emission events, replenishing the energy expended earlier on the emission of a hard photon. In such a regime, which is called the regime of a self-sustaining cascade, the energies of the particles in the cascade do not decrease from one generation to another, but stabilize on average, while the multiplicity of pairs and hard photons increases exponentially with time, and the energy for the formation of a cascade is eventually extracted from the field [239, 240]. Self-sustaining cascades are initiated by particles of moderate rather than high energy with $\chi \gtrsim 1$ (in particular, by those arising at the decay stage of an ordinary cascade [236, 237]) and develop either until all particles escape from the strong field region or until the field is depleted. If the strong-field region is sufficiently large, the latter scenario is realized, in which the resulting cascade multiplicity can reach macroscopic values, and the particle density in the cascade can reach extreme values [241] (see below).

Self-sustaining cascades resemble another well-known process, that of avalanche breakdown of a dielectric in a strong electric field [242] (in which the process of impact ionization is an analog of pair production); for this reason, it is also called an avalanche-type cascade, in contrast to conventional cascades, called shower-type cascades [236]. However, the essential difference again is that the parameter that determines the intensity of the emission of hard photons and photoproduction of a pair in a strong field is not the energy of the incident particle, but its quantum parameter, which must be replenished in the self-sustaining regime when particles are accelerated by a field. This is manifested in subtle differences between the character of particle acceleration required in the cases under consideration. In particular, if a charged particle moves in a strictly constant field, its quantum parameter is conserved; therefore, the inhomogeneity and nonstationarity of laser fields become the decisive factors for the replenishment to be maintained during acceleration [224, 240].

To estimate the threshold intensity required for the development of a self-sustaining cascade, we use a simplified model of a homogeneous uniformly rotating electric field with a strength E and a circular rotation frequency ω, the properties of which are close to those of the field at the antinodes of a plane circularly polarized standing wave [239, 240]. In addition, for simplicity, we assume that, before the emission of a hard photon, the quantum parameter of the electron is $\chi \gtrsim 1$ (consequently, $a_0 \gg 1$ for the LCCF approximation to be applicable), so the probability of emission of a hard photon by an electron per unit time is determined by the lower formula in (38) and, when a hard photon is emitted, the electron almost completely transfers its energy to it (and, consequently, it stops completely) [224, 240]. Immediately after the emission, the electron accelerates again, first along the electric field, rapidly (at times $t \sim m/(eE) \ll \omega^{-1}$, at which the field has time to turn only by a small angle $\omega t \ll 1$) becoming relativistic, and then its Lorentz factor continues to increase with time as $\gamma(t) \simeq eEt/m$. As noted above, during acceleration in a constant field, despite the increase in energy, the parameter χ is strictly conserved, remaining small for an electron initially at rest ($\sim E/E_{\rm cr} \ll 1$). However, in an inhomogeneous (or nonstationary) field, this is no longer the case. In particular, in a purely electric field for an ultrarelativistic electron, Eqn (54) reduces to $\chi(t) \simeq E\gamma(t)\theta(t)/E_{\rm cr}$. It is significant that, due to the rotation of the field, the angle $\theta(t)$ between the field vector and the direction of electron motion also increases in the process of acceleration, in the model under consideration being exactly half of the field rotation angle $\theta(t) = \omega t/2$ [240]. In the general case of acceleration of an electron initially at rest in an arbitrary inhomogeneous nonstationary field, due to inertia, the electron momentum inevitably lags when the Lorentz force acting on it rotates, so the angle between them initially also increases linearly with time, $\theta(t) \simeq \omega t$. For the indicated reasons, at times at which the electron is already relativistic but small compared to the scale of the inhomogeneity or nonstationarity of the field (in our case, ω^{-1}), its quantum parameter increases quadratically with time:

$$\chi(t) \simeq \frac{m}{\omega}\left(\frac{E}{E_{\rm cr}}\right)^2 (\omega t)^2 \,. \tag{59}$$

Substituting the energy $\mathcal{E}(t) = m\gamma(t) \simeq eEt$ and Eqn (59) into the lower formula in (38) and applying the condition that the probability of process (53) is equal to unity, we can estimate the average radiation time $\tau_{\rm r}$, as well as the Lorentz factor $\gamma(\tau_{\rm r})$ and the electron quantum parameter $\chi(\tau_{\rm r})$ at the moment of radiation [224, 240]:

$$\begin{gathered} \tau_{\rm r} \simeq \frac{1}{\omega}\sqrt{\frac{\omega}{\alpha^2 m}}\left(\frac{\alpha E_{\rm cr}}{E}\right)^{1/4}, \\ \gamma(\tau_{\rm r}) \simeq \frac{1}{\alpha}\sqrt{\frac{\alpha^2 m}{\omega}}\left(\frac{E}{\alpha E_{\rm cr}}\right)^{3/4}, \quad \chi(\tau_{\rm r}) \simeq \left(\frac{E}{\alpha E_{\rm cr}}\right)^{3/2}. \end{gathered} \tag{60}$$

Equations (60), which give a rough estimate of the characteristic time of emission or pair production and the average energies $m\gamma$ and quantum parameters $\varkappa \sim \chi$ of particles in a cascade,[13] are presented with the characteristic scales of the considered quantities being indicated explicitly. Note that the factor $\sqrt{\alpha^2 m/\omega}$ appearing in (60), which does not depend on the field intensity, has the meaning of the root of the ratio of the characteristic scale of the binding energy in the hydrogen atom (Rydberg) to the field frequency. For laser fields, it is of the order of several units and, for a rough estimate in order of magnitude, can be omitted with the same accuracy. The field enters the other factors only as a ratio to the characteristic value $E^*_{\rm casc} = \alpha E_{\rm cr}$. In particular, for the emitted photon to be able to subsequently generate a pair, condition $\chi(\tau_{\rm r}) \gtrsim 1$ must be fulfilled. This shows that it is natural to take the value $E^*_{\rm casc}$ as the threshold strength for the development of self-sustaining cascades [240]. In the laser field, $E^*_{\rm casc}$ corresponds to an intensity of $\mathcal{I}^*_{\rm casc} = (E^*_{\rm casc})^2/(4\pi) \simeq 5 \times 10^{25}$ W cm^{-2}. It is important that at $E \gg E^*_{\rm casc}$ condition $\tau_{\rm r} \ll \omega^{-1}$ is also concurrently fulfilled, which implies, notably, that in the field period (and even more so during its duration) the processes of acceleration and emission of a hard photon (as well as the photoproduction of a pair developing on the same time scales) occur repeatedly, leading to the formation of a large-multiplicity cascade. It is easy to check that the conditions $a_0 = eE/(m\omega) \gg \chi^{1/3}(\tau_{\rm r})$ (moreover, with a large margin) and $\gamma(\tau_{\rm r}) \lesssim a_0$ are also fulfilled. The former inequality implies that the LCCF approximation used is really applicable, and the latter implies that, in the process of acceleration by the field, the electron does not have time to

[13] Recall that in the quantum regime the average energies of the emitted photons are comparable to electron energies.

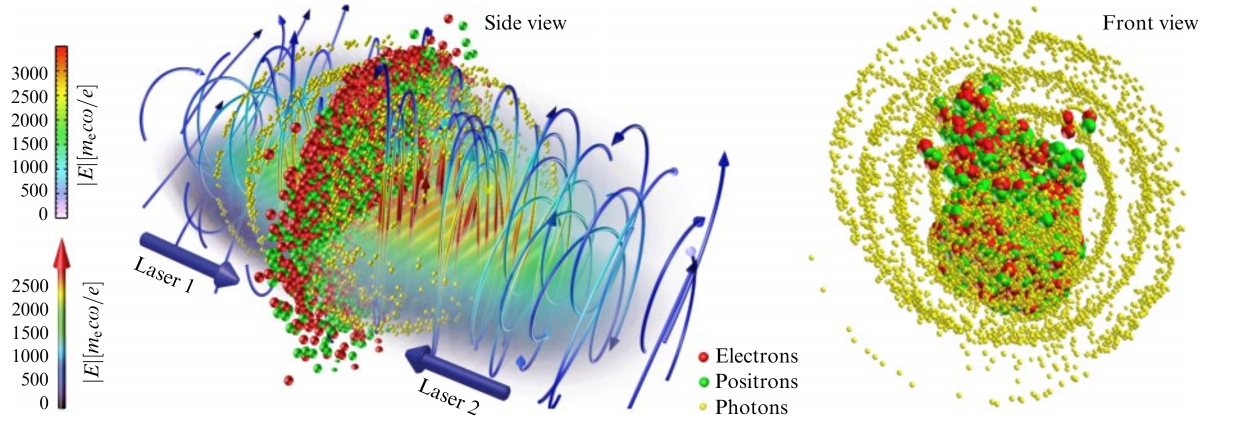

Figure 13. Visualization of a 3D PIC-QED simulation of a self-sustaining cascade in a standing wave. Strength of the electric field resulting from the beating of two laser pulses is represented by a colored band. Curves with arrows show electric field lines. Electrons, positrons, and photons are shown in red, green and yellow, respectively. Particles shown are only a small fraction of those involved in the simulation. (From [254].)

be completely dressed up by interaction with the field to acquire an effective mass prior to emitting the next hard photon.

Of course, the simple estimates presented are intentionally rough and require refinement and factual verification. To simulate the dynamics of a dense plasma in a strong field, PIC-QED codes have been developed [224, 227–229, 241]. In these codes, the implementation of elementary processes by the Monte Carlo method (see Section 5.1) was included in the PIC codes, which model the dynamics of macroparticles in a self-consistent field by means of a joint numerical solution of their equations of motion and Maxwell's equations. QED processes have also been included at the level of macroparticles, and, to control their number, various algorithms for their merging with redistribution of weights have recently been used [243]. In the described scheme, relatively low-frequency radiation associated with collective plasma dynamics is described by a classical field on a grid, while hard photons are described as macroparticles. This does not lead to difficulties, since, as shown in [228], in typical situations the radiation frequency range due to collective plasma processes is much less than the characteristic frequencies of hard photons emitted by ultrarelativistic electrons.

The developed codes were actively used to model cascades generated by individual seed particles in a uniformly rotating field [224, 244], including taking into account the polarization dynamics of photons [245] and electrons [14] [246], and in the field of a standing wave [106, 229, 241, 248, 249]. Typical three-dimensional (3D) modeling is visualized in Fig. 13. In particular, the adequacy of estimates (60) for $E \gg E^*_{\rm casc}$ proposed in [224, 240] was demonstrated in [224]. For fields of a more general form, refinements of estimates were discussed [237, 248], including those based on a detailed analysis of cascade equations [229, 244, 250]. In particular, in Ref. [237], a formula was derived that generalizes Eqn (59) for the case of an arbitrary weakly inhomogeneous electromagnetic field and verified by numerical simulation of cascades generated in the field of a single focused laser pulse (in the case of weak focusing, the properties of such a field differ to the maximum extent possible from those of a homogeneous uniformly rotating field in the original model).

However, according to the simulation results, for $E \sim E^*_{\rm casc}$, the estimates of cascade characteristics (60) yield significantly worse results; in particular, the threshold of cascade generation in a standing wave, which was actually observed in simulation, proved to be almost an order of magnitude lower than $E \gtrsim E^*_{\rm casc}$ and approximately corresponded to an intensity of $\sim 10^{24}$ W cm^{-2} [229, 241, 250–252]. The main reasons for this failure are the strong stochasticity of the process near the threshold, the ambiguity of the very definition of the threshold (for example, its possible dependence on the duration of the field action), and, finally, the fact that hard photons can actually produce pairs not at $\varkappa \gtrsim 1$ but already at slightly lower values [253]. It is a challenging problem to take the listed factors into account in a simple model. The performed PIC-QED simulation has also confirmed that, in the case of a sufficiently large extent of the strong field region at the initial stage of the development of the cascade, its multiplicity first increases exponentially with time, $\propto \exp(t/\tau_{\rm r})$ [224, 229, 241, 246], and, when the critical density determined by Eqn (48) is reached,[15] the external field begins to be depleted (shielded), and the cascade decays. In this mode, up to 10^{14} pairs can be produced per each seed particle, forming a superdense highly nonequilibrium electron–positron plasma with a density of $\sim 10^{26}$ cm^{-3}, the main part of the cascade consisting of GeV-energy γ-quanta [241, 254].

Since it is proposed to attain record high intensities of laser radiation using tight focusing, at which spontaneous production of pairs from a vacuum is predicted already at $\mathcal{I} \sim 10^{28}$ W cm$^{-2} \gg \mathcal{I}^*_{\rm casc}$ [42, 255, 256], the depletion of the field by multiple cascades initiated by the pairs spontaneously generated from the vacuum in the region of maximum field intensity can hinder the attainment of higher laser intensities [237, 240]. We note that, to date, the codes used to model self-sustaining cascades have not included reverse processes, accounting for which *a priori* also enables an alternative scenario of the saturation of cascades by thermalization of the generated plasma at its lower density without significant

[14] It should be noted that in [246] simulation was not carried out using the PIC-QED method but, following [247], by direct solution of kinetic equations on a grid.

[15] For such a density of particles, the cascade energy density $\sim m\gamma n$ is also virtually the same as the energy density of the external field, $\sim E^2/(4\pi)$.

field depletion. Such processes, in particular, include one- and two-photon annihilation of electron–positron pairs (the former process is induced by an external field [31], and the latter one is modified by it). However, according to recent estimates [257, 258], the contribution of both processes to the kinetics of cascades is negligibly small for the considered parameters.

More recent studies have included PIC-QED modeling of cascades for focusing laser pulses on gas [259, 260] and solid [261–265] targets at realistic parameters. In particular, examination is focused on the possible use of cascades as ultra-bright sources of MeV γ rays [266–269] and positron (including polarized [270]) beams [263, 269, 271]. The lowest threshold for the development of cascades is reached in a standing wave formed by isotropic collision of several laser beams [272–274]. An experimental study of cascades in such a situation is planned for the 12-beam 200-petawatt XCELS facility (Exawatt Center for Extreme Light Studies) specially designed with this option in mind [59].

5.3 Radiative corrections and the Ritus–Narozhny conjecture

In addition to affecting standard QED processes (occurring even without a field, such as the scattering of a hard photon or electron on an electron or two-photon pair annihilation) and the above-mentioned induced first-order and tree processes with a large number of final particles, the strong field also modifies the radiative corrections to all processes to which the loop diagrams correspond. The simplest diagrams of this type are shown in Fig. 14: electron (Fig. 14a) [200, 275–277] and photon (Fig. 14b) [278–281] self-energies changing their masses in the field; irreducible correction to the vertex, which determines, inter alia, the dependence of the anomalous magnetic moment of the electron on the field (Fig. 14c) [282, 283]; and the three-photon vertex induced in the field, which corresponds to splitting and merging of photons (Fig. 14d) [284–289]. Due to the number of vertices greater than in tree diagrams with the same external lines, the amplitudes of such processes are proportional to higher powers of α and, therefore, are always small in the absence of a field [76, 137] (the diagram in Fig. 14d only differs from zero in the presence of a field and is dominant among three-photon diagrams). Nevertheless, it is reasonable to take into account and discuss the mentioned processes, since in the presence of an external field they can lead to fundamentally new, albeit subtle, effects [31], which can hopefully be detected in precision experiments. Moreover, we show below that in the strong field regime the contribution of such processes can increase significantly [275] and thus can fundamentally change the behavior of particles in very strong fields.

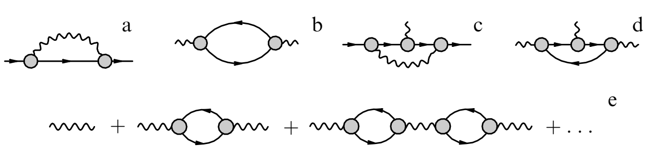

Figure 14. One-loop radiative corrections: (a) mass operator (electron self-energy), (b) polarization operator (photon self-energy), (c) irreducible vertex correction, (d) induced three-photon vertex, (e) photon propagator cumulatively taking into account the one-loop polarization operator. The gray circles represent field-dressed vortices. External lines in the diagrams in panels a–d are assumed to be cut off and are shown solely to indicate the places of their attachment when inserting the considered blocks into diagrams of specific processes.

In the regime that is nonperturbative with respect to the external field, the radiative corrections are calculated by means of standard QED methods [31, 148], described in Sections 4.2 and 5.1, using precise electronic external lines (21) and propagators (55). Loop diagrams are also regularized and renormalized in the standard way, since the divergences arising in these diagrams are the same as in the absence of a field and do not depend on it [31, 278]. In practice, in one-loop corrections, it is convenient to isolate the contribution renormalizable in a standard way in the absence of a field (in particular, that for external lines, which vanishes after renormalization) and the finite contribution due to the influence of the external field per se, which does not require renormalization. This implies that all renormalized quantities (including the scale of the external field itself) are determined in the absence of a field, since the product of the charge and the strength of the external field is a renormalization-invariant quantity.

However, unlike the results of standard QED, due to computational difficulties, reliable results have been only obtained so far for one-particle-irreducible one-loop and partially two-loop corrections and for the corresponding modification of external lines and propagators with cumulative account of one-particle irreducible one-loop mass corrections by summing them or solving the Dyson–Schwinger equation [148, 200, 278] (summing of the cumulative contributions of the one-particle-irreducible correction to the photon self-energy in its propagator dressed with radiative corrections is illustrated in Fig. 14e).

One particle-irreducible one-loop mass corrections to electron and photon lines, called the mass (Fig. 14a) and polarization (Fig. 14b) operators, respectively, are the best studied ones [16] in constant fields [200, 275, 278–280] and in a plane-wave field [276, 277, 281]. As an illustration, we discuss in more detail the results of taking into account the mass corrections to photon lines in the strong field regime, in which they are formed on small scales and due to the exchange by a large number of photons with an external field [278]. In this case, for photons whose frequency substantially exceeds that of the external field, the case of an arbitrary field reduces to a plane wave field [17] and, under the additional condition $a_0 \gg \varkappa^{1/3}$, it can also be considered locally constant [281].

The influence of a constant crossed field on the propagation of a photon with a frequency Ω and wave vector $\mathbf{l}$ directed at an angle ϑ to the Poynting vector of the field is described by a single quantum parameter $\varkappa = eE\Omega(1-\cos\vartheta)/m^3$, which is maximal at $\theta = \pi$, i.e., when the photon propagates in the direction opposite to the Poynting vector of the field. Accounting for cumulative one-particle-irreducible loop mass corrections leads to dynamic generation of masses $\mu_i(\varkappa)$ of the physical (transverse) states of the photon, [18] so

[16] We do not discuss vacuum corrections [290], although they are related to the mass corrections by the gradient expansion [291, 292] but are only relevant when the field strengths approach a critical value (4), or corrections in the Coulomb field, which are beyond the context of the processes in laser fields considered in this review.

[17] It is assumed that the field strength is also much less than the critical value $E_{\rm cr}$; the exact conditions have the form [279] $|\mathcal{F}|/E_{\rm cr}^2,\ |\mathcal{G}|/E_{\rm cr}^2 \ll 1, \varkappa$, where $\varkappa$ is the quantum parameter of a photon, and are fulfilled even in tightly focused fields of available intensity for X-ray and harder photons with $l_0 \gg \omega a_0$.

[18] Since nonphysical modes remain massless, such a dynamically generated mass does not violate gauge invariance.

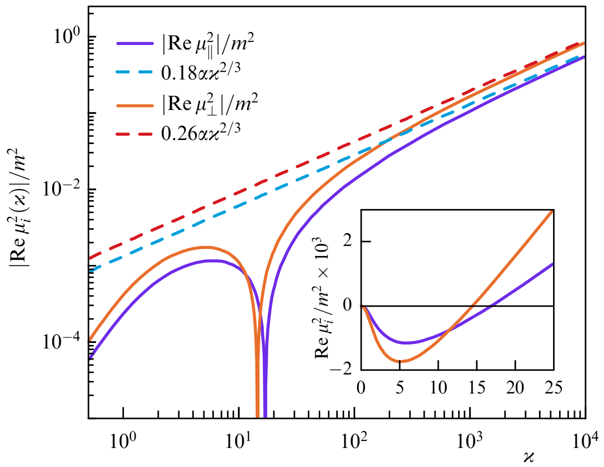

Figure 15. Real part of the effective masses squared of a photon with polarizations along and perpendicular to an electric field in a constant crossed field as a function of the quantum parameter of the photon. Dashed lines show the asymptotic behavior at $\varkappa \gg 1$. Inset shows, on an enlarged scale, the region where the mass squared is negative.

their dispersion equations take the form $\Omega^2 = \mathbf{l}^2 + \mu_i^2(\varkappa)$ [278]. The subscript $i = \{\parallel, \perp\}$ corresponds to the polarizations along the principal axes of the field $\varepsilon_{\parallel,\mu} \propto F_{\mu\nu} l^\nu$ and $\varepsilon_{\perp,\mu} \propto (1/2)\varepsilon_{\mu\nu\alpha\beta} F^{\alpha\beta} l^\nu$. In the frame of reference, where the photon propagates opposite to the wave, the principal axes of the field are directed along the external electric and magnetic fields, respectively. The mass squared of an arbitrarily polarized photon is expressed in terms of the principal values μ_i^2 and the Stokes parameters [293]. The induced masses squared are complex; their imaginary parts, which are negative, are connected by an optical theorem with the probability of producing a pair per unit time by a photon of the corresponding polarization by the relation $R_{\gamma_i \to e^+e^-} = -\mathrm{Im}\,(\mu_i^2)/\Omega$; the probability averaged over photon polarizations was presented in Section 4.3 (see Eqns (4.6) and (47)). In particular, at $\varkappa \ll 1$, they are exponentially small ($\propto \exp(-8/3\varkappa)$). The real part of the photon mass squared is equivalent to the emergence of an effective refractive index $n_i = (1 - \mathrm{Re}\,(\mu_i^2)/\Omega^2)^{1/2}$, the dependence of which on $\varkappa$ is shown in Fig. 15.

In particular, for $\varkappa \ll 1$, we have [278, 295, 296]

$$\mathrm{Re}\,(\mu_{\parallel,\perp}^2) = -\begin{bmatrix} 0.028 \\ 0.050 \end{bmatrix} \alpha m^2 \varkappa^2 \,, \qquad n_{\parallel,\perp}(\mathcal{I}, \theta) \approx 1 + \begin{bmatrix} 0.028 \\ 0.050 \end{bmatrix} \alpha \frac{\mathcal{I}}{\mathcal{I}_{\mathrm{cr}}} \sin^4 \frac{\vartheta}{2} \,, \tag{61}$$

where the result is expressed in terms of the field intensity $\mathcal{I}$ in the laboratory reference system under the assumption that the field is a plane linearly polarized wave. The dependence of the refractive index on polarization is called birefringence; on intensity, Kerr nonlinearity; and on direction (the angle ϑ between the wave vector and the Poynting vector of the external field), anisotropy. All these properties are typical of anisotropic media [297], which, in fact, include an external field. As a result, the propagation of photons in a vacuum in sufficiently strong fields should be accompanied by a wide range of effects typical for the nonlinear optics of anisotropic media [297, 298]; however, in this case, the quantitative magnitude of these effects turns out to be 16 orders of magnitude smaller than in typical crystals. Unfortunately, at currently achievable laser field intensities, all such effects are extremely weak and are either at the limit or beyond the limits of experimental observation. Nevertheless, experimental studies of some of these effects are underway or planned in the foreseeable future [12]. As an illustration, we briefly discuss only a few such effects.

During the propagation of a photon initially linearly polarized at an angle to the principle axes, birefringence leads to the transformation of the photon polarization into an elliptical one. Ellipticity $\delta^2 \sim (\delta\varphi/2)^2$, where $\delta\varphi \sim \Omega d(n_\parallel - n_\perp)$ is the phase difference acquired between the modes corresponding to polarizations along the principal axes at the exit from the strong field region, and d is the propagation length in the field. Experiments to detect this effect in a magnetic field have been carried out for a long time but so far without success [299]. Since laser fields provide much higher field strengths, similar experiments with their use have been discussed and planned. Estimates show that at $\mathcal{I} \sim 10^{22} - 10^{23}$ W cm^{-2}, $\Omega \sim 10$ keV, and $d \sim 10$ μm, the expected signal $\delta^2 \sim 10^{-10}$ [300–302] is at the limit of detection capabilities by modern X-ray polarimetry methods [303], which requires their further development [304, 305].

Furthermore, as can be seen from Fig. 15, at $\varkappa \lesssim 15$, both main values of the effective photon mass are negative, and the refractive index is greater than unity. Therefore, the phase velocity of photons is less than in a vacuum. This condition is characteristic of the emergence of Vavilov–Cherenkov radiation; the corresponding effect was predicted and discussed in papers [306–308]. Since electrons in a strong field undergo immense acceleration, $w \sim m\chi$, they inevitably radiate also due to the synchrotron (for $\chi \gtrsim 1$, quantum) mechanism considered in Section 4.2. Cherenkov radiation in a strong field in a vacuum apparently cannot be observed in its pure form but only in the form of synergistic synchrotron Cherenkov radiation [309–311], i.e., it should manifest itself in a modification of the intensity, angular distribution, and spectrum, and also (due to the presence of birefringence) in a nonlinear dependence of its polarization on the parameters, which is complex compared with that of the usual nonlinear Compton effect.

Finally, according to Eqn (61), the stronger the field, the smaller the phase velocity of photons propagating at an angle to the Poynting vector, which should lead to focusing of the probe photon beam near the maximum of an inhomogeneous strong field, a special case of the nonlinear optical mutual focusing of crossed light beams in strong fields [312]. Since for photons propagating along the wave ($\vartheta = 0$) the effective refractive indices remain equal to unity, and the vacuum polarization does not manifest itself, the issue of possible self-focusing of a strong wave in a vacuum is subtler and, although it has already been discussed [312–314], in our opinion, it has not been definitively clarified yet.

At $\varkappa \gtrsim 1$, the imaginary part of the photon mass squared in a constant crossed field is no longer small, which corresponds to its possible decay into an electron-positron pair (see Section 4.3). At $\varkappa \gtrsim 15$, its real part becomes positive, which corresponds to the superluminal phase velocity and disables a Cherenkov radiation channel. For $\varkappa \gg 1$, we have the asymptotic dependences [278]

$$\mathrm{Re}\,(\mu_{\parallel,\perp}^2) = \begin{bmatrix} 0.18 \\ 0.26 \end{bmatrix} \alpha m^2 \varkappa^{2/3} \,, \qquad \mathrm{Im}\,(\mu_{\parallel,\perp}^2) = -\begin{bmatrix} 0.30 \\ 0.46 \end{bmatrix} \alpha m^2 \varkappa^{2/3} \,, \tag{62}$$

Table. Known asymptotic forms of radiative self-energy corrections for the photon (left) and the electron (right).*

			One loop				
(1a)	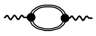	$\boldsymbol{\alpha\chi^{2/3}}$	[278]	(1b)		$\boldsymbol{\alpha\chi^{2/3}}$	[275]
			Two loops				
(2a)	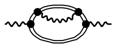	$\alpha^2\chi^{2/3}\log\chi$	[315]	**(2b)**	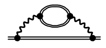	$\alpha^2\chi\log\chi$	[148, 203]
				(2c)		$\alpha^2\chi^{2/3}\log\chi$	[213]
			Three loops				
				(3d)	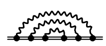	$\alpha^3\chi^{2/3}\log^2\chi$	[316]
(3a)	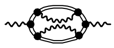	$\alpha^3\chi^{2/3}\log\chi$	[316]	(3e)	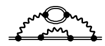	$\alpha^3\chi^{4/3}$	[316]
(3b)	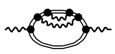	$\alpha^3\chi^{2/3}\log\chi$	[316]	(3f)		$\alpha^3\chi\log^2\chi$	[317]
(3c)	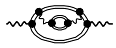	$\alpha^3\chi\log^2\chi$	[317]	**(3g)**		$\boldsymbol{\alpha^3\chi^{5/3}}$	[317]

* For each diagram, asymptotic dependence on the quantum parameter and a reference to the source are displayed. Dependence that grows most rapidly in each order is highlighted in bold.

actually applicable for the imaginary part at $\varkappa \gtrsim 10^2$, and, for the real part, at $\varkappa \gtrsim 10^3$ (see Fig. 15). In this regime, in addition to the above effects, the dependence of the effective refractive indices on frequency becomes significant (dispersion, in particular, $n_i(\Omega \to \infty) = 1$). It is of importance that the radiative correction to the electron mass at $\chi \gg 1$ has the same (up to a common numerical coefficient of the order of unity) asymptotic form $\delta m^2 \simeq \alpha m^2 \chi^{2/3}$, where χ is the quantum parameter of the electron [31, 200]. These arguments and Eqn (62) show that in this regime the radiative corrections for an electron and a photon in a constant crossed field are proportional to the combined parameters $g_\chi = \alpha\chi^{2/3}$ and $g_\varkappa = \alpha\varkappa^{2/3}$, respectively, and grow unboundedly with an increase in the quantum parameter proportional to the field strength and the energy of the corresponding particles. In Ritus's papers [31, 200, 275], this effect was called the amplification of radiative corrections by an external field.

For $g_\chi = \alpha\chi^{2/3} \gtrsim 1$ ($g_\varkappa = \alpha\varkappa^{2/3} \gtrsim 1$), which corresponds to $\chi, \varkappa \gtrsim 1600$, we obtain $\delta m^2 \gtrsim m^2$ (correspondingly $\mu^2 \gtrsim m^2$); at the same time, the probabilities of emission of a hard photon (see Eqn (38)) and photoproduction of a pair (see Eqn (47)) become of the order of unity in the proper frame [19] at Compton times $\tau \sim m^{-1}$, indicating that in such strong fields the interaction of particles with the field should already be completely determined by field-induced radiative corrections [20] [31, 199].

Since the probability is bounded by unity, an unlimited increase in one-loop corrections implies that in such a regime the quantum processes under consideration, which are nonperturbative in interaction with an external field, must also lose their perturbative character with respect to radiative corrections (at least of certain types). In the modern literature, this hypothesis is called the Ritus–Narozhny conjecture [199]. To study the possibility of such a doubly nonperturbative regime in more detail, the well-known two-loop single-particle irreducible mass corrections for a photon and electron in a constant crossed field were analyzed [148, 203, 213, 315], and some three-loop corrections were estimated [316, 317]. The results of these studies are summarized in the table, where for each correction the diagram corresponding to it, the type of the asymptotic behavior for a large value of the quantum parameter, and a reference for detailed acquaintance. It can be seen that, for a given number of loops in higher orders, the leading contributions come from corrections in the form of (3c), (2b), and (3g), the diagrams of which are maximally saturated with single-loop polarization inserts (bubbles) and are called bubble diagrams. In the right column (for an electron), the ratio of successive corrections in the transition from two loops to three loops is $\propto g_\chi = \alpha\chi^{2/3}$, in accordance with the conjecture. In a recent paper [294], all such bubble corrections were considered and summed up (Fig. 16); notably, it was shown that their ratio in sequential orders indeed stabilizes and is preserved in all higher orders. In the first lower orders, however, it is anomalously small, which leads to the suppression of the nonperturbative resummed contribution. In particular, in the left column of the table, all the asymptotic forms (by ignoring the logarithmic factors that are insignificant for our purposes) are shifted by one towards higher orders due to the presence of an extra (not included in the chain of sequential bubbles) common electron–positron loop and, in displayed orders, not yet attained stabilization. However, by analogy, it is natural

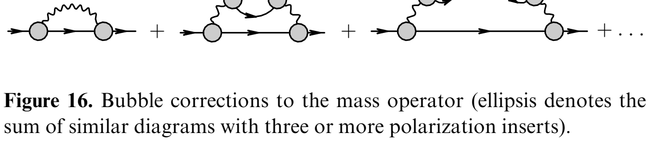

Figure 16. Bubble corrections to the mass operator (ellipsis denotes the sum of similar diagrams with three or more polarization inserts).

[19] To unify the terminology for electrons and photons, here, the 'proper frame of a hard photon' conventionally means such a reference frame in which the photon frequency is of the order of the rest mass of the electron.
[20] Note that the universal asymptotic form $\propto \chi^{2/3}, \varkappa^{2/3}$, characteristic of a crossed field, of the dependences of the probabilities of elementary processes and the squares of effective masses, which are associated with them by virtue of the optical theorem, on the quantum parameter, which are in turn related (see Section 4.4) to their scale of formation, are also unambiguously fixed by their independence from the electron mass as the field strength tends to infinity.

to assume that the stabilization should occur upon transition from three-loop to four-loop corrections.

The meaning of $g = \alpha\chi^{2/3}$ as an expansion parameter for bubble-type corrections in a constant crossed field can be explained without complicated calculations as follows. The analysis and estimates of the characteristic formation time given in Section 4.4, namely, Eqn (51), are applicable to mass-type corrections for an electron. However, since the photon in the loop is now virtual with $l^2 \neq 0$ and $\Omega = (\mathbf{l}^2 + l^2)^{1/2} \approx |\mathbf{l}| + l^2/2|\mathbf{l}|$, one should additionally take into account the contribution of the photon $\simeq l^2/(2\Omega)$ to energy mismatch (50) at the times of loop formation. The characteristic scale of photon virtuality is determined from the condition of commensurability of the electron and photon contributions to the energy mismatch $Q \simeq 1/\tau_{\rm f}$ (where the formation time $\tau_{\rm f}$ of the radiation process is determined in Eqn (51)), whence, taking into account $\varkappa \simeq eE\Omega/m^3$, we find

$$l^2 \simeq m^2 \frac{\varkappa^{4/3}}{(\chi\chi')^{1/3}}\,, \tag{63}$$

where, in this case, $\chi' = \chi - \varkappa$ is the quantum parameter of the virtual electron in the external loop. In bubble diagrams, each photon line is associated with a free propagator $\sim 4\pi/l^2$, and each bubble, with a polarization operator, up to tensor structures $\sim \mu^2$. Hence, it is clear that the characteristic parameter of the loop expansion in terms of the number of bubble inserts is the ratio

$$g = \frac{\mu^2(\varkappa)}{l^2} \simeq \frac{\mu^2(\varkappa)}{m^2\varkappa^{4/3}}(\chi\chi')^{1/3}\,. \tag{64}$$

The nature of the $\mu_i^2(\varkappa)$ dependence was already discussed above; it shows, among other things, that the ratio $\mu_i^2(\varkappa)/\varkappa^{4/3}$ is limited and reaches a maximum of $\sim \alpha m^2$ at $\varkappa \sim 1$. Then, as can be seen from Eqn (64), for $\chi \gg 1$, indeed $g \sim \alpha\chi^{2/3}$, in accordance with the results of [294].

It should be noted that the dominance of bubble corrections [294, 317] assumed on the basis of the analysis of the table is still a hypothesis, since, for the same asymptotic behavior in the one-loop approximation, the suppression of electron mass corrections in comparison with bubble ones remains unclear and, possibly, specific to the studied lowest orders. In addition, since corresponding calculations are very cumbersome, the role of radiative corrections associated with the modification of the vertex (Fig. 14c) has not yet been assessed in any processes, even in the simplest process of photon emission. Based on the experience of calculations in the absence of a field, it was only assumed that it is insignificant.[21] It is this argument that explains the absence of corresponding diagrams in the table. The vertex correction itself (Fig. 14c) was considered in [282, 283], where it was shown that, although the leading contribution in it is also $\mathcal{O}(g)$, it drops out of the amplitudes of the processes, taking into account mass electronic corrections of the same order; thus, at least on the mass shell, only the contributions $\mathcal{O}(\alpha\chi^{1/3}) \ll \mathcal{O}(g)$ [283] are significant. This conclusion implies that a gauge should exist in which the corrections to the vertex can be asymptotically neglected. This conclusion needs confirmation and reliable justification, since it would allow, neglecting the vertex corrections, finding a self-consistent solution of the Dyson–Schwinger equations and systematically taking into account the combined effect of all mass corrections in the nonperturbative regime.

The possibility of experimental implementation of the considered nonperturbative regime was also discussed. It apparently cannot arise in self-sustaining cascades due to doubts regarding the conceptual possibility of generating electric-type fields of the Schwinger intensity (capable of accelerating and concurrently generating particles from a vacuum), since, given estimates (60), for them $\alpha\chi^{2/3} \sim E/E_{\rm cr} \lesssim 1$. Therefore, the only option is to inject sufficiently energetic particles into the field. However, while the processes considered earlier, where the condition $\chi \sim 1$ could be relatively easily implemented using ultrarelativistic particles of GeV energies, and the nonperturbative regime of interaction with the external field was attained already at $a_0 \gtrsim 1$, in the case under consideration, for the nonperturbative character to develop, also with respect to radiative corrections, significantly larger values, $\chi \gg 10^3$, are required and, consequently, a much more stringent restriction on a_0 should be set. The latter requirement is important because, as calculations in the plane wave field clearly demonstrated [318, 319], asymptotic forms like (62) with a power law dependence on the quantum parameter, which provide amplification of single-loop mass corrections in a strong field, as well as asymptotics (38) and (47) for the processes of radiation or decay associated with them by virtue of the optical theorem, only arise if condition $a_0 \gg \chi^{1/3}$ is satisfied, which determines the multiphoton nature of the interaction with the external field and ensures the applicability of the LCCF approximation (see Section 4.4). Moreover, as we have seen, bubble-type electron mass corrections are formed by relatively soft virtual photons with quantum parameter $\varkappa \sim 1 \ll \chi$, for which the formation time of process (51) is even longer and, consequently, the applicability condition for the LCCF approximation is even more stringent: $a_0 \gg \chi^{2/3}$. In addition to providing a sufficiently strong field, for the possible particle interaction with this field in the regime under consideration to be practically implementable, it is also necessary to additionally provide a sufficiently sharp increase in the field when test particles enter it. This is necessary to ensure the quenching (absence of radiative emission) of electrons with large $\chi \gg 1$ or decays of photons from $\varkappa \gg 1$ into pairs before they reach the region of the maximum field [320, 321]. To date, it has already been shown that suitable conditions can in principle be obtained in colliding GeV electron beams in lepton colliders [321], during the passage of ultrarelativistic particles through crystals [322] and also during their interaction with attosecond pulses generated upon reflection of multipetawatt femtosecond laser pulses from a solid target [323, 324].

The search for the characteristic properties and, specifically, the calculation of radiation processes in the described doubly nonperturbative regime, actively continue and are still far from being completed. It is worth mentioning that the most important of these properties is presumably the fundamental instability of all particles with respect to elementary processes of radiation or decay at the times of their formation [199]. For example, the ratio of the characteristic lifetime of a photon to the time of formation of its

[21] Apparently, noting that for $\chi \gg 1$ the imaginary and real parts of the mass and polarization operators are of the same order, and, according to the optical theorem, the imaginary parts of the contributions that do not contain vertex corrections correspond to direct contributions, and those containing such corrections, to the exchange contributions to the probability of emission or decay, and taking into account the fact that for ultrarelativistic particles the latter are suppressed in comparison with the former.

emission is

$$\frac{\tau_\gamma}{\tau_\mathrm{f}} \simeq \left(\frac{R_{\gamma\to \mathrm{e^+e^-}}}{Q}\right)^{-1} \sim \left(\frac{\mathrm{Im}\,\mu^2/\Omega}{l^2/\Omega}\right)^{-1} \sim \frac{l^2}{\mu^2} \sim \frac{1}{g} \ll 1 \quad (65)$$

at $g \gg 1$. Since the kinematics of photon emission and photoproduction of a pair in the ultrarelativistic limit are identical up to the notation, the same estimate also holds for the ratio of the time of emission of a hard photon by an electron to the time of formation of pair photoproduction. This result implies that the observed manifestations of the nonperturbative regime at $g \gg 1$ should be associated with processes of large multiplicity $\propto g$ and moreover, single-stage (coherent) processes, in contrast to the cascades considered in Section 5.2. However, as noted, the possibilities of calculating such processes in an external field are still very limited, so their implementation requires the development of basically new calculation methods.

6. Influence of the laser field on decays of nuclei and elementary particles

Decays play an important role in elementary particle physics, cosmophysics, and nuclear physics [325, 326]. Naturally, the possible influence of external factors on the decay rates attracts the attention of many researchers. Two options seem especially promising: (1) changing the selection rules due to the effect of an external field, as a result of which decays forbidden under normal conditions can be realized and occur with a high probability; (2) a multiple increase in the rate of allowed decay. In the case of the α- or β-decay of atomic nuclei, the problem acquires significant practical interest in connection with the problem of radioactive waste disposal [327]. The idea to accelerate decay by means of an electromagnetic field is also of interest for fundamental physics.

The history of theoretical research on the possibility of controlling decays by means of a strong electromagnetic field is more than half a century long. Although the answer to the question about the strength of the external field required for a significant change in the muon decay rate was given at the dawn of the laser era in [328], which is well known and cited in the scientific community, and similar estimates for β-decays of nuclei have been known since the 1980s [329, 330], erroneous articles devoted to this topic are still published in renowned physics journals. These ‘sensational’ publications usually ‘substantiate’ the possibility of a significant — severalfold or even many orders of magnitude — increase in the decay rate by using large-wavelength laser radiation. In Sections 6.1–6.3, we present estimates showing that a noticeable effect on the decay rate can only be provided by laser fields of extremely high intensity, which is currently unattainable and hardly achievable at all. We also explain the origin of the most typical error, which leads to a significantly overestimated value of the decay rate.

6.1 Threshold field for α- and β-decays

The development of an exact theory of α- and β-decay in an intense external electromagnetic field is not possible for the same reason as in the case of nonlinear ionization of atoms and molecules by strong laser fields: there is no exact analytical solution of the Schrödinger, Klein–Gordon, or Dirac equations that describe the state of a charged particle in a plane electromagnetic wave in the presence of Coulomb, strong, or electroweak interaction. However, there is also a significant difference between the problems of ionization and decay: while the analysis of ionization processes using the numerical solution of non-stationary single-particle Schrödinger or Dirac equations has become a routine procedure in recent decades, in the case of decays in an external field, this approach is unrealizable for the following reasons. First, the characteristic decay time (for example, the half-life $\tau_{1/2}$), which determines the evolution of the wave function, usually exceeds the laser pulse duration by many orders of magnitude. Second, for a correct numerical description of the wave function in the particle localization region, a calculation with a very high spatial resolution on the scale of the size of the nucleus or the radius of the weak interaction would be required. This scale is negligible compared to the amplitude of oscillations of a charged particle in the radiation field. Assuming a laser pulse duration of $\tau_\mathrm{L} \simeq 100$ fs, an intensity of $\mathcal{I} \simeq 10^{26}$ W cm^{-2}, and a wavelength of $\lambda = 1$ μm, it can be easily verified that, in the decay of a uranium-238 nucleus, the ratios of these scales are, respectively, $\tau_\mathrm{L}/\tau_{1/2} \approx 10^{-30}$ and $l_\alpha/l_\mathrm{L} \approx 10^{-7}$. Here, l_α is the spatial scale characteristic of α-decay (see the estimate below), $l_\mathrm{L} = 2eE_\mathrm{m}/(m_\alpha\omega^2)$ is the swing range of a nonrelativistic α-particle in the laser wave field, and E_m is the amplitude of the electric field strength. Thus, the numerical calculation of the wave function of the decay products with the accuracy required to detect its small changes due to the action of a laser wave would require unimaginable computing resources. On the other hand, it is precisely the smallness of the ratios $\tau_\mathrm{L}/\tau_{1/2}$ and l_α/l_L that enables making simple qualitative estimates, which demonstrate the degree of possible influence of a strong electromagnetic field on such processes. The arguments given below basically follow [190, 329–331].

Events of α- and β-decay are localized in a small spatial region and occur in a short time. In the case of the β-decay $\mu^- \to e^-\tilde{\nu}_e\nu_\mu$, the values of these quantities, which are determined by the Compton wavelength for the muon, are $l_\beta \simeq 10^{-13}$ cm and $\tau_\beta \simeq 10^{-23}$ s, respectively. In the α-decay of nuclei, the same values are given by the width of the Coulomb barrier through which the α-particle tunnels, and by its characteristic velocity. Typical values in this case are $l_\alpha \simeq 10^{-12}$ cm and $\tau_\alpha \simeq 10^{-21}$ s. At distances greater than $l_{\alpha,\beta}$, the decay products can be considered free particles, so the influence of the electromagnetic wave field on their motion, although potentially significant, does not lead to a change in the decay probability. It is clear that, for a significant change in the probability, the external field must do significant work on length $l_{\alpha,\beta}$. It is easy to understand, given that times $\tau_{\alpha,\beta}$ correspond to frequencies $\omega \sim 1/\tau \approx 10^{21}$ s^{-1} or higher, i.e., quantum energies $\hbar\omega > 1$ MeV, that, in estimating this work, the field of any laser source can be considered constant. In a constant field with strength E, the energy transferred to a charged particle during the decay time is, in order of magnitude,

$$\Delta\mathcal{E}_{\alpha,\beta} \simeq eEl_{\alpha,\beta}\,. \quad (66)$$

If quantity (66) is comparable to the energy scale $Q_{\alpha,\beta}$, which characterizes the decay, the influence of the external field on the dynamics of the process certainly becomes significant. This implies an estimate for the electric field strength $\tilde{E}$ at which the decay rates should alter significantly:

$$\tilde{E}_{\alpha,\beta} \simeq \frac{Q_{\alpha,\beta}}{el_{\alpha,\beta}}\,. \quad (67)$$

For the α-decay of the uranium nucleus ($Q_\alpha \approx 4.2$ MeV) and the β-decay of the muon ($Q_\beta \simeq m_\mu c^2 \approx 100$ MeV), estimate (67) yields $\tilde{E}_\alpha \simeq 10^{19}$ V cm^{-1}, $\tilde{E}_\beta \simeq 10^{21}$ V cm^{-1}, respectively. Note that $\tilde{E}_\beta = m_\mu^2 c^3/e\hbar$ is just the critical QED field for the muon [328, 332, 333]. For α-decay, the threshold field $\tilde{E}_\alpha$ turns out to be smaller, but it also exceeds the critical QED field (4) by about three orders of magnitude. In nuclear decays and in transitions $p \to ne^+\nu_e$ (forbidden in the absence of an external field), the energy Q_β is much lower than in the muon decay, which, in accordance with Eqn (67), lowers the threshold field, but even then it is comparable to (4) or even exceeds it (see, for example, the estimates reported in [330, 334]). Laser fields of such strength cannot as yet be obtained.

6.2 Semiclassical estimate for the α-decay rate

A more accurate analysis shows that value (67) may turn out to be overestimated and needs to be refined. We show this via the example of α-decay, for which the semiclassical calculation is easily performed using the Gamow model [335]. Given the estimate for τ_α, we can consider the laser wave field to be slowly changing even in the case of X-ray sources with a photon energy of about 1 keV and an oscillation period of 10^{-18} s. To an even greater extent, this applies to lasers in the optical and infrared ranges. Generalizing the Gamow model for the case of a slowly varying external field, for which time can be considered a parameter, we present the decay probability per unit time (decay rate) in the form [331]

$$R \approx \nu_0 \exp\left(-\frac{2}{\hbar}\int_0^b \sqrt{2m_r\left[V(r) - ez_{\text{eff}}\mathbf{E}(t)\,\mathbf{r} - Q_\alpha\right]}\,\mathrm{d}r\right). \quad (68)$$

Here, ν_0 is the oscillation frequency of the α-particle in the nucleus [336], m_r is the reduced mass of the α-particle and the daughter nucleus, $V(r)$ is the potential energy of their interaction, which is the Coulomb repulsive field over most of the trajectory, $z_{\text{eff}} = (2A - 4Z)/(A+4)$ is the effective charge determined by the charge Z and mass A numbers of the daughter nucleus, and finally, $b = 2Ze^2/Q_\alpha$ is the potential barrier width in the absence of a laser field. In Eqn (68), the origin of coordinates coincides with the center of inertia of the parent nucleus. Due to the short time of sub-barrier motion, even in a very strong laser field, an α-particle remains nonrelativistic until the moment it leaves the barrier. The further (for $r > b$) motion of an α-particle may well be relativistic, but it does not affect the probability in any way.

Assuming that the laser field is weak compared to the Coulomb field, the sub-barrier trajectory of the α-particle can be approximated as a straight line, which would be the trajectory in the absence of a laser wave. The same small factor enables the integral in Eqn (68) to be expanded into a series with respect to the external field. Details of the calculations are presented in [331]. As a result, at $E \ll \tilde{E}_\alpha$, the decay rate is represented as

$$R(t) = R_0 R_L(t)\,. \quad (69)$$

Here, $R_0 = \nu_0 \exp(-2\pi\nu_\alpha)$ is the Gamow decay rate in the absence of a field, $\nu_\alpha = 2Ze^2/(\hbar v_\alpha)$ is the Sommerfeld parameter, and $v_\alpha = \sqrt{2Q_\alpha/m_r}$ is the velocity of the α-particle. The field factor R_L describing the change in the decay rate has the form

$$R_L(t) \approx \exp\left(\frac{2E(t)}{E_{\text{eff}}}\cos\theta\right), \quad (70)$$

where θ is the angle between the directions of the particle emission and the electric field of the wave. In Eqn (70), the value of the effective field arise,

$$E_{\text{eff}} = \frac{2\hbar\sqrt{2}\,Q_\alpha^{5/2}}{3\pi Z^2 z_{\text{eff}} e^5\sqrt{m_r}}\,, \quad (71)$$

different from that in Eqn (67).

It follows from Eqn (70) that the influence of the external field on the decay rate becomes significant at $E \simeq E_{\text{eff}}$. It is easy to see that field (71) is $3\pi\nu_\alpha/8 \gg 1$ times smaller than $\tilde{E}_\alpha$, so naive estimate (67) turns out to be overestimated by about an order of magnitude. Nevertheless, field (71) as well is beyond the limits of modern experimental possibilities. Referring the reader for numerical data to Ref. [331], which also gives the next term in the expansion of the exponent in Eqn (70), we only consider a typical example: in the case of the decay of the ^{232}Pu nucleus with $Z = 92$ and $Q_\alpha \approx 5$ MeV, the effective field $E_{\text{eff}} \approx 10^{17}$ V cm^{-1} is almost an order of magnitude greater than the critical QED field (4).

Choosing for evaluation the intensity value $\mathcal{I} = 10^{26}$ W cm^{-2}, which can be achieved in the next 10–20 years, we get that, for the same decay, the factor R_L differs from unity at the field maximum by $\approx 6 \times 10^{-3}$, and, after averaging over oscillations and directions of emission of an α-particle, by 3×10^{-6}. Taking into account the extremely small number of decays that occur in the volume of the laser focus during the pulse duration, these numbers imply that even such a strong laser field has virtually no effect on the α-decay of nuclei.

Two important facts should be noted.

(1) The inequality $E_{\text{eff}} \ll \tilde{E}$ is typical of tunnel processes. A significant influence of the additional interaction on the tunneling probability is achieved already when the correction to the classical action due to this interaction becomes of the order of $\hbar$, while at $E \simeq \tilde{E}_\alpha$ it becomes of the order of the unperturbed action, i.e., $\gg \hbar$. On the contrary, β-decay is not represented as a tunneling process, and such a decrease in the threshold field does not occur for it. The threshold field $\tilde{E}_\beta$, which we obtained from estimates, also appears in a strict quantitative calculation [190, 328].

(2) The expansion of the classical action, leading to Eqns (69) and (70), is carried out in terms of the parameter $E/\tilde{E}$, so the terms in the exponent are not necessarily small. Formula (70) is also applicable for $E \simeq E_{\text{eff}}$.

6.3 Kinematic and dynamic effects

We now discuss the reason for the characteristic error made in solving the problem of the effect of laser radiation on decays, which leads to 'sensational' predictions of possible laser control of radioactive decay processes. Note that, in addition to the *dynamic* effect considered above, which turns out to be vanishingly small, electromagnetic radiation can also cause a significant *kinematic* effect. It consists in a change in the decay rate due to relativistic time dilation for decaying particles oscillating in the wave field and a change in the kinetic energies of the decay products moving under the action of the Lorentz force. By virtue of the inequality $\tau_{\alpha,\beta} \ll 1/\omega$, the latter effect is described even more easily than the dynamic one. Decay can be considered an instantaneous process that sets the initial condition for the motion of a charged particle in a laser field. In most studies devoted to this topic, the laser field is described in the plane wave approximation. The kinematic momentum of a particle $\mathbf{p}(t_0)$ and its kinetic energy $\mathcal{E}$ at the moment of decay t_0 are related to the quantities $\mathbf{P}_\perp$ and P_- conserved in the plane wave field by the relations

$$\mathbf{p}_\perp(\varphi_0) = \mathbf{P}_\perp - \frac{e}{c}\,\mathbf{A}(\varphi_0)\,, \qquad cp_z(\varphi_0) = \mathcal{E} - cP_-\,, \qquad (72)$$

where $A_\mu(\varphi)$ is the 4-potential of the plane wave field propagating along the z-axis, $\mathbf{p}_\perp$ is the momentum in the plane perpendicular to the direction of propagation, and $\varphi_0 = \omega t_0 - kz_0$ is the phase of the field at the spatiotemporal moment of decay. Section 6.2 shows that at $E \ll E_{\text{eff}}$ the decay dynamics does not change under the action of an external field. Consequently, the magnitude of initial momentum $\mathbf{p}(t_0)$ is always the same, and it is distributed isotropically in space. Based on this condition and using Eqn (72), it is easy to find the spectrum of decay products, which turns out to be broad in strong fields. The scale of broadening of the spectrum is set by the dimensionless parameter $a_0 Q_{\alpha,\beta}/\hbar\omega \sim a_0^2/\chi$.

Since the β-decay of an elementary particle or nucleus is not described by the semiclassical tunneling model, the simple qualitative arguments given in Section 6.2 cannot be used, and estimates of the decay rate require rather cumbersome calculations, which can be found in [190, 328, 329, 333]. Calculations are simpler in the case of nonrelativistic β-decays of nuclei [190, 329, 330] with a relatively small value of Q_β, which is equal to 18.6 keV in the case of tritium decay. For α-decay in a strong field, the energy distributions of the emitted particles were obtained in [337]. Despite significant differences in the details of calculations, the kinematic effects in the spectra of α- and β-decays are qualitatively similar. In both cases, the dependence on the kinematic parameters disappears upon integration over the spectrum. For nonrelativistic nuclear decay [190, 329],

$$R = R_0\left(1 + K\,\frac{E_{\text{m}}^2}{\tilde{E}_\beta^2}\right), \qquad (73)$$

where R_0 is the decay probability in the absence of an external field, K is a numerical coefficient, and the threshold field for $Q_\beta \approx 20$ keV turns out to be close to the critical QED field (4), i.e., still very strong.

What is the origin of large errors in estimating the decay rate in the presence of an external field? The complexity of calculating the total decay probability by integrating the spectrum is as follows. The arguments of the Bessel functions in the formulas for the spectral and angular distribution [328, 333] contain the parameters $\simeq a_0^2/\chi$ and $\simeq a_0^3/\chi$, which can be very large in a superstrong field. In calculating the total probability of the process, a large number of oscillating terms are mutually cancelled. Even an insignificant error in the numerical calculation of the Bessel function of an immense argument or insufficient accuracy in using the analytical asymptotic forms can lead to the compensation being incomplete and, as a result, quantities persist that become infinitely large in a constant field, at $\omega \to 0$. Errors of this kind were apparently made in Refs [338–341], which predicted a gigantic increase in the β-decay rate in a laser field of moderate intensity.

Errors leading to the 'survival' of $\sim 1/\omega$ factors in the decay probability can also arise in analytical calculations that use inadequate approximations. As an example, study [342] can be cited, in which the unsubstantiated averaging of a potential oscillating in an external field over the period of this field led to the averaged potential being dependent on a_0 and not having a static limit. This case and the errors made in the papers that followed the publication of [342] are analyzed in detail in [331]. It is apparent that the very presence in the formulas for the probabilities of decays in an alternating external field of factors containing a_0, $Q/(\hbar\omega)$, and other quantities $\propto \lambda$ leads to a conclusion that an arbitrarily weak and slowly varying field can significantly change these probabilities, a conclusion which contradicts elementary physical intuition and, therefore, clearly indicates that these calculations are incorrect.

In conclusion, we note that the issue of the possible effect of a strong laser field on the reaction of fusion of light elements is also of interest (see, for example, recent paper [343], in which the effect of an X-ray laser field on the d–t fusion reaction rate was theoretically studied). Due to the nuclear charge being small compared to that in the case of α-decay, the barrier height turns out to be much lower, which makes it possible to expect a noticeable change in the fusion rate at intensities of $\simeq 10^{23}$ W cm^{-2} and photon energies of $\simeq 1$ keV. The main difficulty that hinders experimental observation of an increase in the fusion rate is that only a small number of reactions can occur in the laser focus during the action of a laser pulse of $\tau_{\text{L}} \simeq 100$ fs.

7. On the concept of Unruh radiation

Recently, various experimental proposals for the detection of 'Unruh radiation' using superpowerful lasers have become popular [344–348]. The essence of the Unruh effect [349] is that a uniformly accelerated observer sees the standard vacuum state as a thermal bath with the Unruh temperature

$$T_{\text{U}} = \frac{\hbar w}{2\pi k_{\text{B}} c}\,, \qquad (74)$$

where w is the observer's acceleration and k_{B} is the Boltzmann constant. The term 'effect' in this context is not very adequate (in our opinion, it would be more correct to speak, for example, about the concept), but it is firmly rooted in publications. In fact, discussed is the assertion that in describing phenomena in a uniformly accelerated reference frame, in addition to the usual account of inertia forces, as in classical and nonrelativistic quantum theories, in quantum field theory [22] it is also necessary to additionally replace the vacuum state of the fields with the state of a thermal bath with temperature T_{U}. To avoid misunderstandings, it is important to emphasize that the Unruh thermal bath consists of so-called Fulling–Unruh particles rather than ordinary particles [349, 350]. These particles have the same spin, charge, and other quantum numbers as the field under consideration, but they are not free (they are in the field of inertia forces); in particular, they are massless and have a specific density of states.

The Unruh effect was discovered in the process of rethinking Hawking's work [351], which predicted the evaporation of black holes, since it is an analogue of the Hawking effect in an eternal black hole. However, these two effects are fundamentally different. While for a black hole what is predicted is the radiation that goes to infinity, for an accelerated observer in the absence of a black hole, predicted

[22] The Unruh effect being specific just for the quantum field theory can be seen in the vanishing of temperature T_{U} at a fixed acceleration and $\hbar \to 0$ or $c \to \infty$.

is the presence of an equilibrium thermal bath localized near event horizons of this observer, to which the Fulling–Unruh particles are confined by the force of inertia and therefore, in principle, cannot go to infinity. (The problems under consideration are identical near the horizons; however, in the case of a black hole, located in front of the horizon is not a centrifugal barrier but a penetrable gravitational barrier vanishing at infinity.)

It should be noted that the concept of the Unruh thermal bath, although popular and recognized by most specialists, was nevertheless repeatedly criticized (see, for example, studies [352–357], the subsequent discussion [358–361], and reviews [362–364]). Such a situation prompts considering its direct experimental verification. The first apparent difficulty is the negligible weakness of the effect under standard conditions (according to Eqn (74) $T_{\rm U}\,[{\rm K}] = 4.06\times10^{-23}w\,[{\rm cm\ s^{-2}}]$). Nevertheless, the necessary immense acceleration values are provided by the ultrarelativistic motion of electrons and atomic nuclei in laser fields. Here, however, a seemingly unobvious unique methodological feature of the Unruh effect emerges, in light of which, in our opinion, it is incorrect to call it an effect. Namely, the Unruh thermal bath, by definition, is only visible to a uniformly accelerated observer, and it is necessary to reconcile their perspective on the observed phenomena with that of an inertial observer. Since any process can always be considered from the perspective of an inertial observer (and, moreover, the laboratory frame of reference in such cases is always inertial with colossal accuracy), it can be asserted that the Unruh effect is unobservable from the inertial frame of reference and therefore basically defies experimental verification. This point of view is well formulated and explained in detail in Ref. [365]. In the currently most comprehensive review of studies on the Unruh effect, the same idea is formulated as follows [362]: "We emphasize that... the Unruh effect itself *does not need experimental confirmation* any more than free quantum field theory.... The assertions follow from the definition and so *do not need to be experimentally verified*. The fact that the 'Rindler and Minkowski perspectives' give consistent physical predictions is a consequence of the validity of these constructions." The way in which the perspectives of uniformly accelerated and inertial observers are reconciled with the Unruh effect taken into account was discussed in detail, inter alia, using the example of radiation by a uniformly accelerated charge [366] and the decay of a uniformly accelerated proton [367]. Note, however, that, from the perspective of a uniformly accelerated frame, particles are emitted in the zero mode, and [356] criticizes just the correctness of taking this mode into account.

Given the foregoing, we finally turn to the above-mentioned proposals [344–348] on the experimental examination of the Unruh effect. They are based on the erroneous notion that, in observing an accelerated charge in an inertial frame of reference, in addition to the 'ordinary' radiation, some 'additional' weak radiation 'due to the Unruh effect' should supposedly be observed. The specific mechanisms of such 'Unruh radiation' being discussed are partly based on an incorrect interpretation of the Unruh thermal bath as consisting of ordinary (rather than Fulling) particles [368], and partly on an incorrect interpretation of the results of Ref. [369]. In this interpretation, the same excitation of a uniformly accelerated detector is explained in a uniformly accelerated frame by the absorption of Fulling particles from a thermal bath and, in an inertial frame, by the radiation of ordinary particles (in the latter case, the energy is taken from the work done by external forces to accelerate the detector [370]). It is erroneous to conclude that in this case some part of the radiation observed in the inertial system should be attributed to the Unruh effect. According to the foregoing, in reality, all radiation observed in an inertial frame is 'ordinary' and can be described without referencing the Unruh effect; therefore, the term 'Unruh radiation' that has been coined in recent years and proposals for experimental verification of the Unruh effect, in our opinion, are absolutely meaningless. For more detailed explanations, we refer the interested reader to the cited papers, especially the brilliant paper [365].

8. Conclusions

The active development of technologies for generating high-intensity laser pulses has stimulated a significant increase in the number of published theoretical studies of the physics of extreme light fields. This review considers selected areas of theoretical research from among those actively discussed in modern publications. An increase in the number of relevant experimental studies is also expected in the near future.

The authors share the moderately optimistic point of view, popular in the scientific community of extreme-field physics, that intensities $\mathcal{I} \simeq 10^{23}-10^{24}$ W cm^{-2} will become available in laboratories in the foreseeable future. In particular, laser systems expected to overcome the 10^{23} W cm^{-2} milestone have already been built. Nevertheless, significant technical problems associated with an insufficiently high contrast of a superhigh-power laser pulse, wavefront distortions, difficulties in tight focusing of high-intensity beams, and other factors, the discussion of which is beyond the scope of our review, significantly slow down implementation of experiments.

Among the processes described in this review, the most realistic in the near future is the experimental study of the nonlinear Breit–Wheeler effect and various features of the spectra of nonlinear Thomson and Compton scattering due to polarization, focusing, and the finite duration of the laser pulse, as well as radiation friction. These effects have already been observed at the limit of experimental capabilities at lower intensities (see references in Sections 3 and 4). The value of quantum parameter (3) sufficient for their detection was previously achieved by using high-energy electron beams. The repetition of such experiments on new multipetawatt laser systems being put into operation will significantly improve the reliability and accuracy of measurements. The effect of birefringence of X-ray photons in a vacuum, induced by a strong field, can apparently also be observed at already achieved intensities, provided that the accuracy of polarimetry is improved.

Among the phenomena that have not yet been studied experimentally, the most immediate goal is the effects associated with the dominance of radiation friction. Intensities of $\mathcal{I} \gtrsim 10^{23}$ W cm^{-2} are required for their observation, which will be achievable as soon as 10-petawatt class lasers start operating in the design mode. In contrast, the observation of the self-sustaining cascades described in Section 5, and even more so of the nonperturbative QED regime, is apparently hardly realistic until the 100-petawatt power level is reached.

Acknowledgments

The authors are grateful to R Alkofer, D Blaschke, S V Bulanov, S S Bulanov, S Weber, M Vranic, E G Gelfer, A A Gonoskov, T Grismayer, M Grech, L L Ji, N V Elkina, D Seipt, A Ilderton, F Karbstein, S P Kim, Ch M Kim, B King, O Klimo, G Korn, I Yu Kostyukov, F Mackenroth, A A Mironov, S Meuren, V D Mur, G Mourou, E N Nerush, A M Pukhov, A di Piazza, D A Reis, E Reicher, C P Ridgers, H Ruhl, S G Rykovanov, A M Sergeev, E S Sozinov, A I Titov, A Hartin, R Shaysultanov, and V Yakimenko, as well as participants in the seminar Extreme Light Technologies, Science and Applications at the Annual International Laser Physics Workshop (LPHYS) and students in the special course Theory of Superstrong Fields delivered to students in the Department of Theoretical Nuclear Physics of the National Research Nuclear University MEPhI, for their helpful discussions of various issues considered in this review.

We would especially like to mention the many years of joint work in the field of superstrong laser fields, which we were lucky to carry out together with N B Narozhny and V S Popov, renowned authorities in this field of physics.

This study was carried out with financial support from the Russian Foundation for Basic Research as part of scientific project no. 20-12-50129.

References

1. Mourou G A, Umstadter D *Sci. Am.* **286** (5) 80 (2002)
2. Reiss H R *J. Math. Phys.* **3** 59 (1962)
3. Nikishov A I, Ritus V I *Sov. Phys. JETP* **19** 529 (1964); *Zh. Eksp. Teor. Fiz.* **46** 776 (1964)
4. Nikishov A I, Ritus V I *Sov. Phys. JETP* **19** 1191 (1964); *Zh. Eksp. Teor. Fiz.* **46** 1768 (1964)
5. Keldysh L V *Sov. Phys. JETP* **20** 1307 (1965); *Zh. Eksp. Teor. Fiz.* **47** 1945 (1964)
6. Nikishov À I, Ritus V I, in *XII Mezhdunarodnaya Konf. po Fizike Vysokikh Energii, Dubna, 5–15 Avg. 1964 g.* (Proc. of 12th Intern. Conf. on High Energy Physics, Dubna, August 5–15, 1964) (Ed. Ya A Smorodinskii et al.) Vol. 1 (Moscow: Atomizdat, 1966) p. 968
7. Nikishov A I, Ritus V I *Sov. Phys. Usp.* **13** 303 (1970); *Usp. Fiz. Nauk* **100** 724 (1970)
8. Kryukov P G et al. *J. Russ. Laser Res.* **15** 351 (1994)
9. Korzhimanov A V et al. *Phys. Usp.* **54** 9 (2011); *Usp. Fiz. Nauk* **181** 9 (2011)
10. Danson C N et al. *High Power Laser Sci. Eng.* **7** e54 (2019)
11. Mourou G A, Tajima T, Bulanov S V *Rev. Mod. Phys.* **78** 309 (2006)
12. Di Piazza A et al. *Rev. Mod. Phys.* **84** 1177 (2012)
13. Burton D A, Noble A *Contemp. Phys.* **55** 110 (2014)
14. Bulanov S V et al. *Plasma Phys. Rep.* **41** 1 (2015); *Fiz. Plazmy* **41** 3 (2015)
15. Bulanov S V et al. *Eur. Phys. J. D* **55** 483 (2009)
16. Macchi A, Borghesi M, Passoni M *Rev. Mod. Phys.* **85** 751 (2013)
17. Marklund M, Shukla P K *Rev. Mod. Phys.* **78** 591 (2006)
18. Ehlotzky F, Krajewska K, Kamiński J Z *Rep. Prog. Phys.* **72** 046401 (2009)
19. Heinzl T *Int. J. Mod. Phys. A* **27** 1260010 (2012)
20. Narozhny N B, Fedotov A M *Contemp. Phys.* **56** 249 (2015)
21. Titov A I et al. *Phys. Part. Nucl.* **47** 456 (2016); *Fiz. Elem. Chastits Atom. Yadra* **47** 834 (2016)
22. Hartin A *Int. J. Mod. Phys. A* **33** 1830011 (2018)
23. Zhang P et al. *Phys. Plasmas* **27** 050601 (2020)
24. Blackburn T G *Rev. Mod. Plasma Phys.* **4** 5 (2020)
25. Shi Y, Qin H, Fisch N J *Phys. Plasmas* **28** 042104 (2021)
26. Bulanov S V *Phys. Wave Phenom.* **29** 1 (2021)
27. Nedorezov V G, Rykovanov S G, Savel'ev A B *Phys. Usp.* **64** 1214 (2021); *Usp. Fiz. Nauk* **191** 1281 (2021)
28. Gonoskov A et al. *Rev. Mod. Phys.* **94** 045001 (2022)
29. Fedotov A et al. *Phys. Rep.* **1010** 1 (2023)
30. Landau L D, Lifshitz E M *The Classical Theory of Fields* 4th ed. (Berlin: Butterworth-Heinemann, 1980); Translated from Russian: *Teoriya Polya* (Moscow: Nauka, 1988)
31. Ritus V I *J. Sov. Laser Res.* **6** 497 (1985); Translated from Russian: *Trudy Fiz. Inst. Akad. Nauk* **111** 5 (1979); Nikishov A I *J. Sov. Laser Res.* **6** 619 (1985); Translated from Russian: *Trudy Fiz. Inst. Akad. Nauk* **111** 152 (1979)
32. Sauter F *Z. Phys.* **69** 742 (1931)
33. Heisenberg W, Euler H *Z. Phys.* **98** 714 (1936)
34. Schwinger J *Phys. Rev.* **82** 664 (1951)
35. Altarelli M et al. (Eds) "The European X-ray Free-Electron Laser", Technical Design Report DESY 2006-097 (Hamburg: DESY, 2007)
36. Bostedt C et al. *Rev. Mod. Phys.* **88** 015007 (2016)
37. Bula C et al. *Phys. Rev. Lett.* **76** 3116 (1996)
38. Bamber C et al. *Phys. Rev. D* **60** 092004 (1999)
39. Cole J M et al. *Phys. Rev. X* **8** 011020 (2018)
40. Poder K et al. *Phys. Rev. X* **8** 031004 (2018)
41. Bulanov S S et al. *AIP Conf. Proc.* **1507** 825 (2012)
42. Bulanov S S et al. *J. Exp. Theor. Phys.* **102** 9 (2006); *Zh. Eksp. Teor. Fiz.* **129** 14 (2006)
43. Bulanov S S et al. *Phys. Rev. Lett.* **104** 220404 (2010)
44. Khazanov E A, Mironov S Yu, Mourou G *Phys. Usp.* **62** 1096 (2019); *Usp. Fiz. Nauk* **189** 1173 (2019)
45. Strickland D, Mourou G *Opt. Commun.* **55** 447 (1985)
46. Dubietis A, Jonušauskas G, Piskarskas A *Opt. Commun.* **88** 437 (1992)
47. Perry M D et al. *Opt. Lett.* **24** 160 (1999)
48. Yanovsky V et al. *Opt. Express* **16** 2109 (2008)
49. Yoon J W et al. *Optica* **8** 630 (2021)
50. Chambaret J-P et al. *Proc. SPIE* **7721** 77211D (2010)
51. Weber S et al. *Matter Radiat. Extrem.* **2** 149 (2017)
52. Papadopoulos D N et al. *High Power Laser Sci. Eng.* **4** E34 (2016)
53. Guo Z et al. *Opt. Express* **26** 26776 (2018)
54. Gan Z et al. *Opt. Express* **25** 5169 (2017)
55. Li W et al. *Opt. Lett.* **43** 5681 (2018)
56. Leng Y X *Chin. J. Lasers* **46** 5 (2019)
57. Sung J H et al. *Opt. Lett.* **42** 2058 (2017)
58. Bashinov A V et al. *Eur. Phys. J. Spec. Top.* **223** 1105 (2014)
59. Shaykin A et al. *Rev. Laser Eng.* **42** 141 (2014)
60. Cartlidge E *Science* **359** 382 (2018)
61. Bahk S-W et al. *Opt. Lett.* **29** 2837 (2004)
62. Kiriyama H et al. *Opt. Lett.* **43** 2595 (2018)
63. Bromage J et al. *High Power Laser Sci. Eng.* **7** E4 (2019)
64. Har-Shemesh O, Di Piazza A *Opt. Lett.* **37** 1352 (2012)
65. He C Z et al. *Opt. Express* **27** 30020 (2019)
66. Blackburn T G et al. *Phys. Rev. Accel. Beams* **23** 064001 (2020)
67. Mackenroth F, Holkundkar A R, Schlenvoigt H-P *New J. Phys.* **21** 123028 (2019)
68. Vais O E et al. *New J. Phys.* **22** 023003 (2020)
69. Chowdhury E A, Barty C P J, Walker B C *Phys. Rev. A* **63** 042712 (2001)
70. Yamakawa K et al. *Phys. Rev. A* **68** 065403 (2003)
71. Link A et al. *Rev. Sci. Instrum.* **77** 10E723 (2006)
72. Ciappina M F et al. *Phys. Rev. A* **99** 043405 (2019)
73. Ciappina M F, Popruzhenko S V *Laser Phys. Lett.* **17** 025301 (2020)
74. Ciappina M F, Peganov E E, Popruzhenko S V *Matter Radiat. Extrem.* **5** 044401 (2020)
75. Sarachik E S, Schappert G T *Phys. Rev. D* **1** 2738 (1970)
76. Berestetskii V B, Lifshitz E M, Pitaevskii L P *Quantum Electrodynamics* (Berlin: Butterworth-Heinemann, 1982); Translated from Russian: *Kvantovaya Elektrodinamika* (Moscow: Nauka, 1989)
77. Kibble T W B *Phys. Rev.* **150** 1060 (1966)
78. Vais O E, Bychenkov V Yu *Appl. Phys. B* **124** 211 (2018)
79. Yandow A, Toncian T, Ditmire T *Phys. Rev. A* **100** 053406 (2019)
80. Popov V S *Phys. Usp.* **47** 855 (2004); *Usp. Fiz. Nauk* **174** 921 (2004)
81. Popruzhenko S V *J. Phys. B* **47** 204001 (2014)
82. Karnakov B M, Mur V D, Popruzhenko S V, Popov V S *Phys. Usp.* **58** 3 (2015); *Usp. Fiz. Nauk* **185** 3 (2015)
83. Popruzhenko S V *JETP Lett.* **117** 281 (2023); *Pis'ma Zh. Eksp. Teor. Fiz.* **117** 279 (2023)
84. Perelomov A M, Popov V S, Terent'ev M V *Sov. Phys. JETP* **23** 924 (1966); *Zh. Eksp. Teor. Fiz.* **50** 1393 (1966)

85. Perelomov A M, Popov V S *Sov. Phys. JETP* **25** 336 (1967); *Zh. Eksp. Teor. Fiz.* **52** 514 (1967)
86. Bagayev S N et al. *Opt. Lett.* **39** 1517 (2014)
87. Sampat S et al. *Appl. Opt.* **57** 9571 (2018)
88. Cerchez M et al. *High Power Laser Sci. Eng.* **7** E37 (2019)
89. Ginzburg V N et al. *Quantum Electron.* **50** 331 (2020); *Kvantovaya Elektron.* **50** 331 (2020)
90. Mourou G et al. *Eur. Phys. J. Spec. Top.* **223** 1181 (2014)
91. Ginzburg V et al. *Opt. Express* **29** 28297 (2021)
92. Giordmaine J, Duguay M, Hansen J *IEEE J. Quantum Electron.* **4** 252 (1968)
93. Fisher R A, Kelley P L, Gustafson T K *Appl. Phys. Lett.* **14** 140 (1969)
94. Yumoto H et al. *Nat. Photon.* **7** 43 (2013)
95. Bulanov S V, Esirkepov T, Tajima T *Phys. Rev. Lett.* **91** 085001 (2003)
96. Bulanov S V et al. *Phys. Usp.* **56** 429 (2013); *Usp. Fiz. Nauk* **183** 449 (2013)
97. Kando M et al. *Phys. Rev. Lett.* **99** 135001 (2007)
98. Kando M et al. *Phys. Rev. Lett.* **103** 235003 (2009)
99. Gordienko S et al. *Phys. Rev. Lett.* **94** 103903 (2005)
100. Abraham M "Prinzipien der Dynamik des Elektrons" *Ann. Physik* **10** 105 (1903)
101. Dirac P A M *Proc. R. Soc. Lond. A* **167** 148 (1938)
102. Jackson J D *Classical Electrodynamics* 3rd ed. (New York: Wiley, 1999); Translated into Russian: *Klassicheskaya Elektrodinamika* (Moscow: Mir, 1965)
103. Ginzburg V L *Applications of Electrodynamics in Theoretical Physics and Astrophysics* 2nd rev. English ed. (New York: Gordon and Breach Science Publishers, 1989); Translated from Russian: *Teoreticheskaya Fizika i Astrofizika. Dopolnitel'nye Glavy* (Theoretical Physics and Astrophysics. Additional Chapters) 3rd ed., rev., exp. (Moscow: Ripol Klassik, 1987)
104. Zel'dovich Ya B *Sov. Phys. Usp.* **18** 79 (1975); *Usp. Fiz. Nauk* **115** 161 (1975)
105. Baier V N, Katkov V M, Strakhovenko V M *Electromagnetic Processes at High Energies in Oriented Crystals* (Singapore: World Scientific, 1998)
106. Kirk J G, Bell A R, Arka I *Plasma Phys. Control. Fusion* **51** 085008 (2009)
107. Sokolov A A, Klepikov N P, Ternov I M *Zh. Eksp. Teor. Fiz.* **24** 249 (1953)
108. Schwinger J *Proc. Natl. Acad. Sci. USA* **40** 132 (1954)
109. Niel F et al. *Phys. Rev. E* **97** 043209 (2018)
110. Di Piazza A *Lett. Math. Phys.* **83** 305 (2008)
111. Tamburini M et al. *New J. Phys.* **12** 123005 (2010)
112. Tamburini M et al. *Nucl. Instrum. Meth. Phys. Res. A* **653** 181 (2011)
113. Tamburini M et al. *Phys. Rev. E* **85** 016407 (2012)
114. Capdessus R, McKenna P *Phys. Rev. E* **91** 053105 (2015)
115. Vshivkov V A et al. *Phys. Plasmas* **5** 2727 (1998)
116. Gelfer E G et al. *Phys. Rev. E* **101** 033204 (2020)
117. Gelfer E, Elkina N, Fedotov A *Sci. Rep.* **8** 6478 (2018)
118. Gelfer E G, Fedotov A M, Weber S *Plasma Phys. Control. Fusion* **60** 064005 (2018)
119. Chen M et al. *Plasma Phys. Control. Fusion* **53** 014004 (2011)
120. Gelfer E, Fedotov A, Weber S *New J. Phys.* **23** 095002 (2021)
121. Nakamura T et al. *Phys. Rev. Lett.* **108** 195001 (2012)
122. Liseykina T V, Popruzhenko S V, Macchi A *New J. Phys.* **18** 072001 (2016)
123. Akhiezer A I, Polovin R V *Sov. Phys. JETP* **3** 696 (1956); *Zh. Eksp. Teor. Fiz.* **30** 915 (1956)
124. Liseykina T V, Macchi A, Popruzhenko S V *Eur. Phys. J. Plus* **136** 170 (2021)
125. Bashinov A V, Kim A V *Phys. Plasmas* **20** 113111 (2013)
126. Pitaevskii L P *Sov. Phys. JETP* **12** 1008 (1961); *Zh. Eksp. Teor. Fiz.* **39** 1450 (1960)
127. Pershan P S *Phys. Rev.* **130** 919 (1963)
128. van der Ziel J P, Pershan P S, Malmstrom L D *Phys. Rev. Lett.* **15** 190 (1965)
129. Capdessus R et al. *Phys. Plasmas* **21** 123120 (2014)
130. Macchi A et al. *Phys. Rev. Lett.* **94** 165003 (2005)
131. Schlegel T, Tikhonchuk V T *New J. Phys.* **14** 073034 (2012)
132. Popruzhenko S V, Liseykina T V, Macchi A *New J. Phys.* **21** 033009 (2019)
133. Oleinik V P *Sov. Phys. JETP* **26** 1132 (1968); *Zh. Eksp. Teor. Fiz.* **53** 1997 (1968)
134. Brown L S, Kibble T W B *Phys. Rev.* **133** A705 (1964)
135. Gol'dman I I *Sov. Phys. JETP* **19** 954 (1964); *Zh. Eksp. Teor. Fiz.* **46** 1412 (1964)
136. Narozhnyi N B, Nikishov A I, Ritus V I *Sov. Phys. JETP* **20** 622 (1965); *Zh. Eksp. Teor. Fiz.* **47** 930 (1965)
137. Peskin M E, Schroeder D V *An Introduction to Quantum Field Theory* (Boca Raton, FL: CRC Press, 2018)
138. Tiesinga E et al. *Rev. Mod. Phys.* **93** 025010 (2021)
139. Kibble T W B *Phys. Rev.* **138** B740 (1965)
140. Frantz L M *Phys. Rev.* **139** B1326 (1965)
141. Glauber R J *Phys. Rev.* **131** 2766 (1963)
142. Bialynicki-Birula I, Bialynicka-Birula Z *Phys. Rev. A* **8** 3146 (1973)
143. Furry W H *Phys. Rev.* **81** 115 (1951)
144. Reiss H R *Laser Phys.* **15** 1486 (2005)
145. Bagrov V G, Gitman D M *Exact Solutions of Relativistic Wave Equations* (Mathematics and its Applications, Soviet Ser., Vol. 39) (Dordrecht: Kluwer Acad. Publ., 1990)
146. Wolkow D M *Z. Phys.* **94** 250 (1935)
147. Taub A H *Rev. Mod. Phys.* **21** 388 (1949)
148. Ritus V I *Ann. Physics* **69** 555 (1972)
149. Bargmann V, Michel L, Telegdi V L *Phys. Rev. Lett.* **2** 435 (1959)
150. Kibble T W B *Phys. Rev. Lett.* **16** 1054 (1966)
151. Bauer D, Mulser P, Steeb W-H *Phys. Rev. Lett.* **75** 4622 (1995)
152. Lau Y Y et al. *Phys. Plasmas* **10** 2155 (2003)
153. Eberly J H, in *Progress in Optics* Vol. 7 (Ed. E Wolf) (Amsterdam: Elsevier, 1969) p. 359
154. Harvey C et al. *Phys. Rev. Lett.* **109** 100402 (2012)
155. Vallée O, Soares M *Airy Functions and Applications to Physics* (Singapore: World Scientific, 2004)
156. Nikishov A I, Ritus V I *Sov. Phys. JETP* **25** 1135 (1967); *Zh. Eksp. Teor. Fiz.* **52** 1707 (1967)
157. Harvey C N, Ilderton A, King B *Phys. Rev. A* **91** 013822 (2015)
158. Di Piazza A et al. *Phys. Rev. A* **98** 012134 (2018)
159. Ilderton A, King B, Seipt D *Phys. Rev. A* **99** 042121 (2019)
160. Harvey C, Heinzl T, Ilderton A *Phys. Rev. A* **79** 063407 (2009)
161. Tamburini M, Meuren S *Phys. Rev. D* **104** L091903 (2021); arXiv:1912.07508
162. Dinu V, Heinzl T, Ilderton A *Phys. Rev. D* **86** 085037 (2012)
163. Boca M, Florescu V *Phys. Rev. A* **80** 053403 (2009)
164. Mackenroth F, Di Piazza A *Phys. Rev. A* **83** 032106 (2011)
165. Heinzl T, Seipt D, Kämpfer B *Phys. Rev. A* **81** 022125 (2010)
166. Seipt D, Kämpfer B *Phys. Rev. A* **83** 022101 (2011)
167. Krajewska K, Kamiński J Z *Phys. Rev. A* **85** 062102 (2012)
168. Seipt D, Kämpfer B *Phys. Rev. A* **88** 012127 (2013)
169. Ivanov D Y, Kotkin G L, Serbo V G *Eur. Phys. J. C* **36** 127 (2004)
170. Krajewska K, Kamiński J Z *Laser Part. Beams* **31** 503 (2013)
171. Seipt D, King B *Phys. Rev. A* **102** 052805 (2020)
172. Baier V N, Katkov V M *Sov. Phys. JETP* **26** 854 (1968); *Zh. Eksp. Teor. Fiz.* **53** 1478 (1968)
173. Bordovitsyn V A, Ternov I M, Bagrov V G *Phys. Usp.* **38** 1037 (1995); *Usp. Fiz. Nauk* **165** 1083 (1995)
174. Heinzl T, Ilderton A, King B *Phys. Rev. Lett.* **127** 061601 (2021)
175. Di Piazza A, Audagnotto G *Phys. Rev. D* **104** 016007 (2021)
176. Di Piazza A *Phys. Rev. Lett.* **117** 213201 (2016)
177. Di Piazza A *Phys. Rev. A* **95** 032121 (2017)
178. Di Piazza A *Phys. Rev. D* **103** 076011 (2021)
179. Abramowicz H et al. *Eur. Phys. J. Spec. Top.* **230** 2445 (2021)
180. Meuren S et al. "Probing Strong-field QED at FACET-II, experimental proposal approved as E-320" (2018) unpublished
181. Krajewska K, Kamiński J Z *Phys. Rev. A* **86** 052104 (2012)
182. Titov A I et al. *Phys. Rev. Lett.* **108** 240406 (2012)
183. Titov A I et al. *Phys. Rev. A* **87** 042106 (2013)
184. Jansen M J A, Müller C *Phys. Rev. D* **93** 053011 (2016)
185. Meuren S, Keitel C H, Di Piazza A *Phys. Rev. D* **93** 085028 (2016)
186. Burke D L et al. *Phys. Rev. Lett.* **79** 1626 (1997)
187. Eberly J H, Reiss H R *Phys. Rev.* **145** 1035 (1966)
188. Mackenroth F et al. *Phys. Rev. E* **99** 033205 (2019)
189. Bassompierre G et al. *Phys. Lett. B* **355** 584 (1995)

190. Akhmedov E Kh *Phys. Atom. Nucl.* **74** 1299 (2011); *Yad. Fiz.* **74** 1326 (2011)
191. Fedotov A M, Mironov A A *Radiophys. Quantum Electron.* **61** 930 (2019); *Izv. Vyssh. Uchebn. Zaved. Radiofiz.* **61** 1147 (2018)
192. Khokonov M Kh, Bekulova I Z *Tech. Phys.* **55** 728 (2010); *Zh. Tekh. Fiz.* **80** (5) 136 (2010)
193. Seipt D et al. *Phys. Rev. Lett.* **118** 154803 (2017)
194. King B *Phys. Rev. A* **101** 042508 (2020)
195. Lv Q Z et al. *New J. Phys.* **23** 065005 (2021)
196. King B *Phys. Rev. D* **103** 036018 (2021)
197. Heinzl T, King B, MacLeod A J *Phys. Rev. A* **102** 063110 (2020)
198. Gelfer E G et al. *Phys. Rev. D* **106** 056013 (2022)
199. Fedotov A *J. Phys. Conf. Ser.* **826** 012027 (2017)
200. Ritus V I *JETP Lett.* **12** 289 (1970); *Pis'ma Zh. Eksp. Teor. Fiz.* **12** 416 (1970)
201. Mitter H, in *Electromagnetic Interactions and Field Theory. Proc. of the XIV Intern. Universitätswochen für Kernphysik 1975 der Karl-Franzens-Universität Graz at Schladming, Steiermark, Austria, 24th February – 7th March, 1975* (Acta Physica Austriaca. Supplementum, Vol. 14, Ed. P Urban) (Wien: Springer-Verlag, 1975) pp. 397–468
202. Baier V N, Katkov V I, Strakhovenko V M *Sov. J. Nucl. Phys.* **14** 572 (1972); *Yad. Fiz.* **14** 1020 (1971)
203. Ritus V I *Nucl. Phys. B* **44** 236 (1972)
204. Hu H, Müller C, Keitel C H *Phys. Rev. Lett.* **105** 080401 (2010)
205. Ilderton A *Phys. Rev. Lett.* **106** 020404 (2011)
206. King B, Ruhl H *Phys. Rev. D* **88** 013005 (2013)
207. Krajewska K, Kaminski J Z *J. Phys. Conf. Ser.* **594** 012024 (2015)
208. Dinu V, Torgrimsson G *Phys. Rev. D* **97** 036021 (2018)
209. King B, Fedotov A M *Phys. Rev. D* **98** 016005 (2018)
210. Mackenroth F, Di Piazza A *Phys. Rev. D* **98** 116002 (2018)
211. Acosta U H, Kämpfer B *Plasma Phys. Control. Fusion* **61** 084011 (2019)
212. Dinu V, Torgrimsson G *Phys. Rev. D* **101** 056017 (2020)
213. Morozov D A, Ritus V I *Nucl. Phys. B* **86** 309 (1975)
214. Lötstedt E, Jentschura U D *Phys. Rev. Lett.* **103** 110404 (2009)
215. Lötstedt E, Jentschura U D *Phys. Rev. A* **80** 053419 (2009)
216. Seipt D, Kämpfer B *Phys. Rev. D* **85** 101701 (2012)
217. Mackenroth F, Di Piazza A *Phys. Rev. Lett.* **110** 070402 (2013)
218. King B *Phys. Rev. A* **91** 033415 (2015)
219. Dinu V, Torgrimsson G *Phys. Rev. D* **99** 096018 (2019)
220. Bogoliubov N N, Shirkov D V *Introduction to the Theory of Quantized Fields* 2nd American ed. (New York: John Wiley, 1980); Translated from Russian: *Vvedenie v Teoriyu Kvantovannykh Polei* 4th ed., rev. (Moscow: Nauka, 1984)
221. Dinu V, Torgrimsson G *Phys. Rev. D* **102** 016018 (2020)
222. Chen P et al. *Nucl. Instrum. Meth. Phys. Res. A* **355** 107 (1995)
223. Rimbault C et al., in *2007 IEEE Particle Accelerator Conf., Proc.* (Piscataway, NJ: IEEE, 2007) p. 2728
224. Elkina N V et al. *Phys. Rev. Accel. Beams* **14** 054401 (2011)
225. Duclous R, Kirk J G, Bell A R *Plasma Phys. Control. Fusion* **53** 015009 (2010)
226. Ridgers C P et al. *J. Comput. Phys.* **260** 273 (2014)
227. Arber T D et al. *Plasma Phys. Control. Fusion* **57** 113001 (2015)
228. Gonoskov A et al. *Phys. Rev. E* **92** 023305 (2015)
229. Grismayer T et al. *Phys. Rev. E* **95** 023210 (2017)
230. Arefiev A V et al. *Phys. Plasmas* **22** 013103 (2015)
231. Di Piazza A, Hatsagortsyan K Z, Keitel C H *Phys. Rev. Lett.* **105** 220403 (2010)
232. Shen C S, White D *Phys. Rev. Lett.* **28** 455 (1972)
233. Blackburn T G et al. *Phys. Rev. Lett.* **112** 015001 (2014)
234. Sokolov I V et al. *Phys. Rev. Lett.* **105** 195005 (2010)
235. Bulanov S S et al. *Phys. Rev. A* **87** 062110 (2013)
236. Mironov A A, Narozhny N B, Fedotov A M *Phys. Lett. A* **378** 3254 (2014)
237. Mironov A A, Gelfer E G, Fedotov A M *Phys. Rev. A* **104** 012221 (2021)
238. Dobrotin N A et al. *Usp. Fiz. Nauk* **49** 185 (1953)
239. Bell A R, Kirk J G *Phys. Rev. Lett.* **101** 200403 (2008)
240. Fedotov A M et al. *Phys. Rev. Lett.* **105** 080402 (2010)
241. Nerush E N et al. *Phys. Rev. Lett.* **106** 035001 (2011)
242. Raether H *Electron Avalanches and Breakdown in Gases* (Washington, DC: Butterworths, 1964)
243. Vranic M et al. *Comput. Phys. Commun.* **191** 65 (2015)
244. Nerush E N, Bashmakov V F, Kostyukov I Yu *Phys. Plasmas* **18** 083107 (2011)
245. King B, Elkina N, Ruhl H *Phys. Rev. A* **87** 042117 (2013)
246. Seipt D et al. *New J. Phys.* **23** 053025 (2021)
247. Artemenko I I et al. *Plasma Phys. Control. Fusion* **61** 074003 (2019)
248. Bashmakov V F et al. *Phys. Plasmas* **21** 013105 (2014)
249. Jirka M et al. *Phys. Rev. E* **93** 023207 (2016)
250. Slade-Lowther C, Del Sorbo D, Ridgers C P *New J. Phys.* **21** 013028 (2019)
251. Brady C S et al. *Phys. Plasmas* **21** 033108 (2014)
252. Jirka M et al. *Sci. Rep.* **7** 15302 (2017)
253. Fedotov A, Narozhny N, Mironov A *J. Phys. Conf. Ser.* **691** 012023 (2016)
254. Grismayer T et al. *Phys. Plasmas* **23** 056706 (2016)
255. Narozhny N B et al. *Phys. Lett. A* **330** 1 (2004)
256. Fedotov A M *Laser Phys.* **19** 214 (2009)
257. Tang S, Ilderton A, King B *Phys. Rev. A* **100** 062119 (2019)
258. Bragin S, Di Piazza A *Phys. Rev. D* **102** 116012 (2020)
259. Tamburini M, Di Piazza A, Keitel C H *Sci. Rep.* **7** 5694 (2017)
260. Artemenko I I, Kostyukov I Yu *Phys. Rev. A* **96** 032106 (2017)
261. Ridgers C P et al. *Phys. Rev. Lett.* **108** 165006 (2012)
262. Kirk J G, Bell A R, Ridgers C P *Plasma Phys. Control. Fusion* **55** 095016 (2013)
263. Zhu X L et al. *Nat. Commun.* **7** 13686 (2016)
264. Samsonov A S, Nerush E N, Kostyukov I Yu *Sci. Rep.* **9** 11133 (2019)
265. Samsonov A S, Kostyukov I Y, Nerush E N *Matter Radiat. Extremes* **6** 034401 (2021)
266. Ridgers C P et al. *Phys. Plasmas* **20** 056701 (2013)
267. Nerush E N et al. *Phys. Plasmas* **21** 013109 (2014)
268. Ji L L et al. *Phys. Plasmas* **21** 023109 (2014)
269. Gu Y-J et al. *Commun. Phys.* **1** 93 (2018)
270. Wan F et al. *Phys. Lett. B* **800** 135120 (2020)
271. Vranic M et al. *Sci. Rep.* **8** 4702 (2018)
272. Gelfer E G et al. *Phys. Rev. A* **92** 022113 (2015)
273. Gonoskov A et al. *Phys. Rev. X* **7** 041003 (2017)
274. Magnusson J et al. *Phys. Rev. A* **100** 063404 (2019)
275. Ritus V I *Sov. Phys. JETP* **30** 1181 (1970); *Zh. Eksp. Teor. Fiz.* **57** 2176 (1970)
276. Baier V N et al. *Sov. Phys. JETP* **42** 400 (1975); *Zh. Eksp. Teor. Fiz.* **69** 783 (1975)
277. Meuren S, Di Piazza A *Phys. Rev. Lett.* **107** 260401 (2011)
278. Narozhnyi N B *Sov. Phys. JETP* **28** 371 (1969); *Zh. Eksp. Teor. Fiz.* **55** 714 (1969)
279. Batalin I A, Shabad A E *Sov. Phys. JETP* **33** 483 (1971); *Zh. Eksp. Teor. Fiz.* **60** 894 (1971)
280. Baier V N, Katkov V M, Strakhovenko V M *Sov. Phys. JETP* **41** 198 (1975); *Zh. Eksp. Teor. Fiz.* **68** 405 (1975)
281. Meuren S, Keitel C H, Di Piazza A *Phys. Rev. D* **88** 013007 (2013)
282. Morozov D A, Narozhnyi N B, Ritus V I *Sov. Phys. JETP* **53** 1103 (1981); *Zh. Eksp. Teor. Fiz.* **80** 2113 (1981)
283. Di Piazza A, Lopez-Lopez M A *Phys. Rev. D* **102** 076018 (2020)
284. Adler S L et al. *Phys. Rev. Lett.* **25** 1061 (1970)
285. Bialynicka-Birula Z, Bialynicki-Birula I *Phys. Rev. D* **2** 2341 (1970)
286. Adler S L *Ann. Physics* **67** 599 (1971)
287. Papanyan V O, Ritus V I *Sov. Phys. JETP* **34** 1195 (1972); *Zh. Eksp. Teor. Fiz.* **61** 2231 (1972)
288. Papanyan V O, Ritus V I *Sov. Phys. JETP* **38** 879 (1974); *Zh. Eksp. Teor. Fiz.* **65**1756 (1974)
289. Baier V N, Mil'shtein A I, Shaisultanov R Zh *Sov. Phys. JETP* **63** 665 (1986); *Zh. Eksp. Teor. Fiz.* **90** 1141 (1986)
290. Gies H, Karbstein F, Kohlfürst C *Phys. Rev. D* **97** 036022 (2018)
291. Karbstein F *Phys. Rev. D* **88** 085033 (2013)
292. Karbstein F *J. High Energy Phys.* **2021** 1 (2021)
293. Goldstein D H *Polarized Light* (Boca Raton, FL: CRC Press, 2017) https://doi.org/10.1201/b10436
294. Mironov A A, Meuren S, Fedotov A M *Phys. Rev. D* **102** 053005 (2020)
295. Baier R, Breitenlohner P *Nuovo Cimento B* **47** 117 (1967)
296. Kotkin G L, Serbo V G *Phys. Lett. B* **413** 122 (1997)
297. Landau L D, Lifshitz E M, Pitaevskii L P *Electrodynamics of Continuous Media* 2nd ed. (Amsterdam: Elsevier, 2013); Translated

from Russian: *Elektrodinamika Sploshnykh Sred* (Moscow: Nauka, 1982)
298. Boyd R W *Nonlinear Optics* (San Diego, CA: Academic Press, 2020)
299. Zavattini G et al. *Int. J. Mod. Phys. A* **27** 1260017 (2012)
300. Heinzl T et al. *Opt. Commun.* **267** 318 (2006)
301. Karbstein F et al. *Phys. Rev. D* **92** 071301 (2015)
302. Shen B et al. *Plasma Phys. Control. Fusion* **60** 044002 (2018)
303. Marx B et al. *Phys. Rev. Lett.* **110** 254801 (2013)
304. Schmitt A T et al. *Optica* **8** 56 (2021)
305. Bernhardt H et al. *Phys. Rev. Res.* **2** 023365 (2020)
306. Becker W *Physica A* **87** 601 (1977)
307. Dremin I M *JETP Lett.* **76** 151 (2002); *Pis'ma Zh. Eksp. Teor. Fiz.* **76** 185 (2002)
308. Macleod A J, Noble A, Jaroszynski D A *Phys. Rev. Lett.* **122** 161601 (2019)
309. Schwinger J, Tsai W Y, Erber T *Ann. Physics* **281** 1019 (2000)
310. Bulanov S V et al. *Phys. Rev. D* **100** 016012 (2019)
311. Artemenko I I, Nerush E N, Kostyukov I Yu *New J. Phys.* **22** 093072 (2020)
312. Soljačić M, Segev M *Phys. Rev. A* **62** 043817 (2000)
313. Rozanov N N *Sov. Phys. JETP* **86** 284 (1988); *Zh. Eksp. Teor. Fiz.* **113** 513 (1998)
314. Sauerbrey R, Kohlfürst C, arXiv:2105.08006
315. Morozov D A, Narozhnyi N B *Sov. Phys. JETP* **45** 23 (1977); *Zh. Eksp. Teor. Fiz.* **72** 44 (1977)
316. Narozhny N B *Phys. Rev. D* **20** 1313 (1979)
317. Narozhny N B *Phys. Rev. D* **21** 1176 (1980)
318. Podszus T, Di Piazza A *Phys. Rev. D* **99** 076004 (2019)
319. Ilderton A *Phys. Rev. D* **99** 085002 (2019)
320. Blackburn T G et al. *New J. Phys.* **21** 053040 (2019)
321. Yakimenko V et al. *Phys. Rev. Lett.* **122** 190404 (2019)
322. Di Piazza A et al. *Phys. Rev. Lett.* **124** 044801 (2020)
323. Baumann C et al. *Sci. Rep.* **9** 9407 (2019)
324. Baumann C, Pukhov A *Plasma Phys. Control. Fusion* **61** 074010 (2019)
325. Blatt J M, Weisskopf V F *Theoretical Nuclear Physics* (New York: Dover Publ., 1991)
326. Pfützner M et al. *Rev. Mod. Phys.* **84** 567 (2012)
327. Qi C, Liotta R, Wyss R *Prog. Part. Nucl. Phys.* **105** 214 (2019)
328. Ritus V I *Sov. Phys. JETP* **29** 532 (1969); *Zh. Eksp. Teor. Fiz.* **56** 986 (1969)
329. Akhmedov E Kh *Sov. Phys. JETP* **58** 883 (1983); *Zh. Eksp. Teor. Fiz.* **85** 1521 (1983)
330. Nikishov A I, Ritus V I *Sov. Phys. JETP* **58** 14 (1983); *Zh. Eksp. Teor. Fiz.* **85** 24 (1983)
331. Pálffy A, Popruzhenko S V *Phys. Rev. Lett.* **124** 212505 (2020)
332. Becker W et al. *Phys. Lett. A* **94** 131 (1983)
333. Narozhny N B, Fedotov A M *Phys. Rev. Lett.* **100** 219101 (2008)
334. Wistisen T N, Keitel C H, Di Piazza A *New J. Phys.* **23** 065007 (2021)
335. Gamow G *Z. Phys.* **51** 204 (1928)
336. Fermi E *Nuclear Physics* (Chicago, IL: Univ. of Chicago Press, 1950)
337. Cortés H M C et al. *New J. Phys.* **13** 063007 (2011)
338. Becker W et al. *Phys. Rev. Lett.* **47** 1262 (1981)
339. Reiss H R *Phys. Rev. C* **27** 1199 (1983)
340. Reiss H R *Phys. Rev. C* **27** 1229 (1983)
341. Liu A H, Li S M, Berakdar J *Phys. Rev. Lett.* **98** 251803 (2007)
342. Delion D S, Ghinescu S A *Phys. Rev. Lett.* **119** 202501 (2017)
343. Queisser F, Schützhold R *Phys. Rev. C* **100** 041601 (2019)
344. Darbinyan S M et al. *JETP Lett.* **51** 110 (1990); *Pis'ma Zh. Eksp. Teor. Fiz.* **51** 97 (1990)
345. Chen P, Tajima T *Phys. Rev. Lett.* **83** 256 (1999)
346. Schützhold R, Schaller G, Habs D *Phys. Rev. Lett.* **97** 121302 (2006)
347. Brodin G et al. *Class. Quantum Grav.* **25** 145005 (2008)
348. Thirolf P G et al. *Eur. Phys. J. D* **55** 379 (2009)
349. Unruh W G *Phys. Rev. D* **14** 870 (1976)
350. Fulling S A *Phys. Rev. D* **7** 2850 (1973)
351. Hawking S W *Commun. Math. Phys.* **43** 199 (1975)
352. Nikishov A I, Ritus V I *Sov. Phys. JETP* **67** 1313 (1988); *Zh. Eksp. Teor. Fiz.* **94** 31 (1988)
353. Silaev P K, Khrustalev O A *Theor. Math. Phys.* **91** 481 (1992); *Teor. Mat. Fiz.* **91** 217 (1992)
354. Belinskii V A et al. *JETP Lett.* **65** 902 (1997); *Pis'ma Zh. Eksp. Teor. Fiz.* **65** 861 (1997)
355. Fedotov A M et al. *Phys. Lett. A* **254** 126 (1999)
356. Narozhny N B et al. *Phys. Rev. D* **65** 025004 (2001)
357. Gelfer E G et al. *Theor. Math. Phys.* **182** 356 (2015); *Teor. Matem. Fiz.* **182** 405 (2015)
358. Grib A A *JETP Lett.* **67** 95 (1998); *Pis'ma Zh. Eksp. Teor. Fiz.* **67** 86 (1998)
359. Belinskii V A et al. *JETP Lett.* **67** 96 (1998); *Pis'ma Zh. Eksp. Teor. Fiz.* **67** 87 (1998)
360. Fulling S A, Unruh W G *Phys. Rev. D* **70** 048701 (2004)
361. Narozhny N B et al. *Phys. Rev. D* **70** 048702 (2004)
362. Crispino L C B, Higuchi A, Matsas G E A *Rev. Mod. Phys.* **80** 787 (2008)
363. Arageorgis A, Earman J, Ruetsche L *Philos. Sci.* **70** 164 (2003)
364. Earman J *Stud. Hist. Philos. Sci. B* **42** 81 (2011)
365. Peña I, Sudarsky D *Found. Phys.* **44** 689 (2014)
366. Higuchi A, Matsas G E A, Sudarsky D *Phys. Rev. D* **45** R3308 (1992)
367. Vanzella D A T, Matsas G E A *Phys. Rev. Lett.* **87** 151301 (2001)
368. Zeldovich I B, Rozhanskii L V, Starobinskii A A *JETP Lett.* **43** 523 (1986); *Pis'ma Zh. Eksp. Teor. Fiz.* **43** 407 (1986)
369. Unruh W G, Wald R M *Phys. Rev. D* **29** 1047 (1984)
370. Birrell N D, Davies P C W *Quantum Fields in Curved Space* (Cambridge: Cambridge Univ. Press, 1982); Translated into Russian: *Kvantovannye Polya v Iskrivlennom Prostranstve–Vremeni* (Moscow: Mir, 1984)